In Vivo Bio-Safety Evaluations and Diagnostic/Therapeutic Applications of Chemically Designed Mesoporous Silica Nanoparticles

Yu Chen, Hangrong Chen, and Jianlin Shi**

The remarkable progress of nanotechnology and its application in biomedicine have greatly expanded the ranges and types of biomaterials from traditional organic material-based nanoparticles (NPs) to inorganic biomaterials or organic/inorganic hybrid nanocomposites due to the unprecedented advantages of the engineered inorganic material-based NPs. Colloidal mesoporous silica NPs (MSNs), one of the most representative and well-established inorganic materials, have been promoted into biology and medicine, and shifted from extensive in vitro research towards preliminary in vivo assays in small-animal disease models. In this comprehensive review, the recent progresses in chemical design and engineering of MSNs-based biomaterials for in vivo biomedical applications has been detailed and overviewed. Due to the intrinsic structural characteristics of elaborately designed MSNs such as large surface area, high pore volume and easy chemical functionalization, they have been extensively investigated for therapeutic, diagnostic and theranostic (concurrent diagnosis and therapy) purposes, especially in oncology. Systematic in vivo bio-safety evaluations of MSNs have revealed the evidences that the in vivo bio-behaviors of MSNs are strongly related to their preparation prodecures, particle sizes, geometries, surface chemistries, dosing parameters and even administration routes. In vivo pharmacokinetics and pharmacodynamics further demonstrated the effectiveness of MSNs as the passively and/or actively targeted drug delivery systems (DDSs) for cancer chemotherapy. Especially, the advance of nano-synthetic chemistry enables the production of composite MSNs for advanced in vivo therapeutic purposes such as gene delivery, stimuli-responsive drug release, photothermal therapy, photodynamic therapy, ultrasound therapy, or anti-bacteria in tissue engineering, or as the contrast agents for biological and diagnostic imaging. Additionally, the critical issues and potential challenges related to the chemical design/synthesis of MSNs-based "magic bullet" by advanced nano-synthetic chemistry and in vivo evaluation have been discussed to highlight the issues scientists face in promoting the translation of MSNs-based DDSs into clinical trials.

1. Introduction

According to the definition by the US National Nanotechnology Initiative in 2000, nanotechnology refers to the materials and systems whose structures and components exhibit novel and significantly improved physical, chemical and biological properties due to their nanoscale size.[1] It has been accepted and demonstrated that the nanoparticles (NPs) can bring forth the novel chemical and physical properties when their sizes are reduced into nanoscale, which endows them with broad and promising application potentials in catalysis, separation, sensors, optics, energy, electronics, environmental treatment, etc.[2–5] The convergence and application of nanotechnology in biological-, pharmaceutical- and medical-related areas have produced an interdisciplinary research field designated as nanomedicine, which can be traced back to late 1990s.[4,6–8] With the development of modern society, ever greater attention and efforts have been devoted to the heath issues of human beings. Nanomedicine, as one of the most developing multi-disciplinary research frontiers, seeks to accomplish two clinical goals: precisely diagnosing the diseases at their early stage and effectively treating the diseases upon positioning and identifying them. From chemical point of view, the cornerstone of nanomedicine relys on the chemically engineered nanobiomaterials obtained by various advanced nano-synthetic chemistry such as sol-gel chemistry, supramolecular chemistry, nanocrystal-growth chemistry, etc. Nanobiomaterials have been extensively explored in the following nanomedicine-related fields: as drug delivery systems (DDSs) for drug/gene transport,[9,10] as probes for diagnosis,[11,12] as repair materials for tissue engineering,[13] as synergistic[14,15] or radiosensitive[16,17] agents for ultrasound therapy or radiotherapy, etc. Several other therapeutic modalities, such as photothermal,[18–20] photodynamic[21–23] and magnetic hyperthermia-based[24–29] therapies have also been developed to

Dr. Y. Chen, Prof. Dr. H. R. Chen, Prof. Dr. J. L. Shi
State Key Laboratory of High Performance Ceramics and Superfine Microstructures
Shanghai Institute of Ceramics
Chinese Academy of Sciences
1295 Ding-Xi Road, Shanghai 200050, P. R. China
E-mail: hrchen@mail.sic.ac.cn; jlshi@sunm.shcnc.ac.cn

DOI: 10.1002/adma.201205292

address the complex requirements in cancer therapy based on synthetic nanobiomaterials.

Typically, NPs have the nature of high surface-to-volume ratio and abundant surface chemistry. The high surface-to-volume ratio facilitates the loading and delivery of drugs, genes and/or contrast agents (CAs) either in the interior or on their surface, while the abundant surface chemistry makes the surface modification using organic biomacromolecules or targeting ligands possible, resulting in excellent bio-behaviors in the biological media in vitro and in vivo. Many material systems have been introduced into nano-biomedicine, taking the advantages of their intrinsic physical, chemical and biological natures and merits, which can be roughly divided into three categories: (1) organic, (2) inorganic and (3) organic/inorganic hybrid nanoparticulate systems. The organic material systems (OMSs) are relatively mature in clinical translations after decades of development, and several nanotechnology-based organic DDSs (liposomes, emulsions, albumins, etc.) have been commercially driven to the clinical stage for tumor chemotherapy by improving the bioavailability and targeting efficacy of original drugs, such as DaunoXome, Myocet, Doxil, Abroxane, etc.[6,30] However, the intrinsic instability and low drug-loading capacity/efficiency of organic DDSs leave many of them in the preclinical stage and inhibit their further clinical translations.[6,30,31]

Recently, inorganic nanobiomaterials have attracted the increasing attention due to their unprecedented advantages. Compared to OMSs, inorganic materials systems (IMSs) show the unique nature of high thermal/chemical stability and resistance to corrosion under physiological conditions. They also exhibit the good biocompatibility but relatively low degradable rates. Especially, the IMSs can be easily endowed with unique structural features and chemical/physical properties to show the specific functions and properties, such as well-defined mesoporosity, magnetism, fluorescence, plasmonic absorbance, etc. For instance, our recent results have demonstrated that SiO_2 nanoparticles with well-defined mesoporosity and unique hollow interior could store as much as 35.1% hydrophobic anticancer drugs (camptothecin), which was difficult to be achieved by traditional OMSs.[32] Therefore, tailoring the structures of inorganic nanobiomaterials with similar or even better functions than OMSs while preserving their unique structural characteristics and physical/chemical properties can further promote the nanomedical products into clinical stage. Various IMSs, such as magnetic NPs,[33–35] semiconductor quantum dots (QDs),[36–38] metallic NPs,[39–41] carbon-based nanomaterials,[42–44] layered double hydroxide (LDH),[45,46] etc., have showed the excellent performance and broad applications in nanomedicine. A large number of in vitro results of inorganic nanobiomaterials are very attractive and encouraging. However, their in vivo translocations have encountered the great debate and challenge today. The bio-safety of IMSs, especially the degradability, is one of the crucial issues now under consideration and debate. Among numerous IMSs, silica is one of the most biocompatible materials manifested by the facts that it is an endogenous substance present mainly in bones and it has been used commercially as the excipient in tablet-form oral-taken drugs. Additionally, silica is "Generally Recognized As Safe (GRAS)" by the U. S. Food and Drug Administration (FDA).[47–50] Heart-stirringly, dye-doped fluorescent silica NPs, well-known as "Cornell dots" (C dots) have been approved by FDA for human stage I molecular imaging of cancer, which gives the great confidence about future clinical translation potentials of silica-based NPs for cancer diagnosis and therapy.[51] Additionally, recently developed organic-inorganic hybrid nanomaterials combine the merits of both organic and inorganic materials. Thus, these hybrid nanosystems can be endowed with unique characteristics such as improved biocompatibility, stimuli-responsive drug release, co-delivery of multi-drugs, etc.[52–57]

Dr. Y. Chen received his Bachelor degree in Polymer Material Sciences and Engineering at the Nanjing University of Technology (NJUT) and PhD degree in Shanghai Institute of Ceramics, Chinese Academy of Sciences (SICCAS). He is now the assistant professor in SICCAS. His research focuses on the design, synthesis and nano-biomedical applications of multifunctional mesoporous materials, including hollow mesoporous material for drug delivery, contrast agents for molecular imaging (fluorescent, MR, PAT, PET and ultrasonic imaging), chemo-/HIFU-therapy and non-virus gene delivery vehicles.

Prof. Dr. H. R. Chen received her PhD degree in SICCAS. She is a full professor and PhD supervisor in SICCAS since 2006. Her recent research interest focuses on nano-scale materials with novel mesoporous and/or specific structures as drug delivery systems for controlled drug release.

Prof. Dr. J. L. Shi received his PhD degree in SICCAS. He is now the professor of SICCAS and the director of the State Key Lab of High Performance Ceramics and Superfine Microstructures. His research areas include synthesis of mesoporous materials and mesoporous-based nano-composites, and their catalytic, biomedical and optical applications.

Adv. Mater. 2013,
DOI: 10.1002/adma.201205292

Mesoporous silica, discovered in the early 1990s[58,59] and typically synthesized by co-assembly of organic structural directing agents (SDAs, e.g., surfactants or block copolymers) and inorganic silicate species via the sol-gel chemistry and supramolecular chemistry,[59–61] is expected to provide an ideal platform in nano-theranostics by the generation of a new family of nanoformulations.[9] A large number of researches have focused on the development of using mesoporous silica nanoparticles (MSNs) for biomedical applications such as controlled/sustained drug delivery, biological imaging, biosensors and tissue engineering based on the attractive features of MSNs, e.g., large surface area, high pore volume, tunable pore sizes, abundant inner/outer surface chemistries and their intrinsic biocompatibility. In 2001, Vallet-Regí et al for the first time reported that MCM41-type mesoporous materials exhibited the sustained release profiles of a common anti-inflammatory drug (ibuprofen, IBU) encapsulated.[62] Until 2003, Lin et al introduced surface-modified MCM41-type MSNs into intracellular stimuli-responsive controlled release of vancomycin and adenosine triphosphate by using CdS NPs as the nanovalves and disulfide bond-reducing molecules as the release triggers.[63] Since then, the exploration of MSNs in nanobiotechnological and nanobiomedical areas have entered an era of fast development and become one of the hottest research frontiers, which was reflected by the exponential growth of scientific publications (**Figure 1**).

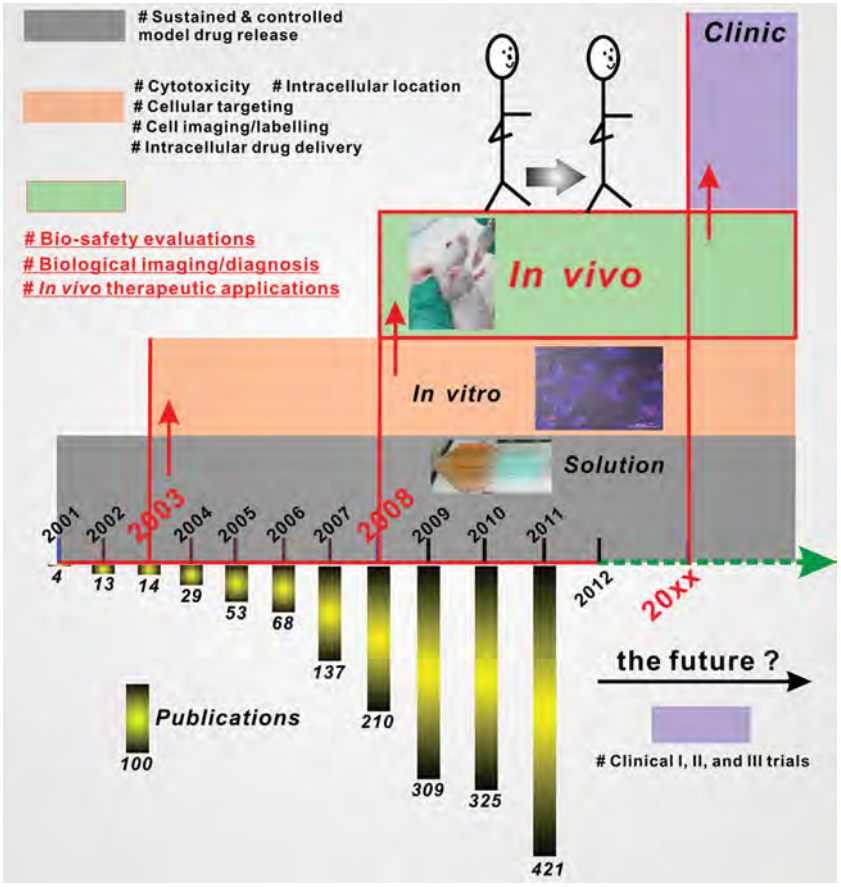

Figure 1. The timeline scheme for the development of MSNs-based nanobiomedical applications and the number of scientific publications each year ranging from year 2001 to 2011 on the nanomedical applications of MSNs (data obtained from ISI web of science in 2012).

A large number of MSNs-based NPs with largely varied compositions, structures and morphologies have been chemically designed and synthesized, which show very promising application prospects in nano-biomedicine due to their low cytotoxicity, enhanced therapeutic efficiency, excellent supports for CAs and good biocompatibility. The substantial progress of in vitro therapeutic outcomes of MSNs-based nanocarriers has been made recently by Brinker et al.[64] They designed a new type of multicomponent cargo by coating MSNs with a lipid bilayer to combine the properties of liposomes and nanoporous particles (**Figure 2**).[64] Targeting peptide (SP94) modifications endow them with a 10,000-fold greater affinity to human hepatocellular carcinoma than to hepatocytes, endothelial cells or immune cells. Further loading of therapeutic combinations (drugs, siRNA and toxins) and diagnostic agents (QDs) within MSNs can produce synergistic agents to kill the drug-resistant human hepatocellular carcinoma cells or imaging agents for cancer cell labeling. Such multifunctional MSNs-based DDSs represented a 10^6-fold in vitro improvement on the therapeutic efficiency over comparable liposomes.[64]

Although the well-established in vitro researches are consistent with the in vivo results in some respect, the in vivo evaluations always exhibit unexpected results due to the complicated physiological environment. For example, the opsonization of NPs in vivo, transportation of NPs in blood stream, enhanced permeability and retention (EPR) effect, etc., are difficult to imitate in vitro. Therefore, only when comprehensive in vivo assays on the bio-safety and therapeutic efficacy are demonstrated successfully and sufficiently, the clinical trials can then be permitted. In this respect, the in vivo assays of MSNs concerning bio-safety, diagnostic imaging and therapeutic efficiency were started only several years before in 2008 for promoting the translation of MSNs into preclinical stage (Figure 1).[65] Mou et al fabricated tumbler-like superparamagnetic (Fe_3O_4) and fluorescent (fluorescein isothiocyanate, FITC) MSNs (designated as Mag-Dye@MSNs) for cell labeling and small-animal MRI.[65] They also used MRI to assess the biodistributions of Mag-Dye@MSNs. Since then, great efforts have been devoted to boosting the in vivo assays of MSNs-based NPs, especially related to cancer diagnosis and treatment. Generally, two main issues should be concerned when MSNs are considered for in vivo cancer-related therapy. On the one hand, the types of tumor should be determined before designing MSNs because the heterogeneity among different tumors is very significant, leading to the differences in the vascularity, lymphatic drainage, and EPR effect thereby. In addition, the specificity of tumor cells for

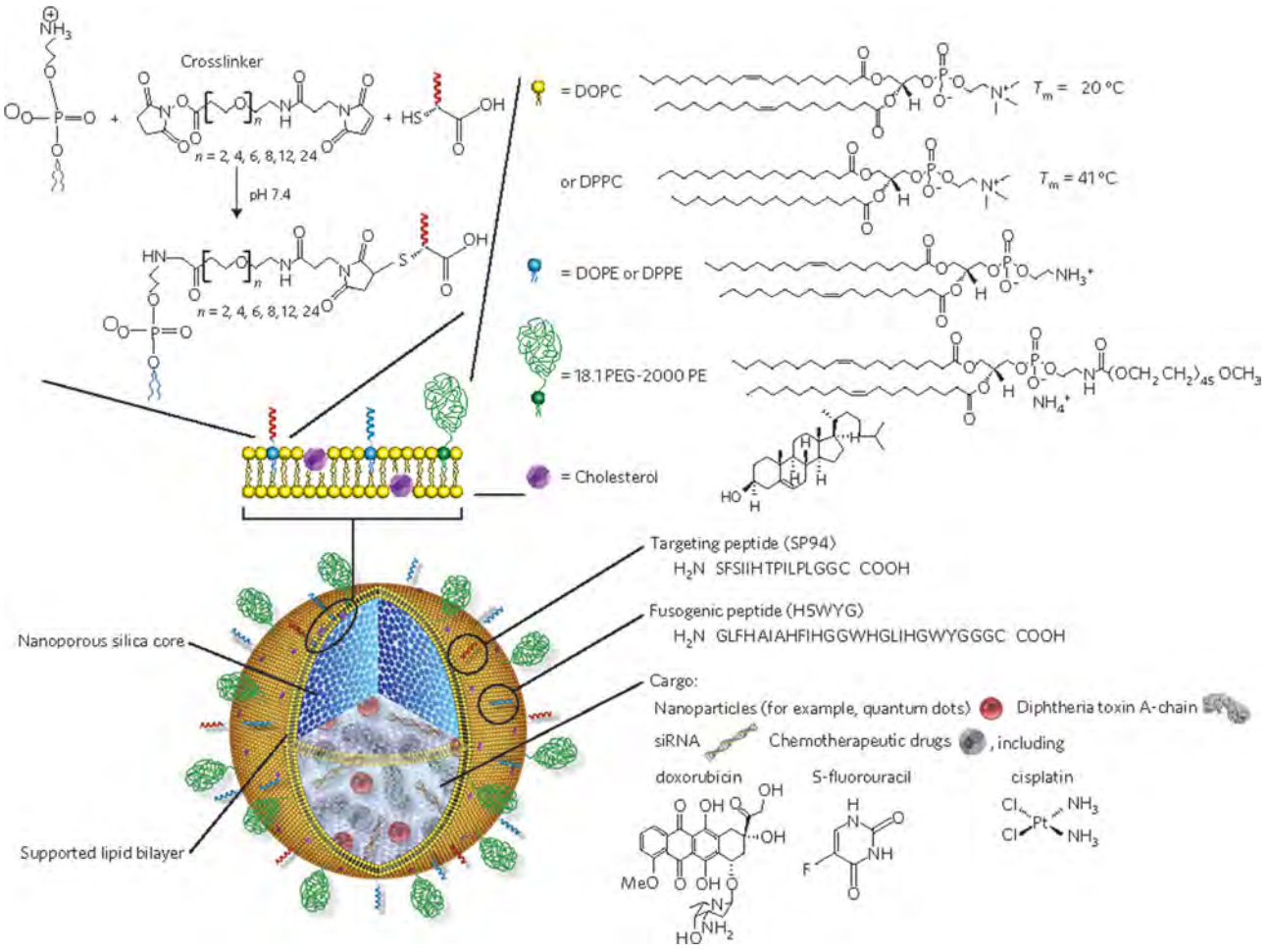

Figure 2. Schematic illustration of the nanoporous particle-supported lipid bilayer, depicting the disparate types of therapeutic and diagnostic agents that can be loaded within the nanoporous silica core, as well as the ligands that can be displayed on the surface of the supported lipid bilayer (SLB). Reproduced with permission.[64] Copyright 2011, Nature publishing group

cell-specific targeting is also highly dependent. However, if the type of tumors is unknown, the main and first issue is to precisely diagnose them at the early stage by designing efficient MSNs-based nanoprobes as CAs for molecular imaging. On the other hand, MSNs should be designed and synthesized elaborately to meet the strict physiological standards. For instance, MSNs with relatively large particle sizes are easily recognized and uptaken by mononuclear phagocytic cells in the reticuloendothelial system (RES) such as liver and spleen,[66,67] which can cause severe cytotoxicity to these organs and prevent the therapeutic agents from being efficiently delivered via MSNs to tumor tissues. The surface modifications of MSNs with biomacromolecules such as hydrophilic polyethylene glycol (PEG) derivatives can provide the effective steric hindrance to improve the particle dispersion in saline, interference in particle opsonization, increase the circulatory half-life, reduce the uptake of MSNs by RES as well as enhance the EPR effect.[67,68]

To date, there are four types of MSNs-based nanostructures being chemically designed and synthesized for bio-medical use, including traditional MSNs with small pores, large pore-sized MSNs, hollow MSNs and multifunctional MSNs-based composites (**Figure 3**A). Traditional MSNs (Figure 3A) are the best candidates for fundamental researches on their biological behaviors due to the mature synthetic protocols to obtain MSNs with high quality and repeatability. Small pore-sized MSNs are typically synthesized by hydrolysis and condensation of silicate alkoxides (e.g., tetraethyl orthosilicate) based on the sol-gel chemistry, by which the hydrolyzed silicate species were co-assembled with SDAs such as cetyltrimethylammonium bromide (CTAB), cetyltrimethylammonium chloride (CTAC) or octadecyltrimethoxysilane (CTMS). MSNs obtained using CTAB or CTMS as the SDAs usually possess relatively ordered pore arrays but their sizes are usually larger than 50 nm.[69–71] Comparatively. the particle sizes of MSNs obtained using CTAC as the SDAs and triethanolamine (TEA) as the base catalyst can be tailored to less than 50 nm, but the pores are disordered.[71–74] Large pore-sized MSNs (Figure 3B) are fabricated via the additional pore-expanding processes employing diverse pore-expanding agents (e.g., 1,3,5-trimethylbenzene, TMB) to meet the prerequisites for the encapsulation and delivery of large biomacromolecules such as siRNA and DNA.[75–78] Hollow MSNs (Figure 3C), typically

Adv. Mater. 2013,
DOI: 10.1002/adma.201205292

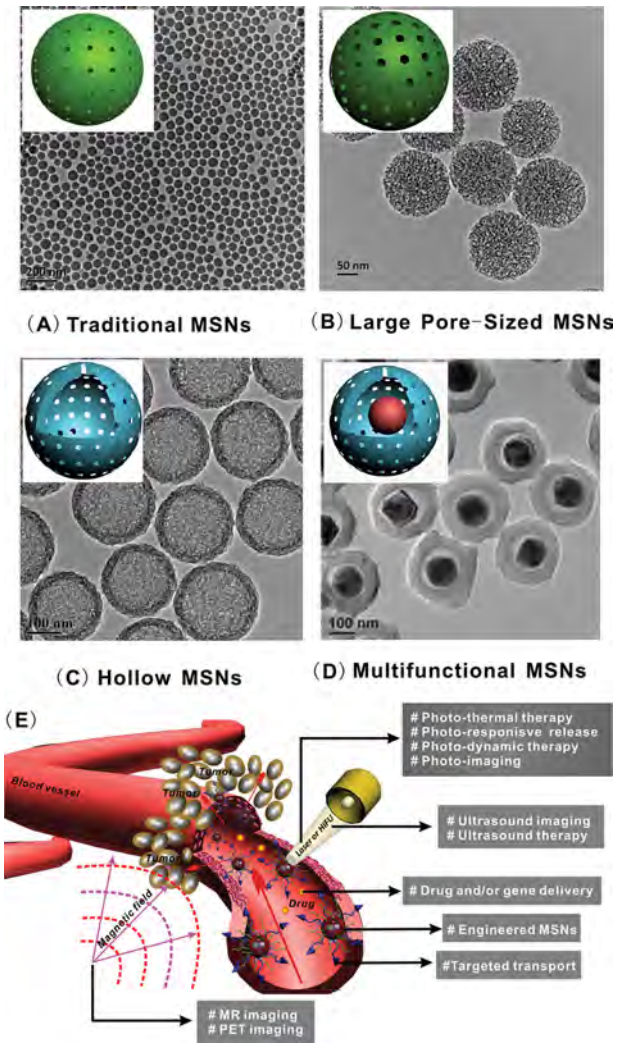

Figure 3. TEM images of four representative types of MSNs synthesized for biomedical applications, including traditional MSNs with small pore sizes (A), large pore-sized MSNs (B), hollow MSNs (C) and multifunctional MSNs (D). Insets in A-D are their corresponding structural schematics. (E) Schematic illustration of the transport of engineered MSNs in the blood vessel and their possible functions and options for the diagnostic and treatment of tumors.

synthesized via the soft-/hard-templating method,[71,79–81] can store much larger amounts of cargos than MSNs, thus the amounts of in vivo administrated carriers can be substantially reduced for improved bio-safety and/or reduced doses and dosing frequency. Multifunctional MSNs composites (Figure 3D) are elaborately designed for some special therapeutic modalities, such as magnetic hyperthermia therapy, photothermal therapy, photodynamic therapy, ultrasound therapy, especially in the theranostic field with diagnostic imaging capacities, such as optical, MR and/or PET imagings. These multifunctional MSNs (MMSNs) are typically synthesized by coating processes to deposit a mesoporous silica layer onto the surface of as-prepared functional nanocrystals (e.g., Fe_3O_4,[82–84] QDs,[85] Au,[86,87] upconversion NPs[88]), or by the modification processes to graft functional molecules (e.g., fluorescent[89,90] or paramagnetic tags[91,92]) or nanocrystals[93,94] into the mesopores, or anchoring procedures to link targeting ligands,[95–98] biomacromolecules[68] or nanocrystals[99] on their surface. Based on these four types of NPs, there have been many design options for MSNs to improve or optimize their pharmacokinetics, pharmacodynamics, biodistribution, excretion and delivery of therapeutic agents to tumors. The flexibility of MSNs as the platform for in vivo applications is illustrated in Figure 3E.

The extensive reports on MSNs-based DDSs for in vitro nanomedical applications have been summarized and discussed in several reviews by us[100] and other groups.[101–113] Alternatively, the scope of this comprehensive review covers the very recent progress on chemically engineered MSNs-based biomaterials for in vivo applications. Firstly, the summary of recent bio-safety evaluations of MSNs is provided to discuss their in vivo biodistribution, tolerance threshold, degradation, clearance and hematological/histological biocompatibility. Secondly, we highlight the very recent progresses in the researches of MSNs-based nanocarriers for in vivo therapeutic use. It is not restricted to the encapsulation and delivery of traditional anticancer drugs or siRNAs. Some special in vivo therapeutic modalities, such as photothermal/photodynamic therapy, ultrasound therapy, and even anti-bacteria in tissue engineering, are also involved. Thirdly, we review the chemical design of MMSNs for diagnostic imaging and further theranostic applications. Finally, we finish with a brief discussion on the critical issues and potential difficulties related to the chemical design/synthesis of MSNs by advanced nano-synthetic chemistry and subsequent in vivo assays in an attempt to further promote the translation of MSNs-based DDSs into clinical trials.

2. In Vivo Bio-Safety Evaluations

Silica-based materials are generally regarded biocompatible and suitable for in vivo use.[47,51,114] With the same compositions to traditional silica NPs, MSNs exhibit the well-defined mesostructures with high surface area and pore volume. Such structural characteristics would result in altered biological behaviors. For example, MSNs induced substantially lower hemolytic effect than non-porous silica NPs due to the decreased silanol density by the presence of mesopores.[115,116] In addition, MSNs exhibited higher accumulation in the lung than non-porous silica NPs due to the relatively large hydrodynamic size of MSNs in serum, which are caused by the enhanced inter-particle interaction of MSNs with high surface area and thereafter more likely to cause obstruction in vessels.[117] Although numerous in vitro results have demonstrated the low cytotoxicities of MSNs against different cell lines, our recent researches showed that the SDAs, especially ionic surfactants, could cause the severe cytotoxicities when they were not completely removed from MSNs by the traditional extraction.[66,118,119] We also demonstrated that PEGylation of MSNs could substantially improve the blood compatibility (e.g., much lowed hemolysis effect) of MSNs and reduce their non-specific binding to serum proteins.[68] These results give the direct evidences that the bio-behaviors of MSNs are strongly related to their preparation procedures,[118,119] particle sizes,[66] particle

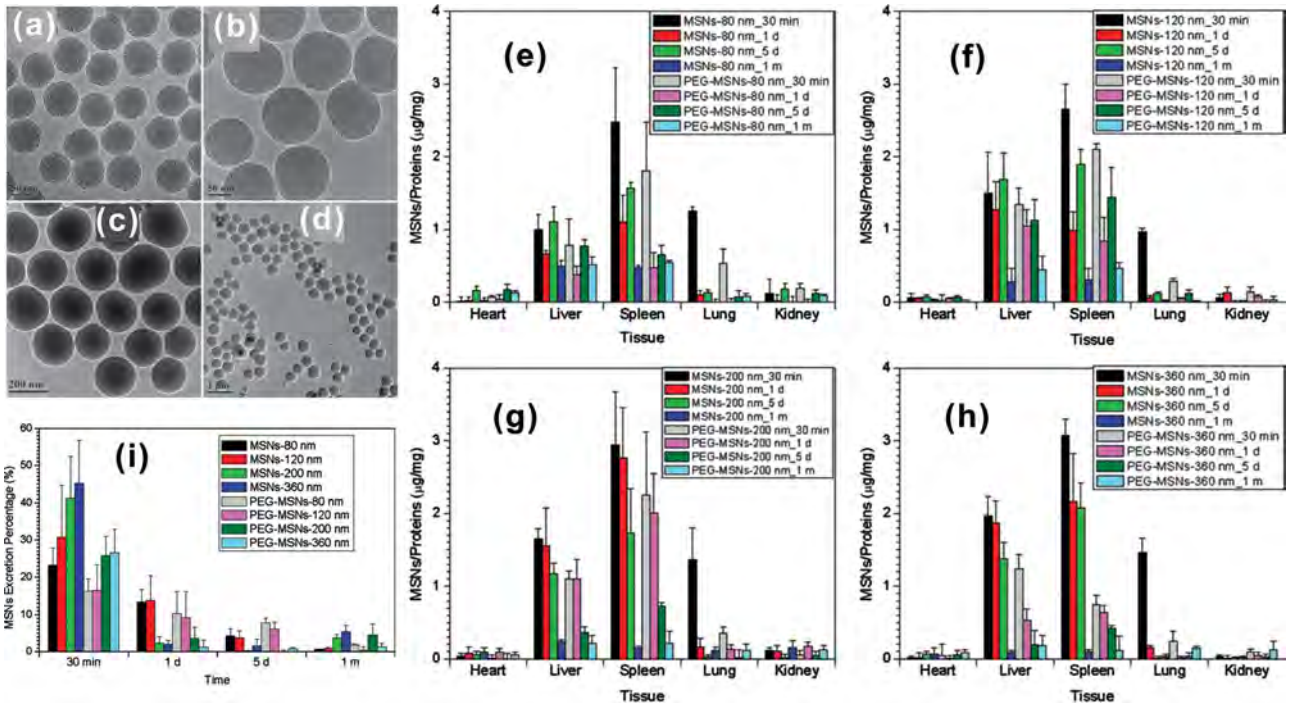

Figure 4. TEM images of PEGylated MSNs of different particle sizes: PEG-MSNs-80 (a), PEG-MSNs-120 (b), PEG-MSNs-200 (c) and PEG-MSNs-360 (d). Biodistribution amounts of MSNs and PEG-MSNs of particle sizes 80 (e), 120 (f), 200 (g) and 360 nm (h) in heart, liver, spleen, lung and kidney of ICR mice after tail intravenous injection for different time periods of 30 min, 1 day, 5 day, and 1 month. (i) Excretion percentages of degraded products of MSNs and PEG-MSNs of different particle sizes in urine up to 1 month after tail intravenous injection. Reproduced with permission.[66]

shape[120] and surface chemistries.[66] The in vitro studies have also demonstrated that the cell uptake of MSNs is cell-type-, dosage- and time-dependent.[103,109] Unfortunately, Tang et al recently reported that MSNs could promote the human malignant melanoma growth though MSNs themselves had no toxicity to human malignant melanoma, which was attributed to the decreased endogenous reactive oxygen species (ROS) in cells, upregulated anti-apoptotic molecules Bcl-2 expression and inhibited NF-κB activation.[121] However, Tamanoi et al found that blank MSNs did not affect tumor growth in mice using two human pancreatic cancer xenografts, PANC-1 and MiaPaCa-2, but the camptothecin-loaded MSNs showed the much enhanced tumor-suppression effect.[122] These results revealed that more extensive and detailed researches are necessary to obtain clearer and more accurate understanding on the in vivo bio-behaviors of MSNs, though the recent bio-safety evaluations of MSNs, such as dosing parameters, absorption, distribution, metabolism, excretion, etc., have revealed some respects of MSNs's bio-behaviors.

2.1. In Vivo Biodistribution and Tolerance Threshold of MSNs

The cargo-loaded MSNs are highly expected to target tumors to reach the desired therapeutic doses. In term of this, the accumulation of MSNs in the healthy tissues should be substantially reduced to ensure the maximum tumor accumulation and meanwhile to mitigate the side-effects because these accumulations are detrimental to healthy tissues. The optimized biodistributions of MSNs play a decisive role in achieving the desired therapeutic effects and reduced toxicities. However, the biodistributions of MSNs are strongly related to their size, shape and surface status, and the in vivo biodistribution assay was typically carried out either in the presence or absence of tumors. Mou et al for the first time reported the biodistribution of MSNs-based fluorescent, magnetic and porous NPs (Mag-Dye@MSNs) in ICR mice by direct MRI observations thanks to the T_2-weighted MRI (MRI-T_2) capability of magnetic cores.[65] The Mag-Dye@MSNs tended to accumulate in the liver and spleen, and a few in the kidney in 30 min post-injection,[65] and, these NPs were still detectable in up to 3 months, indicating that they were resistant to degradation and decomposition. We systematically investigated the biodistributions of MSNs of different particle sizes (**Figure 4**a–d, 80, 120, 200 and 360 nm) and their corresponding PEGylated counterparts (PEG-MSNs).[66] PEGylation was selected because it could reduce the opsonization of NPs in vivo, facilitate the escape of NPs from phagocytosis and increase the blood-circulation time.[123–125] MSNs and PEG-MSNs of different particle sizes were mainly accumulated in liver and spleen after tail intravenous injection due to the recognition and phagocytosis of MSNs by liver and spleen phagocytes, and a few MSNs were found in lung, kidney, and very few in heart (Figure 4e–h). The PEGylation could significantly prevent MSNs from being captured by liver, spleen and lung, thus the blood-circulation lifetime of PEG-MSNs was relatively longer. Both MSNs and PEG-MSNs of larger particle sizes

Adv. Mater. **2013**,
DOI: 10.1002/adma.201205292

were more easily captured by the organs. The time-dependence profiles of the MSNs' in vivo biodistribution are also affected by particle sizes and PEGylation, and correlated to the different capture features of various organs and the in vivo degradation behaviors. This study further revealed that the PEG-MSNs of smaller particle size escaped more easily from the capture by liver, spleen and lung tissues, possessed longer blood-circulation lifetime, and were more slowly biodegraded and consequently had a lower excreted rates (Figure 4i).[66]

The influence of geometric feature on the biodistribution, clearance and biocompatibility was investigated by adopting MSNs with varied aspect ratios (ARs) through the easy morphological tailoring of MSNs.[117,120,126] It was found that short-rod MSNs mainly accumulated in the liver, but long-rod MSNs were more easily trapped in the spleen.[120] After PEGylation, the content of MSNs in lung increased. The effect of geometry of MSNs on biocompatibility, such as hematology, serum chemistry and histopathology, was not apparent. Although no apparent toxicity was observed under experimental doses, the potential glomerular filtration dysfunction was indicated.[120] Ghandehari et al found that amine-modified MSNs with high ARs were still captured mainly by liver and spleen due to the passive entrapment in the discontinuous openings in the endothelium of liver and spleen or in the pulmonary capillaries.[117] Comparatively, MSNs with high ARs showed the enhanced lung accumulation compared to amine-modified MSNs with such a spherical morphology.[117] To enhance the accumulation of MSNs to tumors, Zink et al chose polyethylene imine-polyethylene glycol (PEI-PEG) copolymers to modify the surface of 50 nm-sized MSNs,[67] thus the opsonization of MSNs could be reduced, which led to the enhanced passive accumulation of NPs within tumors. They compared three types of MSNs with different surface modifications: NP1 with phosphonate modification, NP2 with 5kD PEGylation and NP3 with PEI-PEG coating. NP1 was mainly captured by liver and spleen while NP2 exhibited less prominent liver uptake. The prominent particle uptake in tumor tissue was found in NP3 due to the enhanced EPR effect by PEI-PEG modification. There results indicate that biodistributions of MSNs can be optimized by choosing adequate particle sizes, geometries and surface engineering protocols.

Zink et al investigated the maximum tolerated dose of fluorescent MSNs (FMSNs) via intravenous administration into female nude mice with the dosage ranging from 10 mg/kg to 200 mg/kg, once per day for 10 d.[127] They found that all mice were healthy but the mice treated with FMSNs higher than 100 mg/kg showed mild elevation of liver transaminase aspartate aminotransferase (AST). Long-term toxicity evaluations using healthy nude mice with the dose of 1 mg mouse^{-1}d^{-1} showed that no unusual responses or behaviors could be found during a 2 month period. The fluorescence and inductively coupled plasma optical emission spectrometry (ICP-OES) results confirmed the renal excretion of MSNs. However, Ghandehari et al reported that the maximum tolerated dose (MTD) of MSNs was only 30 mg/kg on female CD-1 mice. Above MTD, the major affected organ was kidney and lung.[126] The toxicity was alleviated using surface modifications of MSNs by primary amine groups (MTD = 150 mg/kg). By the blood chemistry analysis, it was found that the blood urea nitrogen level and creatinine concentration increased significantly, suggesting that kidney was the target organ of intravenous toxicity of MSNs, and such an effect was irrespective of geometrical features or surface characteristics. Additionally, the surface area and surface characteristics play crucial roles in determining their biological activity. It was also found that the MTD of Stöber-based non-porous silica NPs was about 450 mg/kg, significant higher than MSNs (30 mg/kg).[126] Hudson et al reported that intraperitoneal or intravenous administration of 1.2 g/kg MSNs is lethal to SV 129 mice but is safe when reduced to 40 mg/kg.[128] For MSNs with hollow interiors, Tang et al reported that the lethal dose 50 (LD_{50}) of 110 nm rattle-type MSNs (RMSNs) was higher than 1000 mg/kg after single dose administration, and no death was observed by repeated administration of RMSNs at the dose of 80 mg/kg for 14 days.[129] The biodistribution tests revealed that HMSNs mainly accumulated in liver and spleen with abundant mononuclear phagocytic cells. Importantly, the introduced RMSNs could be excreted from the body, but the entire clearance time duration was over 4 weeks. It was also suggested that the major adverse reaction above MTDs was caused by the mechanical obstruction of MSNs in the vasculature, which could lead to congestion in major organs to induce the organ failure.[126]

2.2. In Vivo Degradation and Clearance of MSNs

MSNs have been proposed to be used for in vivo diagnosis and therapy of diseases recently. Therefore, their biodegradation and biodissolution behaviors must be taken into serious account. Bein et al investigated the influence of different surface functionalities on the biodegradation of MSNs.[130] They chose unfunctionalized, phenyl-, chloropropyl-, aminopropyl- and PEG-functionalized MSNs for in vitro simulated body fluids (SBF) evaluations. The small particle sizes (50–70 nm), the low condensation degrees, the highly mesoporous texture (pore of 3–4 nm) and high surface area can accelerate the surface reactions. The phenyl-functionalized MSNs exhibited the fastest degradation kinetics while the PEGylated MSNs had the lowest degradation rate. The formation of hydroxyapatite on the surface of MSNs was also observed. We found that the degradation of surfactant-extracted MCM41-type MSNs exhibited the three-stage degradation behavior in SBF.[131] MSNs were firstly degraded very fast on hour-scale (within 2 h), followed by the decelerated degradation stage due to the formation of calcium/magnesium silicate layer on the surface of MSNs. Finally, MSNs maintained the slow degradation in the third stage on day-scale. It should be pointed out that only these MSNs without high temperature treatment (e.g., calcination for surfactant removal) demonstrated fast and three stage degradation behavior in SBF in about two weeks of immersion in SBF, those experienced high temperature treatment can be hardly degraded in two weeks and are not featured with such a three stage degradation behavior. The incomplete -Si-O- tetrahedral network in the framework of MSNs without high temperature treatment, in which plenty of Si-R and/or Si-OH groups are present, is believed to be responsible for their easy degradation. We also showed that the bio-degraded byproducts (e.g., monomeric silicic acid and polysilicic acids) from MSNs

are non-toxic to different cell lines.[119] Very recently, Kuroda et al investigated the degradation behaviors of MSNs by dialysis process in SBF.[132] The dialysis process could exclude the dissolved silica continuously to reduce the redeposition of dissolved silica. They found that the degradation of MSNs was independent of the particle diameter, while the total specific surface area dominated the degradation process. By immersing MSNs in SBF for varied time intervals, it was found that the degradation proceeded from the outer surfaces of particles and simultaneous from inner cores. However, this degradation process was not homogeneous, but heterogeneous. Kuroda et al compared the degradation rates of organic group-bridged silsesquioxane frameworks with traditional MSNs featured with pure Si-O-Si frameworks in phosphate buffered solution (PBS) solution.[116] The ethenylene-bridged silsesquioxane framework showed extremely high hydrolysis resistance under aqueous conditions compared to traditional MSNs.

The well-defined porous structures and corresponding large surface area of MSNs are quite beneficial for accelerating the degradation of MSNs. However, the chemical stability of MSNs is generally higher than that of organic DDSs, which leaves a big bio-safety issue for their in vivo translations. The biological effect of undegraded MSNs remained in vivo for a relatively long period is still unknown. Additionally, the in vitro degradation results performed in PBS or SBF are in many cases not applicable to the in vivo bio-behaviors. Thus, it is very important to determine the biodegradation behaviors of MSNs in vivo. However, such a in vivo degradation assay will encounter several technological obstacles. Firstly, it is difficult to *in-situ* detect the complex degradation process of MSNs in vivo. Secondly, the in vivo presence of both degraded species of MSNs and intrinsic silicate species makes it difficult to distinguish the exact amount of degraded products from the total detected amount. To date, no systematic in vivo results about the degradation process of MSNs have been reported. It should be noted that the excretion of MSNs does not mean the degradation.

For in vivo clearance, we found that both MSNs and PEG-MSNs could be excreted through urinary system of mice due to their in vivo degradation.[66] In 30 min post-administration, a number of silica degradation products were excreted from urine, and MSNs with larger particle sizes excreted faster than smaller ones. Almost 15–45% of the total injected amount of MSNs with different particle sizes and PEGylation could be cleared in only 30 min post-injection. The excretion of MSNs in vivo is strongly dependent on their surface charge. Lo et al synthesized MSNs with highly positive charge and grafted near-infrared fluorescent indocyanine green (ICG) to trace the extraction of MSNs.[133] By using in vivo fluorescence imaging and ICP test of harvested tissues, urine and feces, it was found that MSNs with highly positive charge (+34.4 mV at pH 7.4) were quickly excreted from the liver into the gastrointestinal tract and eliminated via feces subsequently, while less charged MSNs (–17.6 mV at pH 7.4) remained within the liver, which was attributed to the charge-dependent adsorption of serum proteins to facilitate the hepatobiliary excretion of MSNs. The morphology does influence the excretion behaviors of MSNs. It was found that the excretions of MSNs with different ARs were mainly by urine and feces, but comparatively, short-rod MSNs showed a more fast extraction than long-rod ones.[120] By using TEM observations, Tamanoi et al found that MSNs with intact structures and morphologies could be excreted through urine without obvious breakdown or degradation,[122] which is in consistence with Lo's observations.[133] According to Kuroda's in vitro research, the degradation of MSNs proceeds from the outer surfaces and inner cores simultaneously but heterogeneously.[132] The initial particle morphology remains almost intact after degradation to a low extent, thus they can be found in urine by TEM. It is surprising that MSNs can be excreted through urine because it is generally accepted that only NPs with the particle sizes of less than 5.5 nm can be cleared through kidney.[134] Obviously, these MSNs are all beyond this size limit. Therefore, the exact urine process still remains unclear in this case. According to the degradation results,[130–132] the excreted products of MSNs are composed of two parts: silicate species from degraded MSNs with small sizes which can be easily cleared via urine, and intact MSNs after degradation which also can be excreted via urine. Tang et al found that the administration of MSNs caused the dysfunctions of biliary excretion and glomerular filtration, which might be the reason of the excretion of MSNs with such large particle sizes by urine.[120,121]

A series of in vivo experiments have demonstrated that MSNs can be excreted through renal and hepatic routes in the form of urines and feces containing either solid NPs or degraded products, and the renal clearance was the major route. The physicochemical properties of MSNs, such as particle sizes, morphologies and surface charges, affect the clearance routes and rates. However, a major issue that should be considered is that the specific quantitative results of the biodistribution and clearance of MSNs were obtained by either fluorescence intensity or the ICP result of Si amount. However, the fluorescence of MSNs may suffer from quenching after being administrated into mice or interference by the background fluorescence signals. In addition, the quantitative tests of Si amount by ICP may become inaccurate due to the intrinsic in vivo Si background. These semi-quantitative methods may lead to the error of experimental results. Thus, more accurate quantitative methods are highly needed to give the more reliable information of biodistributions, degradation routes and excretion of MSNs in vivo.

2.3. In Vivo Hematological and Histological Biocompatibility of MSNs

MSNs are supposed to be administrated intravenously, by which MSNs may interact with the blood components. Consequently, their hematological biocompatibility determines their administration routes. The surface chemistry of MSNs has the most important effect on the hemolysis of MSNs against red blood cells (RBCs). Lin et al found that the mesostructures of MSNs decreased the silanol density compared to non-porous silica NPs.[115] Thus, the hemolytic effect could be substantially reduced because of the reduction in the interactions between negatively charged MSNs and positively charged trimethylammonium groups of the membrane lipid of RBCs.[115,135] PEGylation could further improve the hemocompatibility of MSNs.[68,135] Recently, Kuroda et al synthesized aqueous colloidal mesoporous NPs with ethenylene-bridged silsesquioxane frameworks.[116] The presence

Adv. Mater. **2013**,
DOI: 10.1002/adma.201205292

of ethenylene groups on the surface of MSNs showed lower hemolytic activity against RBCs than traditional colloidal MSNs, which provides an alternative route to improve the hemocompatibility of MSNs by molecularly integrated organic-inorganic hybridization. Tang et al tested the in vivo effect of differently shaped and PEGylated MSNs on blood, hematology and serum biochemical indicators in 1 day and 18 days after the intravenous administration of MSNs.[120] All hematology marker values, such as RBC, HGB, HCT, MCV, MCH, MCHC, PLT and WBC, were mostly within the normal ranges and did not show significant trends of toxicity of all tested samples, indicating the excellent biocompatibility in hematology.

We found that MSNs and PEG-MSNs do not cause the significant tissue toxicity and inflammation in one month in vivo.[66] Tang et al investigated the tissue toxicity of MSNs with different shapes and PEGylation.[104] It was found that the introduced MSNs could induce the dysfunction of biliary excretion and glomerular filtration by testing representative serum biochemical indicators,[120] but the histological assessment of major tissues did not indicate significant tissue damage, inflammation or lesion. The cytotoxicity of MSNs was also found to be dependent on the administration modes. Kohane et al found that subcutaneous injection of MSNs of different particle sizes (150 nm, 800 nm and 4 μm) showed good biocompatibility at all time points, while the intraperitoneal and intravenous administrations in mice resulted in death or euthanasia.[128] Histological assay indicated that the death might be due to the thrombosis. Tang et al found that rattle-type MSNs had no apparant toxicity in any of organs at the dose of 20 mg/kg. However, the lymphocytic infiltration and microgranulation of hepatocytes in the liver were observed at the doses of 40 and 80 mg/kg while the spleen, kidney and lung were not influenced,[129] indicating that the administration of such NPs could induce the liver injury at high doses.[136] After intraperitoneal injection of RMSNs at the doses of 10, 25 and 50 mg/kg twice a week for 6 weeks, blood biochemistry assays and proinflammatory cytokine measurements revealed that the liver injury markers in serum, such as alanine aminotransferase (ALT), inflammatory cytokines interleukin-1 beta (1L-1β) and tumor necrosis factor-alpha (TNF-α), increased significantly at 50 mg/kg. The activated kupffer cells (KCs) played a key role in the liver damage caused by introduction of RMSNs, which was similar to alveolar macrophage in the process of silicosis.

Based on above mentioned bio-safety evaluations, it can be concluded that the in vivo bio-behaviors of MSNs, such as the biodistributions, biodegradations, possible excretion paths, tolerate thresholds and hematological/histological biocompatibilities, are strongly related to their synthetic processes, particle sizes, morphologies, surface modifications, doses and even administration routes. Although extensive bio-safety assays have been carried out to give the confidence of clinical translation of MSNs, there are still many unanswered questions regarding their in vivo behaviors. For example, the thorough understanding of some specific issues, such as neurotoxicity, brain toxicity and reproductive toxicity, still remains unknown. More importantly, the long term in vivo bio-safety issue for up to one year, for example, must be addressed seriously for future clinical translation, not only in small animals such as mice and rabbits, but also in big mammals such as dogs or pigs. However and encouragingly, the rapid progress of the related knowledge on in vivo bio-behaviors will, without doubt, promote the future clinical translations of MSNs-based biomaterials.

3. In Vivo Therapeutic Applications of MSNs

A series of bio-safety assays have provided a large amount of evidences that MSNs are highly biocompatible in vivo at the desirable dosage, and they can be degraded in vivo and extracted from the body through the urine and feces afterwards.[137] Based on the excellent biocompatibility and unique structural characteristics for drug delivery, MSNs are expected to be among the ideal candidates as the DDSs for transporting various guest cargos, such as anticancer drug for chemotherapy, siRNA delivery for gene therapy, photosensitizers for photodynamic therapy, precious metals for photo-thermal therapy, magnetic nanoparticles for hyperthermia and fluorocarbon compounds for ultrasound therapy (**Table 1**). Specially, MSNs can be used in oral drug delivery and tissue engineering. A great number of successful in vitro therapeutic demonstrations have been made which will promote the applications of MSNs into small-animal disease models, especially for cancer therapy.

However, the successful in vitro therapeutic results can not warrant the same in vivo effect because the in vivo therapeutic use needs more strict compositional, structural and morphological modulations to meet the complicated physiological environment, and the bio-performances of MSNs are usually compromised due to the unwanted phenomena in such complex physiological environment. For example, to enhance the accumulation of drug-loaded MSNs within tumor tissues, particle size distributions and surface modifications of MSNs should be optimized to increase the blood circulation half-life time and decrease the uptake by RES. In addition, the administration route, whether systemic, oral, intraperitoneal, or subcutaneous, is equally important.

3.1. In vivo Drug & siRNA Delivery

Tamanoi et al conjugated folic acid (FA) onto the surface of MSNs for in vivo tumor targeting (**Figure 5**a).[127] Non-targeted MSNs could accumulate into tumors via the EPR effect while the folate-receptor-targeting conjugation further promoted the tumor accumulation of MSNs to some extents. No acute toxicity was observed after the injection of MSNs into mice as indicated by the similar body weight evolution compared to the control (Figure 5a_1). The tumor growth inhibition results showed that camptothecin (CPT)-loaded MSNs induced faster tumor-shrinkage compared to that by the free drug (Figure 5a_2 and a_3). Comparatively, CPT-loaded targeting FA-MSNs only showed a slight and insignificant increase in the tumor-suppressing effect (Figure 5a_2). The major reason might be due to the low expression of folate receptor of the MCF-7 tumor xenografts investigated. Furthermore, the same group tested the effectiveness of CPT-loaded MSNs against two different human pancreatic cancer xenografts, PANC-1 and MiaPaCa-2. Significant tumor growth suppressing could be achieved by MSNs-mediated CPT delivery. The complete elimination of tumor was found after the treatment with CPT-loaded

Table 1. Summary of representative in vivo therapeutic applications using MSNs-based NPs.

MSNs type	Surface modifications	Particle size (nm)	Loaded drugs	Administrati-on mode	Animal models	Performance	Ref.
MSNs	FA	100–130	CPT	Intraperitoneal injection	Nude mice xenograft of human breast cancer MCF-7	Enhanced tumor growth inhibition/no obvious targeting effect	[127]
MSNs	PEI-PEG	50	DOX	Intravenous injection	Nude mice xenograft of human squamous carcinoma xenograft KB-31	Enhanced rate of tumor shrinking	[67]
MSNs	FA	100–130	CPT	Intraperitoneal injection	Nude mice xenograft of human pancreatic cancer MiaPaca-2 and PANC-1 in SCID mice	Enhanced rate of tumor shrinking/significant targeting efficiency/reduced side-effects	[122]
Rattle-type MSNs	PEG	152	Dtxl	Intravenous injection	ICR female mice xenograft of marine hepatocarcinoma 22 subcutaneous model	15% enhanced tumor inhibition rate via RMSNs as DDSs	[146]
Rattle-type MSNs	FA	131	DOX	Intravenous injection	Nude mice of human cervical carcinoma HeLa cells	Enhanced rate of tumor shrinking/significant targeting efficiency	[147]
Rattle-type MSNs	Monoclonal CD73 or CD90 antibody	152.9	DOX	Intratumor injection	Male nude mice with subcutaneous U251 xenografts	Enhanced drug retention and tissue penetration in tumor tissues/enhanced cell apoptosis	[138]
HMSNs	PEG	44 ± 2	DOX	Intravenous injection	ICR female mice of liver cancer Hep-A-22	Enhanced tumor growth inhibition	[149]
MSNs MSMs	/	< 100 (MSNs)	TEL	Oral administration	Beagle dogs	The relative bioavailability: MSNs/154.4 ± 28.4%; MSMs/129.1 ± 15.6%	[150]
pGSNs	PEG	159	Doc	Intravenous injection	ICR mice of H22 subcutaneous model	Enhanced rate of tumor shrinking/reduced toxicity of drugs	[185]
pGSNs-Tf	PEG and Tf	185	Doc	Intravenous injection	MCF-7 tumor-bearing BALA/c nude mouse	Enhanced rate of tumor shrinking/enhanced and special targeting effect	[184]
MSNs	Mannose derivative	118	PS	Intravenous injection	Nude mice bearing HCT-116 xenografts	Enhanced rate of tumor shrinking and reduced macrometastasis	[189]
MSNs	Rotaxane	60	Curcumin	Local brain injection	Zebrafish larvae	Excellent photothermal drug release behaviors	[155]
MSNs	MMP-sensitive polymer layer	94	DOX	Intratumor injection	Human sarcoma (HT-1080) xenografts in immune-compromised nude mice	Protease-responsive DOX release in vivo	[156]
MSNs	PEG	200	siVEGF	Intratumor injection	Nude mice of MDA-MB-23 xenografts	Effective gene therapy/ enhanced rate of tumor shrinking	[78]
HMSNs	/	300	PFH	Intravenous injection	Rabbits with VX2 liver tumors	Enhanced damage of tumor tissues	[191]
MCNCs	/	342	PFH	Intravenous injection	Rabbits with VX2 liver tumors	Enhanced damage of tumor tissues	[15]
MSNs	/	400	INH & RFP	Local implantation	New Zealand rabbits with bone defect	Long term and sustained in vivo drug release	[197]
Fe_3O_4@mSiO_2	PEG	70	DOX	Intravenous injection	Nude mice bearing MCF-7 tumors	Simultaneous MR and fluorescent imaging, and enhanced DOX accumulation	[99]
Fe3O4@SiO2@ NaYF4/Yb, Er	/	115	DOX	Intravenous injection	Nude mice bearing H22 tumors	Enhanced rate of tumor shrinking	[242]

Adv. Mater. **2013**,
DOI: 10.1002/adma.201205292

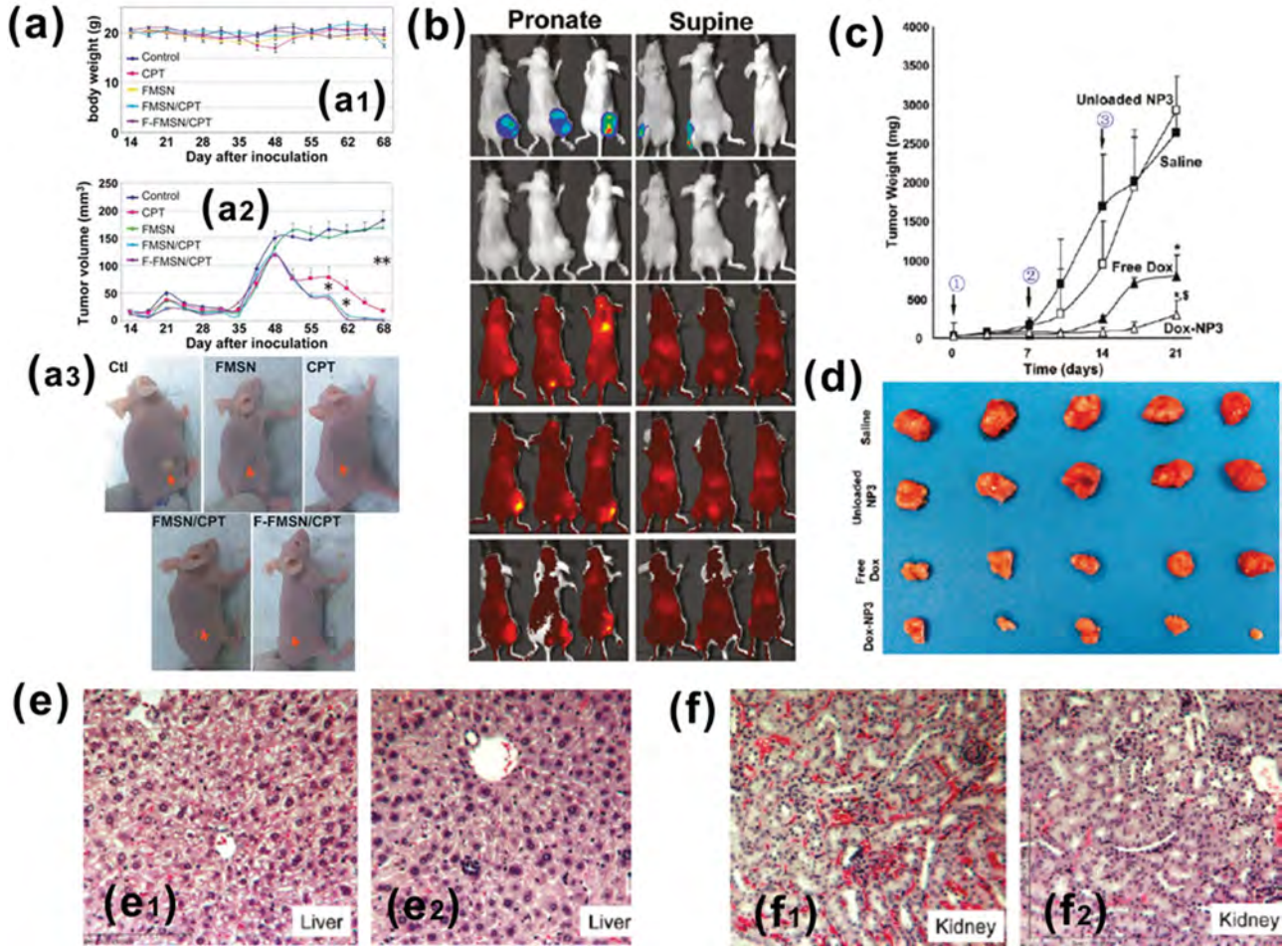

Figure 5. (a) Antitumor effects of CPT-load MSNs: average body weights of treated mice (a_1), average tumor volumes (a_2) and representative images of mice from differently treated groups (a_3); Reproduced with permission.[127] Biodistribution of NIR dye-labeled MSNs to the KB-31-luc tumor xenograft in nude mice (left: PEGylated MSNs and right: PEI-PEG grafted MSNs); (c, d) Tumor growth inhibition rate (c) and photograph (d) of the tumor tissue of tumor-bearing nude mice after the treatment of DOX-loaded MSNs, pure MSNs, free DOX and saline; (e, f) Histological analyses of liver (e, e_1: free DOX and e_2: DOX-MSNs) and kidney (f, f_1: free DOX and f_2: DOX-MSNs). Reproduced with permission.[67] Copyright 2011, American Chemical Society.

MSNs.[122] Recently, Zink et al decorated the surface of MSNs with PEI-PEG to dramatically enhance the EPR effect for passively targeted drug delivery.[67] More MSNs could accumulate into the tumor by the administration of PEI-PEG grafted MSNs compared to injection of PEGylated MSNs (Figure 5b). A more significant tumor shrinkage and apoptosis were induced compared to those by the free doxorubicin (DOX) drug (Figure 5c and d), and dramatically improved safety profile of systemic drug delivery was achieved as well, as indicated by less damaged liver (Figure 5e) and kidney (Figure 5f). The accumulation of MSNs caused by EPR effect was around 12% after 72 h post-administration, and DOX-loaded PEI-PEG-MSNs could inhibit 85% tumor growth compared to 70% inhibition by the free DOX drugs.

Compared to traditional MSNs, hollow MSNs (HMSNs) or rattle-type MSNs (RMSNs) with large hollow interiors exhibit extraordinarily enhanced drug loading capacity due to the contributions of interstitial hollow space, which leaves much more rooms for drug molecules, while their well-defined mesoporous shell provides the diffusion pathways for guest molecules. The high drug loading capacity can simultaneously reduce carrier amounts used and the dosing frequency. In this respect, their bio-safety would be higher than traditional MSNs. Our group has developed several synthetic routes towards the construction of hollow nanostructures of MSNs, which mainly based on the traditional soft-/hard-templating protocols.[71,79,138–144] The fabricated HMSNs showed the high loading capacity for hydrophobic IBU,[140,142] hydrophobic CPT,[32] hydrophilic DOX[71] and siRNA.[145] Using HMSNs as the matrix, we have demonstrated the new concepts of "inorganic nanoemulsion" and "inorganic nanoliposome" to realize the functions of representative OMSs while preserving the advantages of IMSs.[32] As shown in **Figure 6**a and b, the large hollow interiors of HMSNs can function as the reservoir for hydrophobic agents, similar to the function of organic nanoemulsion to encapsulate water-insoluble agents. In addition, the well-defined hydrophilic

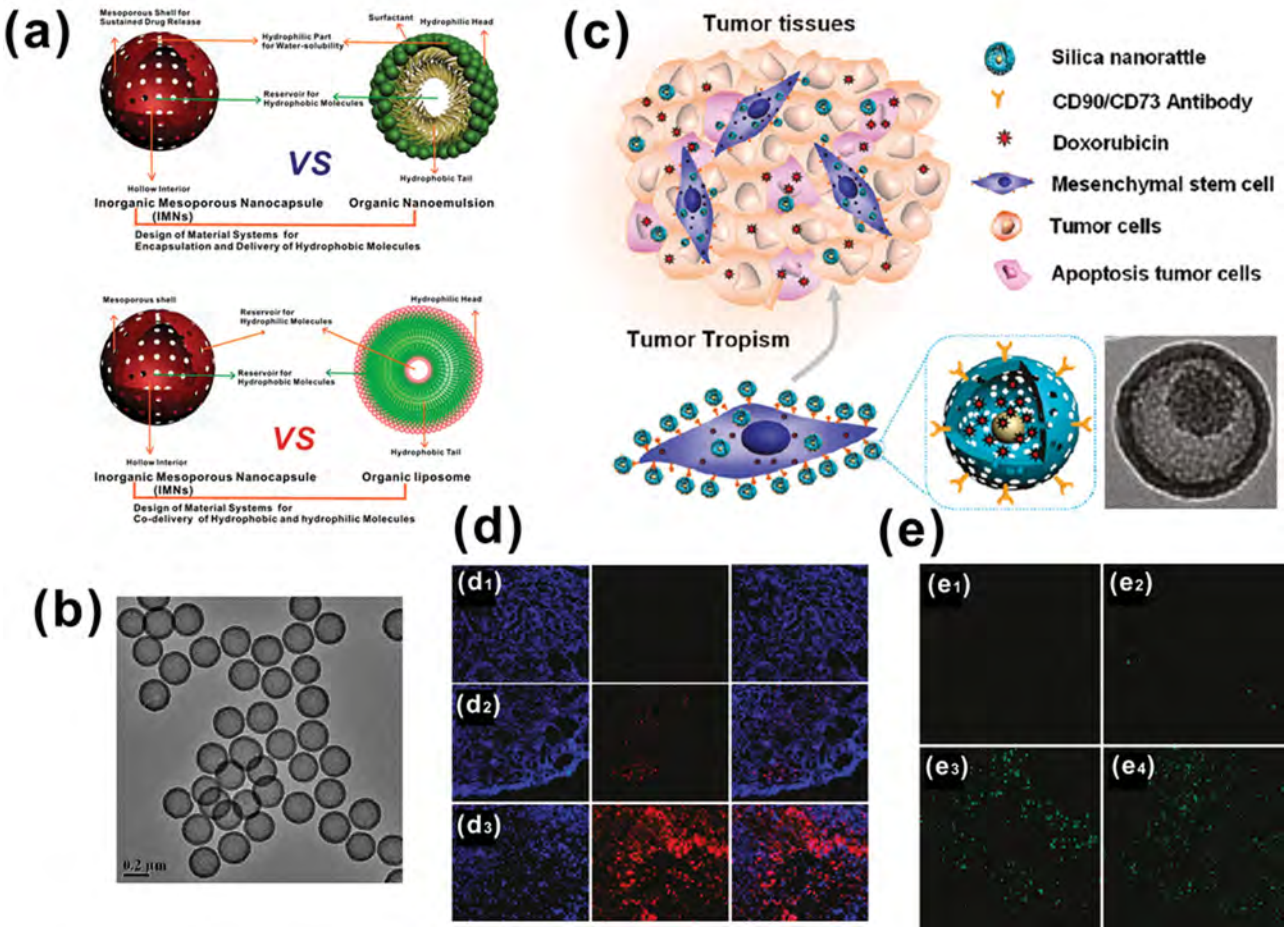

Figure 6. (a) Strutural comparison between HMSNs and organic nanoemulsions for the delivery of hydrophobic drugs (upper image), and structural similarity between HMSNs and organic nanoliposomes for the co-delivery of hydrophilic and hydrophobic drugs (down image); (b) Typical TEM image of HMSNs; Reproduced with permission.[32] (c) Scheme of silica nanorattle (SN)-DOX-anchored MSCs for tumor-tropic therapy; (d) Fluorescent microscopy images of tumor tissue sections in 7 d post intratumor injetion of (d_1) free DOX, (d_2) SN-DOX and (d_3) MSC-SN-Ab(CD90)-DOX (The blue fluorescence showed the nuclear staining with DAPI, and red fluorescence represented the location of DOX); (e) TUNEL staining assay showing the apoptosis and cell death treated by (e_1) control, (e_2) free DOX, (e_3) SN-DOX and (e_4) MSC-SN-Ab(CD90)-DOX in 7 day post intratumor injection. Reproduced with permission.[138] Copyright 2011, American Chemical Society.

mesopores within the shell can encapsulate hydrophilic agents to realize the co-loading of hydrophobic and hydrophilic agents simultaneously, similar to the functions of organic nanoliposome. The co-loading of dual drugs in one matrix can restore the anti-proliferative effect of drugs to circumvent the multidrug resistance (MDR) of cancer cells.[32] The in vivo research on the pharmacokinetics of MSNs with hollow interiors was carried out by Tang's group.[146] They firstly employed RMSNs as the carriers for docetaxel (Dtxl).[146] The Dtxl-loading amount on RMSNs could reach as high as 32% (48 mg Dtxl/100 mg RMSNs) due to the contribution of hollow cavity. After PEGylation, the Dtxl-RMSNs could accumulate within tumors to inhibit the tumor growth via EPR effect. The inhibition rate of tumor growth reached 72% while the free Taxotere only inhibited the tumor growth by about 57%. The sustained release of Dtxl from RMSNs continuously killed the cancer cells while the free Taxotere was easily metabolized from body. As another benefit, the delivery of Dtxl via RMSNs substantially mitigated the systemic toxicity of free drugs as indicated by the results of normal body-weight growth, hematological/histological analysis and liver function tests. Further FA modifications of RMSNs promoted the actively targeting delivery of DOX. The same high therapeutic efficiency and reduced systemic toxicity were also achieved by using FA-conjugated RMSNs for the in vivo transport of DOX.[147] We recently modified the surface of rattle-type multifunctional Fe_3O_4@mSiO_2 NPs by FA for efficient targeted anticancer drug delivery and simultaneously biological imaging.[148] In addition, the magnetic nanorattles could be transported to the designated organs under an external magnetic field, implying that these special multifunctional DDSs possess molecularly and magnetically double-targeted drug transport capabilities.

By binding monoclonal CD73 or CD90 antibody-conjugated RMSNs with mesenchymal stem cells (MSCs), the laden MSCs could actively find and migrate to solid tumor tissues to achieve the targeted drug delivery using RMSNs (Figure 6c).[138] The

Adv. Mater. 2013,
DOI: 10.1002/adma.201205292

loaded cargos could be released upon arriving at tumors. The cytotoxicity assay revealed that this anchored RMSNs-based DDSs did not compromise the key cellular function and caused the apparent cytotoxicity. The in vivo cancer homing effects of laden MSCs was examined by using DOX as the anticancer agent and subcutaneous U251 xenografts in male nude mice as the disease model. The retention and tissue penetration ability of free DOX, DOX-loaded RMSNs and DOX-RMSNs in MSCs were examined after intratumor administration. Interestingly, the free DOX (Figure 6d$_1$) and DOX-loaded RMSNs (Figure 6d$_2$) within tumors exhibited decreased red fluorescence and shrunken distribution area of DOX, while the DOX-RMSNs in MSCs (Figure 6d$_3$) still remained high level and broad distribution of DOX within tumor tissue, which was considered to be associated with tumor-tropic migration properties of MSCs including targeting the tumor hypoxic area. The cancer cell apoptosis assay using a terminal deoxynucleotidyl transferase dUTP nick end labeling (TUNEL) analysis (Figure 6e) showed that DOX-RMSNs in MSCs caused the highest cell apoptosis due to the enhanced DOX retention and penetration effect caused by MSCs. However, as a matter of fact, the solid core part of RMSNs can be removed to enhance the drug loading capacity because such solid cores contribute nothing to the drug delivery. For this purpose, Wang et al prepared hollow mesoporous silica nanocages (HMSNCs) by using cubic PbS as the hard template.[149] After surface PEGylation to protect NPs from immune scavengers, such nanocages were used as the carriers for the delivery of DOX by using Hep-A-22 xerograft in ICR mice as the animal disease model. It was found that enhanced tumor growth inhibition rate could be achieved by using PEGylated HMSNCs as the DOX carriers (39.10%) compared to that by using free DOX (22.33%), which was attributed to the enhanced accumulation of DOX-loaded HMSNCs via EPR effect by PEGylation.

Wang et al encapsulated poorly water soluble drug-telmisartan (TEL) into MSNs and mesoporous silica microparticles (MSMs) to test the oral drug delivery potentials of MSNs in beagle dogs.[150] After the administration of drugs by gavage, the mean plasma drug concentrations were determined by high pressure liquid chromatography (HPLC). After the pharmacokinetic calculations, they found that the relative bioavaibilities of TEL-loaded MSNs and MSMs were 154.4 ± 28.4% and 129.1 ± 15.6%, respectively, of commercial product Micardis. This research demonstrated the significant potential of using MSNs (or MSMs) to promote the drug dissolution and drug permeability, thus enhance the oral bioavailability of drugs.[150]

MSNs provide an ideal platform for multicomponent drug administration, especially for the combinations of small drug molecules and large therapeutic biomolecules. The large surface area and high pore volume of inner mesopores function as the reservoirs for small drug molecules and the outer hydrophilic surface provides the anchors for biomacromolecules such as DNA or siRNA (**Figure 7**A). Chen et al encapsulated DOX within mesopores and Bc1-2-targeted siRNA on the outer surface to reverse the MDR of A2780/AD human ovarian cancer cells.[151] The Bc1-2 siRNA can effectively silence the Bc1-2 mRNA, resulting in the exceedingly suppressed non-pump DOX resistance and substantially enhanced DOX cytotoxicity against MDR cancer cells thereby. Similarly, Meng et al

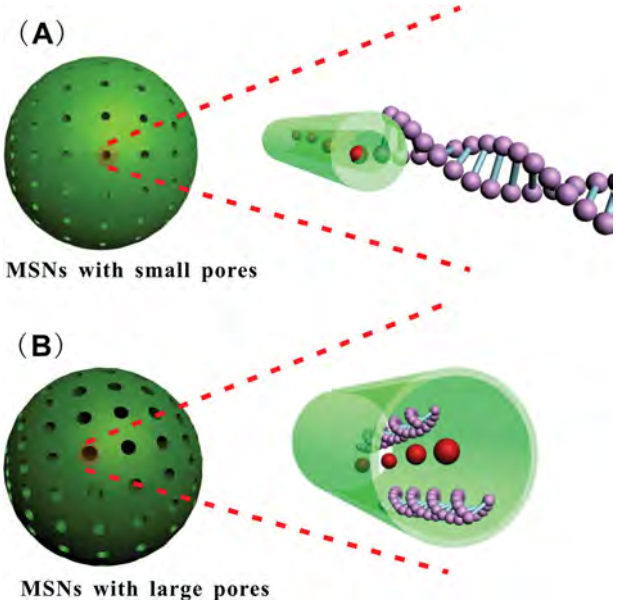

Figure 7. Two typical routes of adopting MSNs for gene encapsulation and delivery, including anchoring gene molecules onto the outer surface of small pore-sized MSNs (A) and inner pore-encapsulation of genes within the large pores of MSNs (B).

functionalized the MSNs by PEI to effectively deliver DOX and Pgp siRNA into a drug-resistant cancer cell line (KB-V1 cells) simultaneously.[152] The introduced siRNA could knock down the gene expression of the drug exporter, resulting in the enhanced drug cytotoxicities. Lin et al used honeycomb MSNs to transport DNA and chemicals into isolated plant cells and intact leaves.[153] Chemicals could be released to trigger the gene expression in the plants under the controlled release conditions, indicating the possible applications of MSNs-based nanotechnology in plant fields.

However, most MSNs-based gene-delivery systems immobilized DNA or siRNA on their outer surfaces due to limitation by their relatively small mesopore sizes. As a result, the anchored genes were highly vulnerable to enzyme-mediated degradation in vivo, and such a loading style does not show any advantage of mesoporous structure of MSNs in delivering gene molecules. The relatively low progress of MSNs for gene delivery lies in a big challenge in preparing small particle-sized MSNs with large enough pores for gene encapsulation (Figure 7B).[77,154] Recently, Min et al constructed a MSNs-based DNA[76] and siRNA[78] delivery system using monodispersed MSNs with ultra-large pores (23 nm, denoted as MSN23). The pore-expansion process was performed by hydrothermally treating as-prepared 2 nm pore-sized MSNs in a co-solvent of TMB (swelling agent) and distilled water for 4 days at 140 °C. Negatively charged siRNAs were encapsulated into large pores of amine-functionalized positively charged MSNs (P-T-MSNs), by which confined siRNAs within mesopores could be enabled of cellular delivery and to resist the RNase-mediated degradation by the pore protection (**Figure 8**a and 8b). They tested the green fluorescent protein (GFP) gene silencing in the HeLa xenografts by intratumor injection. The GFP green fluorescence significantly decreased after the treatment with siGFP-P-T-MSN23 in xenograft tumor

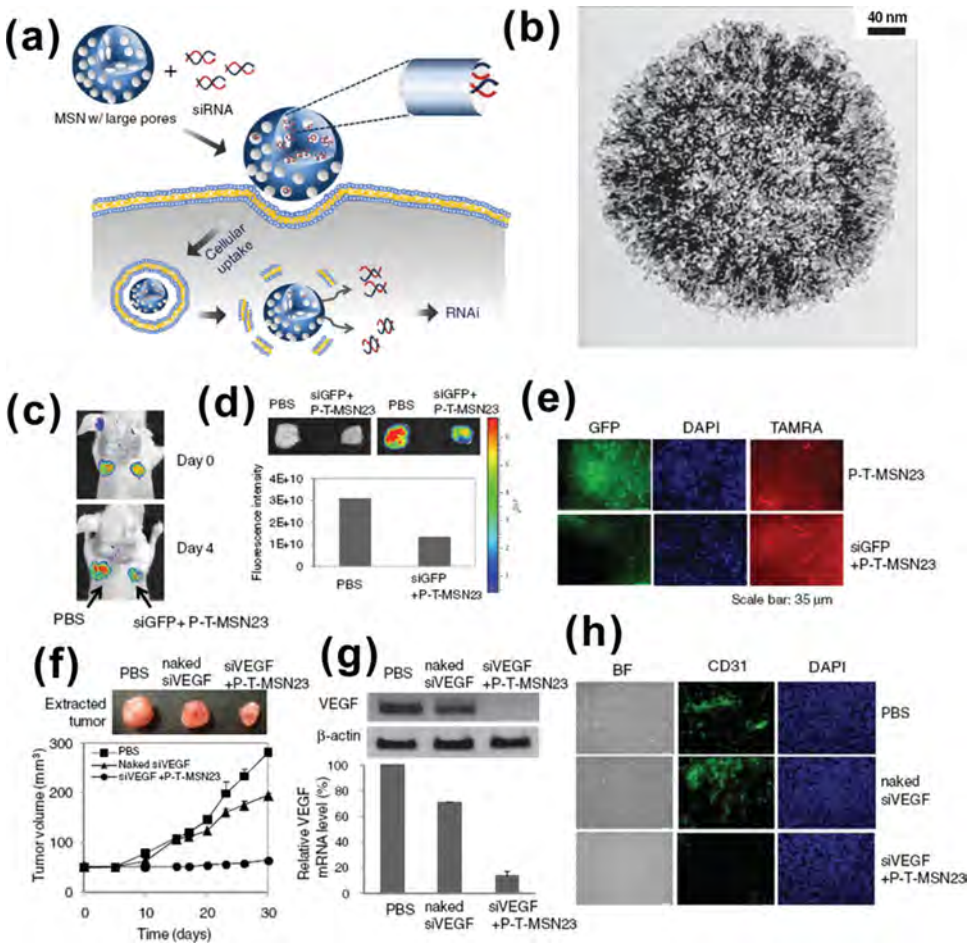

Figure 8. (a) The scheme of delivering siRNA intracellularly using large pores of MSNs as the siRNA reservoirs; (b) TEM image of MSN23; (c, d) Quantitative optical analysis of GFP-expressing tumors before (c) and after (d) the removal of tumors; (e) Optical microscopic images of the tissue section showing the GFP expression after the treatment with siGFP-P-T-MSN23 and P-T-MSN23; (f) Tumor inhibition results after the treatment with naked siVEGF and siVEGF-P-T-MSN23; (g) Quantitative analysis of relative VEGF mRNA levels in the tumors; (h) The results of inhibition of blood vessel growth in tumors by immunohistochemistry of tumor tissue sections with anti-CD31 antibody. Reproduced with permission.[78]

(Figure 8c, 8d and 8e), indicating that P-T-MSN23-mediated functional GFP delivery in vivo had been a success. To further down-regulate a therapeutically relevant gene, vascular endothelial growth factor (VEGF), siRNA against VEGF (siVEGF) was loaded into P-T-MSN23 for the in vivo inhibition of tumor growth. A significant tumor growth inhibition was observed after the treatment with siVEGF-P-T-MSN23, compared with naked siVEGF or PBS-treated tumors (Figure 8f). In addition, the remarkable down-regulation of VEGF mRNA was achieved in tumors after the treatment with siVEGF-P-T-MSN23 (Figure 8g). Immunohistochemistry tests of tumor tissue sections with anti-CD31 antibody revealed that the treatment of tumors with siVEGF-P-T-MSN23 could effectively inhibit the blood vessel growth compared to the xenografts treated with naked siVEGF and PBS (Figure 8h). Although this in vivo evaluation was performed by intratumor injection of gene-loaded NPs, this MSN23 may find the applications for tissue amenable to topical or localized therapy. Of course, the parameters of MSNs, such as particle size or surface modifications, could be further tailored for intravenous administration and gene therapy.

3.2. In Vivo Stimuli-Responsive Drug Delivery and Release

Chemical design and synthesis of stimuli-responsive drug carriers are the promising approach to mitigate the systemic toxicity and enhance the therapeutic outcome of therapeutic agents.[155,156] These intelligent DDSs can release the cargos on demand in the targeted tissues triggered by inner and/or outer environmental changes such as pH, temperature, enzymes, light, etc.[157–159] Thus, the dose magnitude and timing can be controlled, and the near zero-premature drug release can be achieved when they circulate in the blood stream. The mesopores provide the doors to be sealed by a series of "nanovalves", such as supramolecules, nanocrystals, polyelectrolytes, genes, etc., which are opened by the responsiveness

Adv. Mater. 2013,
DOI: 10.1002/adma.201205292

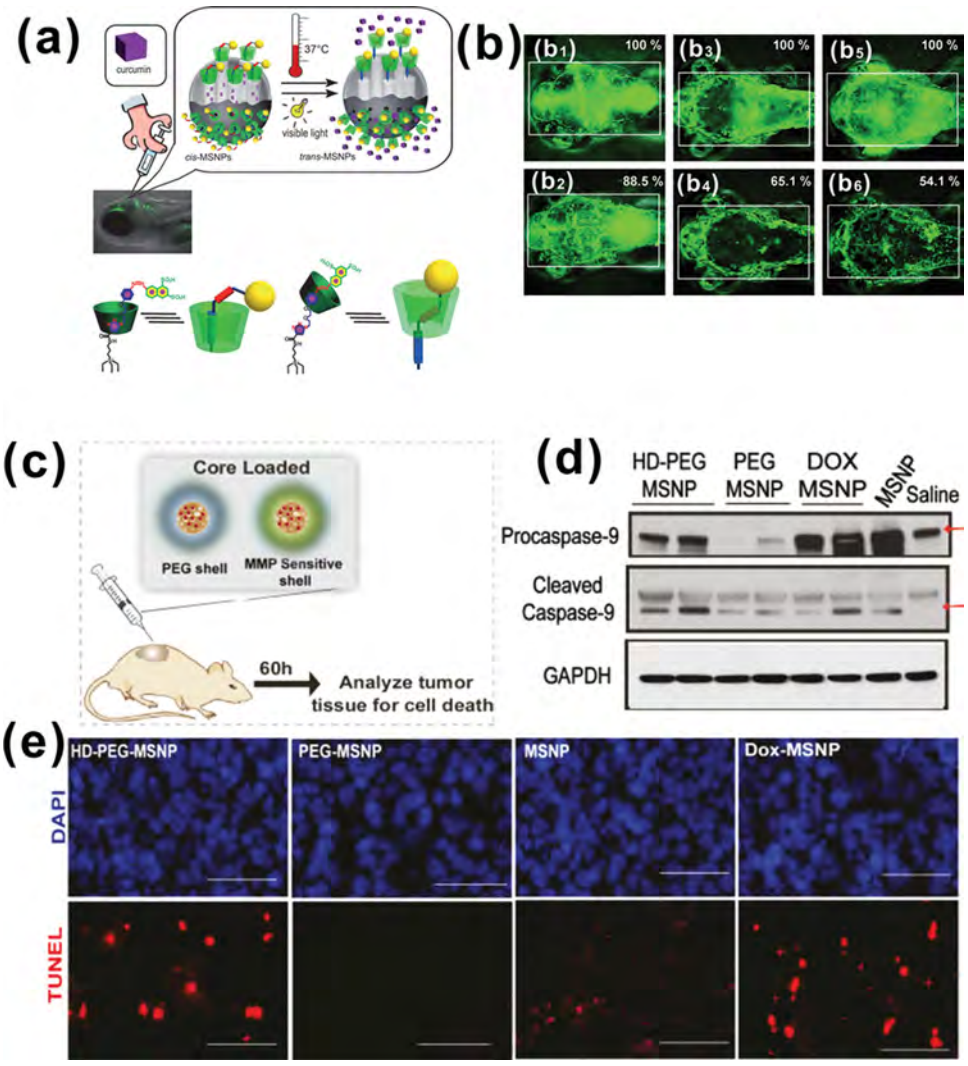

Figure 9. (a) The schematic presentation of the administration of drug-loaded MSNs into zebrafish larvae for in vivo controlled drug release, triggered by either heating or visible light irradiation; (b) Fluorescence intensities of zebrafish brains microinjected with curcumin-loaded photothermal MSNs (b_1 and b_2: images at 24 °C without photo and thermal treatments immediately after injection (b_1) and in 1 h post-injection (b_2); b_3 and b_4: images at 24 °C immediately after injection (b_3) and in 1 h after continuous visible light illumination (b_4); b_5 and b_6: images in the dark at 24 °C (b_5) and in 1 h after being in the dark at 37 °C (b_6); Reproduced with permission.[155] Copyright 2012, Wiley-VCH Verlag GmbH & Co. KGaA, Weinheim. (c) Scheme of the in vivo evaluation of protease-triggered DOX release from MSNs; (d) Immunoblots for protein levels of caspases and GAPDH from tumor lysates of animals after 60 h post-treatment; (e) TUNEL staining for apoptotic cells in tumor sections (Red: TUNEL, blue: DAPI). Reproduced with permission.[156] Copyright 2011, American Chemical Society.

to the changes of in vitro or in vivo environments to realize the photo-,[160–163] redox-,[63,164,165] pH-,[166–171] ultrasound-,[172] enzyme-,[173–177] temperature-,[178–180] antibody-antigen reaction-,[181] glucose-responsive triggered drug release.[182]

Unfortunately, many well-established MSNs-based stimuli-responsive systems were evaluated in vitro. How to realize the in vivo stimuli-responsive drug release is crucial for further clinical translations. The major breakthrough on MSNs-based in vivo controlled drug release was preliminarily achieved recently.[155,156] Zhao et al prepared rotaxane-functionalized MSNs with photothermal-responsive behaviors (**Figure 9**a).[155] They demonstrated the in vivo remote-controlled drug release on wild-type, optically transparent zebrafish larvae (Figure 9b). Curcumin was further delivered to zebrafish larvae for the treatment of heart failure. Figure 9a shows the proposed protocol of controlled drug release. Upon irradiation with 365 nm UV light, the *trans-to-cis* photoisomerization of the azobenzene unit cause a shift of the α-CD ring from the azobenzene unit to the triazole/ethylene glycol position, thus the drugs could be trapped within the mesopores. The *cis-to-trans* isomerization of the azobenzene unit upon exposure to visible light or heating induced the recovering of the α-CD ring to the original *trans*-azobenzene position, resulting in the opening of the nanopores for the release of loaded cargos. In vivo evaluation using optically transparent zebrafish larvae showed that 34.9% (Figure 9b_3 and b_4) and 45.9% (Figure 9b_5 and b_6) reduction

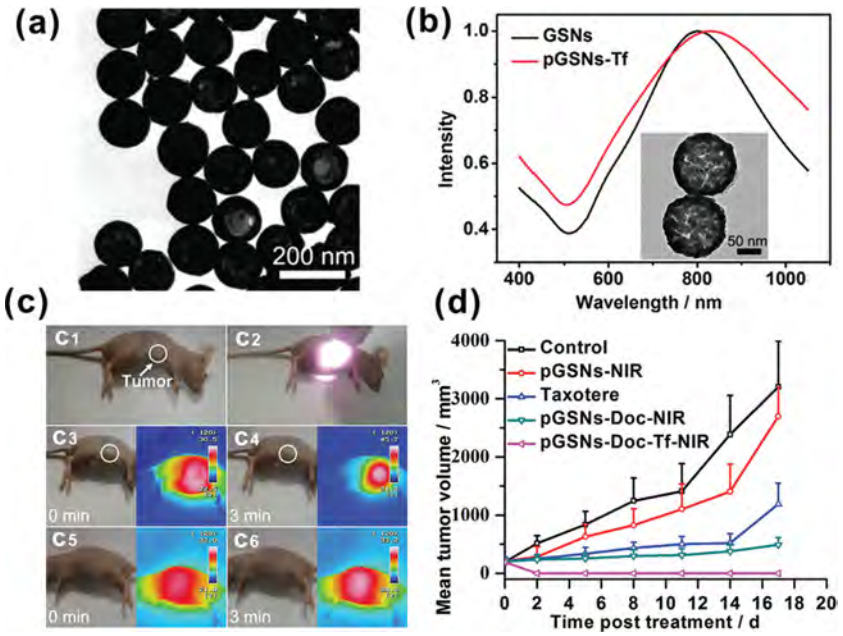

Figure 10. (a) TEM image of GSNs; (b) Extinction spectra of pGSNs and pGSNs-Tf (inset: TEM image of pGSNs-Tf); (c) Infrared thermal imaging under the 808 nm laser irradiation (c_1: photo image of tumor-bearing mouse; c_2: photo image of tumor-bearing mouse under the 808 nm NIR laser light irradiation; c_3: photo and infrared thermal images of the tumor side in 6 h post-intravenous injection of pGSNs-Tf before (c_3) and after (c_4) NIR laser light irradiation; photo and infrared thermal images of non-tumor side before (c_5) and after (c_6) NIR laser light irradiation; (d) In vivo tumor inhibition results of control group, pGSNs-NIR, Taxotere, pGSNs-Doc-NIR, pGSNs-Doc-Tf-NIR group on MCF-7 bearing nude BALA/c mice. Produced with permission.[184] Copyright 2011, Wiley-VCH Verlag GmbH & Co. KGaA, Weinheim.

in the mean fluorescence intensity of curcumin in 1 h post-treatment under visible light and thermal treatment (37 °C), while only 11.5% (Figure 9b_1 and b_2) reduction of curcumin in zebrafish was found without the photothermal treatment. The decrease of fluorescence intensity was due to the in vivo metabolism of the released curcumin, thus curcumin-loaded MSNs showed an effective in vivo photothermal responsive behavior.

The in vivo controlled drug release using mammalian was successfully demonstrated recently by Bhatia and coworkers.[156] They used PEGDA-peptide macromer possessing matrix metalloproteinases (MMPs) substrate polypeptides with a highly degradable (HD-MMP) sequence to coat onto the surface of MSNs (denoted as HD-PEG-MSNs). The HD-PEG layer could be degraded by MMPs abundant in the tumor cells (Figure 9c). The tumor model was established by injecting a human sarcoma cell line (HT-800) with elevated levels of MMPs subcutaneously in the flanks of immune-compromised mice. In 60 h post-injection of DOX-loaded HD-PEG-MSNs NPs into tumors, the DOX-induced apoptosis was measured by means of TUNEL staining and caspase levels testing (Figure 9d-e). It was found that DOX-loaded HD-PEG-MSNs and DOX-loaded uncoated MSNs generated higher levels of the caspases than DOX-loaded undegradable PEG-MSNs and saline controls (Figure 9d). Additionally, the TUNEL staining of the tumor sections revealed that DOX-loaded HD-PEG-MSNs exhibited the higher amount of DOX-induced cell death compared with DOX-loaded undegradable PEG-MSNs (Figure 9e). This effect was attributed to the MMP-sensitive PEG layers of HD-PEG-MSNs which could be degraded to facilitate the release of the loaded DOX, while non-MMP-sensitive PEG layers of PEG-MSNs inhibited the release of DOX. This MSNs-based stimuli-responsive drug release system takes the advantages of PEG layers for improved biocompatibility and stability in physiological system and of the protease-cleavable moiety on the PEG molecules to achieve triggered drug delivery and release in the tumor locations, thus is very promising for the further clinical applications.

3.3. In vivo Photothermal and Photodynamic Therapy

The progress of nano-synthetic chemistry makes the engineering of MMSNs for photothermal therapy possible. Such a therapeutic modality can customize the therapy with accurate lesion positioning and controlled power input/duration of the applied laser pulse while the penetration depth is sometimes restricted.[183] Therefore, it is suitable for the treatment of superficial tissues rather than the deep tissues. Combining plasmonic nanomaterials, such as gold nanorods[86,87] or gold nanoshells[184,185] with MSNs, simultaneous chemotherapy and photothermal therapy could be realized. Tang et al recently coated a uniform Au layer onto the surface of mesoporous silica nanorattles to produce a new type of plasmonic NPs (designated as GSNs) for the synergistic docetaxel (Doc) delivery and photothermal therapy.[185] After the further PEGylation (pGSNs), the pGSNs could accumulate into the tumor tissues via the typical EPR effect. The in vivo results demonstrated that the mouse group treated by pGSNs-Doc and combined with 808 nm NIR laser light irradiation induced the average tumor inhibition rate of as high as 85.4% while the free drug Taxotere group only reached 57.4%. Furthermore, they anchored transferring (Tf) onto the surface of pGSNs for targeted transportation (denoted as pGSNs-Tf).[184] The fabricated GSNs exhibited the uniform and spherical morphology and high dispersity (**Figure 10**a). The pGSNs-Tf exhibited the broadened and red-shifted extinction spectra compared to the initial GSNs in the NIR region (Figure 10b). In 6 h intravenous post-injection of pGSNs-Tf and subsequent 808 nm NIR laser light irradiation (2 W cm^{-2}), the temperature of the tumor increased from 30.5 °C to 45.7 °C (Figure 10c). No apparent temperature fluctuation occurred in non-tumor side under the same NIR light irradiation condition. The in vivo tumor inhibition results demonstrated that the tumors receiving pGSNs-Doc-Tf-NIR via a single NIR light irradiation were almost completely regressed (Figure 10d). Such a high therapeutic outcome was due to the Tf-based targeting accumulation, and synergistic therapy based on chemotherapy (Doc) and NIR photothermal therapy. These plasmonic mesoporous NPs have the nature of excellent biocompatibility and could be cleared from the body via urine and feces.

Adv. Mater. **2013**,
DOI: 10.1002/adma.201205292

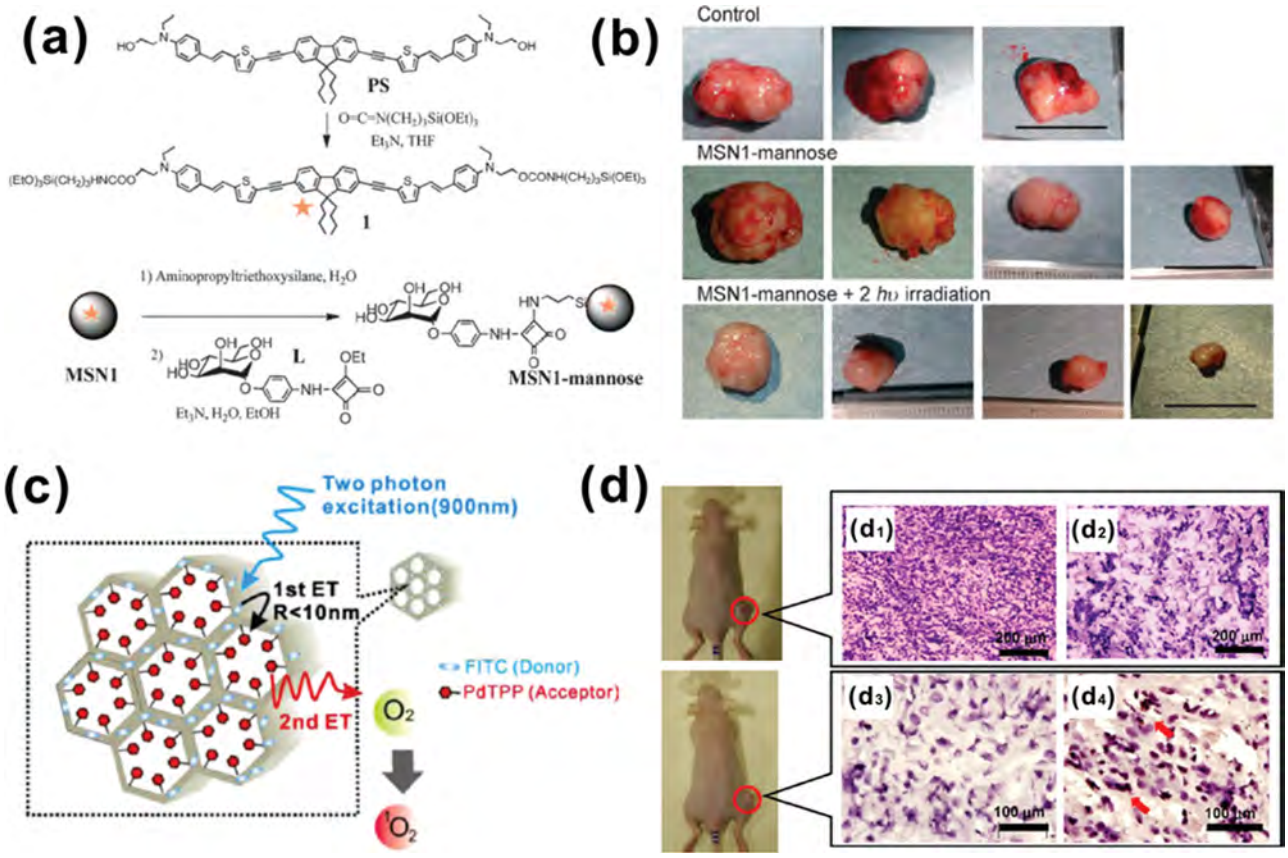

Figure 11. (a) Scheme of the synthetic procedure for mannose-modified MSN1 (denoted as MSN1-mannose); (b) The effect of TPE-PDT on tumor growth; Reproduced with permission.[189] Copyright 2011, Wiley-VCH Verlag GmbH & Co. KGaA, Weinheim. (c) Two-step intra-MSNs energy transfer from FITC in the framework to PdTPP in the nanochannels to generate singlet oxygen by two-photon excitation; (d) In vivo two-photon PDT effect by intratumor injection of NPs (d_1 and d_3: control; d_2 and d_4: FITC@MSN-PdTPP (16 mg/kg)). Histological specimens of tumors were evaluated with hematoxylin and eosin staining (d_1 and d_2) and caspase-3 immuno-histogram (d_3 and d_4). Reproduced with permission.[190] Copyright 2011, Elsevier.

Photodynamic therapy (PDT) is a promising therapeutic modality alternative to chemo- and radiotherapy because of its non-invasive and selective destruction of tumors.[186,187] The PDT process involves the accumulation of photosensitizers into tumor sites, irradiation of photosensitizers by outer light and the generation of toxic singlet oxygen species to destruct the tumor cells. However, the photosensitizers suffer from the drawbacks of low targeting efficiency, instability and easy excretion from the animal bodies. Encapsulation of photosensitizers within the NPs is a promising route to enhance the selectivity of therapeutic efficacy towards tumor cells. The unique mesoporous structure of MSNs provides an ideal platform for the delivery of photosensitizers for PDT.[188]

To establish PDT with large two-photon absorption (TPA) cross-section in the biological spectral window, Gary-Bobo et al covalently encapsulated the synthetic photosensitizer PS inside MSNs, followed by surface grafting of mannose derivative to target lectins over-expressed cancer cells (**Figure 11**a).[189] The PS-functionalized MSNs were nontoxic under daylight illumination. After the irradiation at 760 nm for three periods of 3 min on three different tumor areas, a significant tumor weight reduction (ca.70%) was found in comparison to the tumors treated with saline solution or MSNs without subsequent irradiation (Figure 11b). No significant systemic and organ-specific toxicities were found within two weeks, and the macrometastasis of MSN1-mannose group could be effectively prevented.

To achieve spatially selective treatment of cancers and enhanced penetration depth of incident light, Mou et al developed a hybrid system with two-photo absorption dyes (FITC) in the framework of MSNs and photosensitizers (Pd-meso-tetra(4-carboxyphenyl), PdTPP) in the mesopores.[190] FITC acts as a medium for two-photon harvesting and thereafter a donor for energy transfer, and PdTPP functions as the acceptor of the transferred energy for the generation of toxic singlet oxygen. Such a Förster resonance energy transfer (FRET) process induced highly efficient two-photon excited PDT both in vitro and in vivo (Figure 11c). After the intratumor injection of FITC@MSNs-PdTPPs (16 mg/kg) followed by irradiation with a 920 nm femtosecond laser for 1 h at a total energy of 150 J cm^{-2}, hematoxylin and eosin stain (H&E stain) and caspase-3 immuno-histogram of tumor sections showed that extensive cell death via combined necrosis and apoptosis could be found in the tumor tissues (Figure 11d_1 and d_3), while the injection of FITC@MSNs did not show such an effect (Figure 11d_2 and d_4).[190]

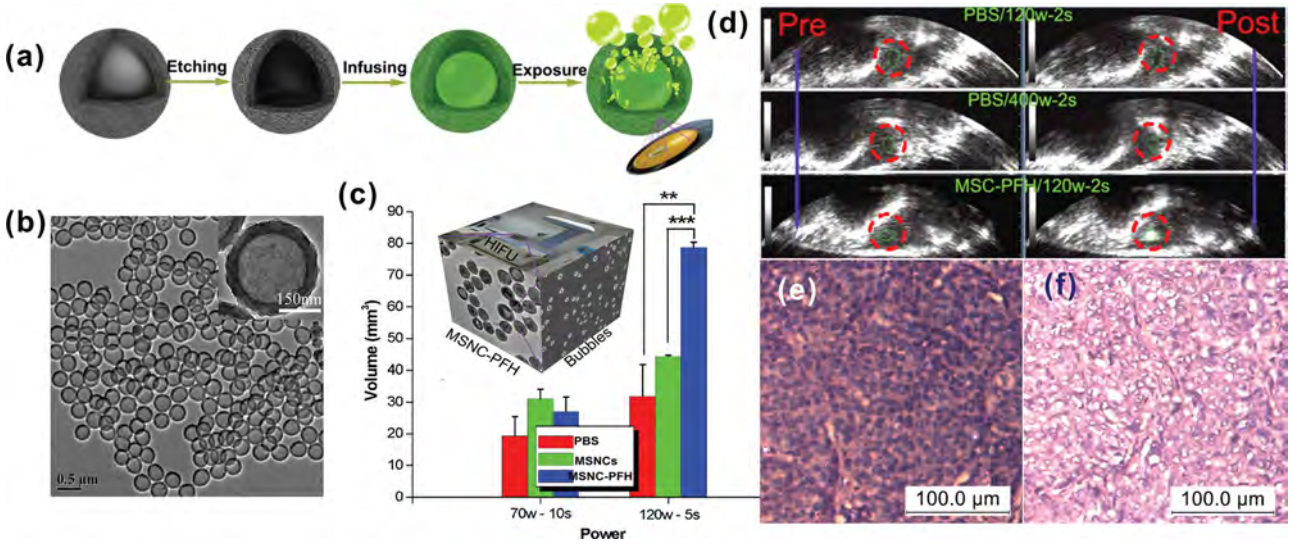

Figure 12. (a) Preparation procedure of PFH encapsulated mesoporous silica nanocapsules (MSNC-PFH); (b) TEM image of prepared MSNC; (c) *Ex vivo* results of HIFU exposure by the administration of different agents at different ultrasound exposures using bovine liver as the model tissue; (d) The typical in vivo B-mode ultrasonic images before (left) and after (right) HIFU exposure on rabbit liver tumors; (e and f) Pathological examinations of related tumor tissue after HIFU ablation at 400 W/cm^2 for 2 s using PBS as the control (e) and at 120 W/cm^2 for 2s using MSNC-PFH (f). Reproduced with permission.[191]

3.4. In vivo Ultrasound Therapy

Conventional cancer chemotherapy always brings about high side-effects due to the severe toxicity of therapeutic agents. High intensity focused ultrasound (HIFU), as the representative non-invasive and nonradioactive transcutaneous therapeutic mode, has been clinically used for cancer surgery with high efficacy and low side-effects, which was based on the tissue-penetrating nature of ultrasound to destroy the tumor vasculature and cause coagulative necrosis of cancer cells by thermal, mechanical and cavitation effects.[191–195] We recently introduced nanobiotechnology into HIFU-based cancer surgery by engineering mesoporous silica nanocapsules (MSNCs) for HIFU synergistic therapy,[191] which concurrently suffers from low therapeutic efficiency for some deep tissues and the possible damages to the normal tissues in the acoustic propagation channels due to the relatively high ultrasound power input clinically adopted. By impregnating perfluorohexane (PFH) with a phase transition temperature of ~56 °C into the hollow interiors of MSNCs (**Figure 12**a and b), the ex vivo results demonstrated that MSNC-PFH caused the substantially larger volume tissue ablation than either MSNC or PBS (Figure 12c). The in vivo assessment on rabbit VX2 liver xenograft further demonstrated the high synergistic effect of MSNC-PFH (Figure 12d–f).

To completely eradicate the microscopic tumor foci, the accurate positioning of the therapeutic targets for ultrasound focusing by clinical imaging modalities is of equivalent importance compared to the enhancement of HIFU surgical efficacy. Additionally, the accurate focusing of ultrasound in vivo can reduce the chances of the ablation to healthy tissues. We further decorated MnOx NPs into the mesopores of HMSNs (**Figure 13**a) to provide the T_1-weighted MRI contrast-enhanced imaging performance of HMSNs (MCNCs, r_1 = 1.84 $mM^{-1}s^{-1}$).[15] For ultrasound focusing, the T_1-weighted MR imaging of VX2 liver tumor was carried out on rabbits after intravenous injection of PFH loaded MCNCs (PFH-MCNCs). The boundary between tumor and normal tissues could be clearly distinguished after the intravenous administration of either MCNCs or PFH-MCNCs in MRI-T_1 images, respectively (Figure 13b). Comparatively, the administration of PBS as a control did not show significant MRI-T_1 signal enhancement. The principal for MRI-guided HIFU surgery is shown in Figure 13c. The tumor tissues can be precisely positioned/determined in MRI-T_1 images using MCNCs as the CAs. The low-energy ultrasound waves launched by the ultrasonic transducer can be focused on the tumor tissue to produce the high temperature to ablate the tumor tissues using MCNCs as the synergistic agents (SAs). The *ex vivo* assay choosing degassed bovine liver as the modal tissue showed that the MCNCs could efficiently encapsulate and deliver PFH molecules to remarkably enhance the therapeutic efficiency of HIFU. The relatively low power (150 W/5 s, 86.5 mm^3) ultrasound exposure in the group received PFH-MCNCs/PBS caused the larger coagulated tissue volume than that even under the ultrasound exposure of much higher power (250 W/5 s, 66.6 mm^3) in the group received only PBS (Figure 13d). Importantly, the coagulated tumor volumes by HIFU irradiation (Figure 13e) in the rabbits received PFH-MCNCs (10.2 mm^3) are 8.3 and 1.8 times larger than those in the rabbits received only PBS (1.1 mm^3) and MCNCs (3.7 mm^3). This work gives an alternative but effective solution to solve the issues of safety and efficacy in HIFU clinical therapy, which will open new avenues and enlighten the future work of introducing nano-biotechnology into some specific therapeutic modalities, such as radiation treatment, microwave therapy and radiofrequency surgery for significantly enhanced efficacies of these clinically therapeutic protocols. Additionally, the mesopores within MCNCs can be loaded with guest therapeutic molecules, which makes the simultaneous chemotherapy and HIFU surgery possible.

Adv. Mater. **2013**,
DOI: 10.1002/adma.201205292

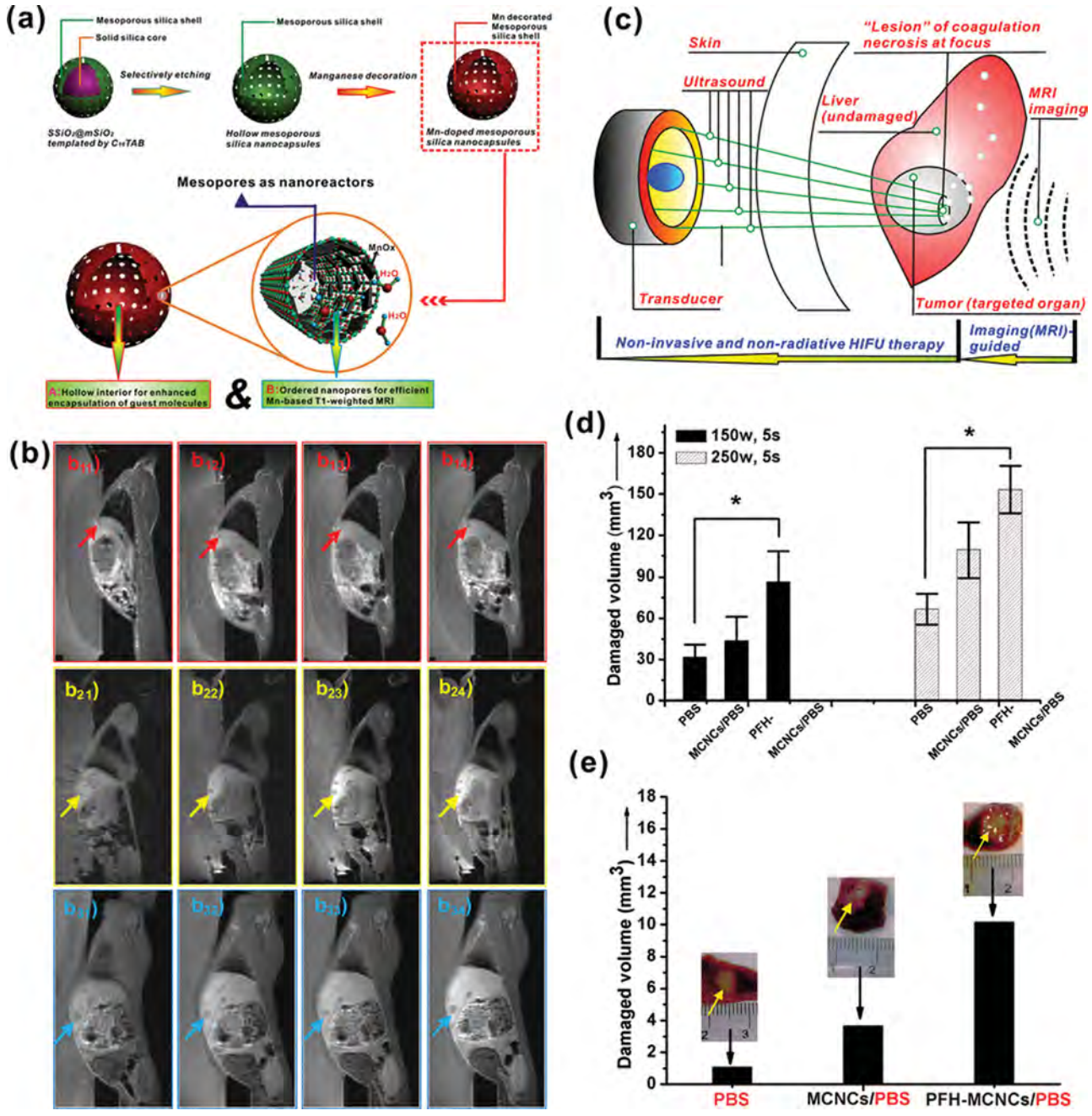

Figure 13. (a) Schematic diagram of the synthetic procedure for multifunctional composite nanocapsules (MCNCs) and their corresponding microstructures; (b) In vivo T_1-weighted MRI of rabbits bearing VX2 tumor before (b_{11}, b_{21} and b_{31}) and after 5 min (b_{12}, b_{22} and b_{32}), 15 min (b_{13}, b_{23} and b_{33}) and 30 min (b_{14}, b_{24} and b_{34}) administration of different agents (PBS: b_{11}-b_{14}; MCNCs/PBS: b_{21}-b_{24}; PFH-MCNCs/PBS: b_{31}-b_{34}) via ear vein; (c) Technical principal of MRI-guided HIFU for the cancer surgery; (d) Coagulated-tissue volumes of degassed bovine liver after intratissue injection of PBS, MCNCs/PBS and PFH-MCNCs/PBS under the same irradiation power and duration; (d) In vivo coagulated necrotic-tumor volumes by MRI-guided HIFU exposure under the irradiation power of 150 W/cm^2 and duration of 5 s in rabbit liver tumors after the administration of different agents through the ear vein (inset: digital pictures of tumor tissue after HIFU exposure). Reproduced with permission.[15]

3.5. In vivo Drug Delivery for Tissue Engineering

Mesoporous silica-based materials possess intrinsic bioactivity because their silanol groups on the large surface areas can react with physiological fluids to generate the nanosized carbonated apatites.[196–198] Thus, they are considered as the potential repairing materials for bone tissue regeneration.[199–201] As shown in **Figure 14**a, mesoporous silica materials can load and deliver diverse guest molecules for bone regeneration.[196] The well-defined mesopores can storage and *in-situ* release

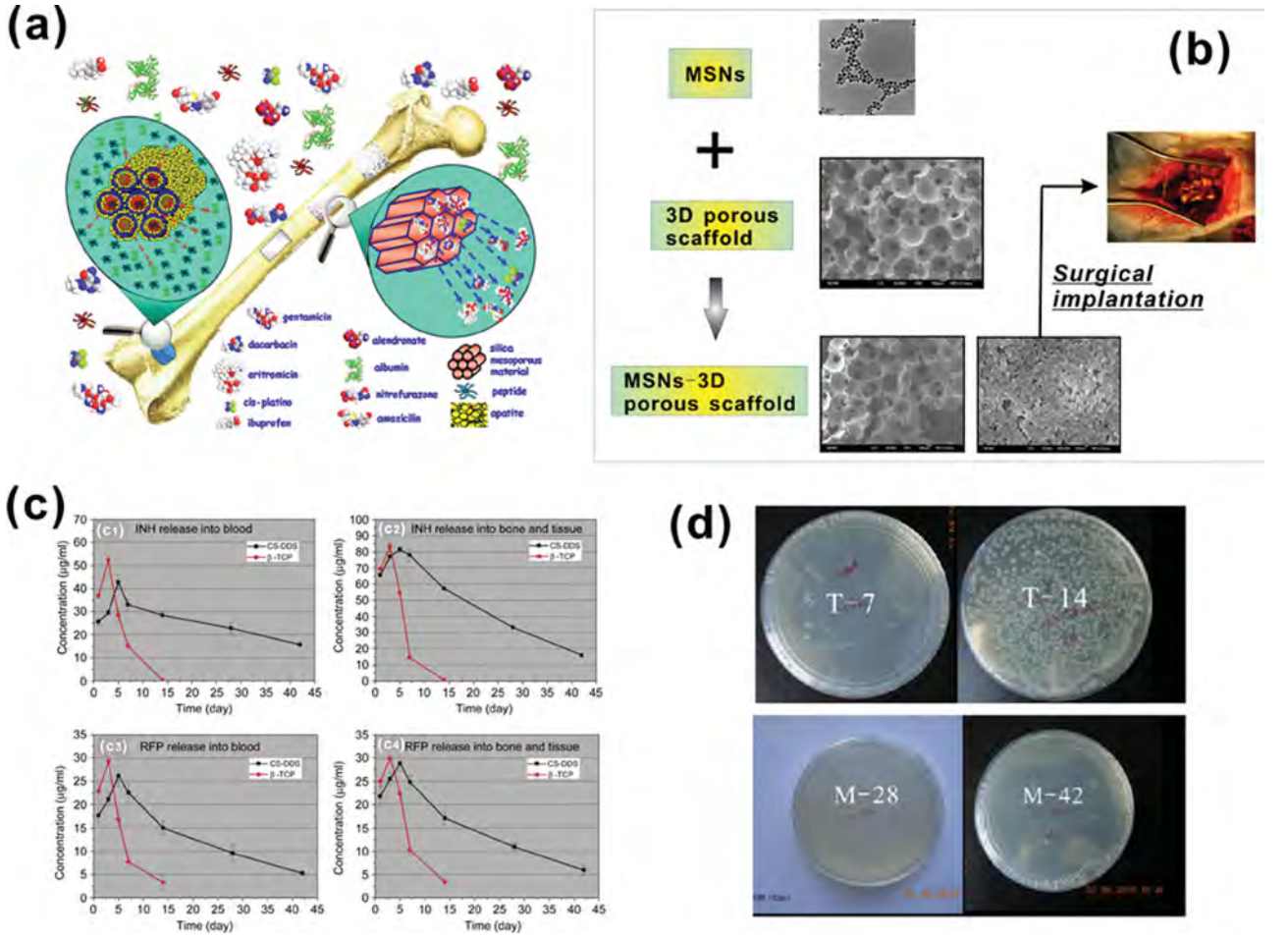

Figure 14. (a) Scheme of the possibilities of mesoporous silica for the delivery and release of drugs and proteins in the application of implant materials; Reproduced with permission.[196] Copyright 2008, Elsevier. (b) The synthetic procedure for MSNs-β-TCP composite scaffold and their corresponding morphology and microstructure; (c) Drug concentrations with respect to the time period of the antitubercular drug INH (c_1, c_2) and RFP (c_3, c_4) releases from implanted CS-DDSs and β-TCP in blood, bone and the surrounding tissues; (d) Digital photos of the agar plates on which different extraction liquids containing antitubercular drugs were smeared. Reproduced with permission.[197] Copyright 2011, Elsevier.

antibiotic and/or anti-infection drugs to defense against the inflammation and/or infection caused by the introduction of foreign materials in the surgical process of implant fixation. Vallet-Regí et al reported that SBA-15-type mesoporous silica loaded with parathyroid hormone-related protein (PTHrP) could significantly promote local bone induction compared to the unloaded material, which was due to the regulation nature of PTHrP for bone formation and remodeling.[202]

We used nanometer-sized MSNs to co-deliver antitubercular drugs for long-term in vivo drug releasing in the therapy of osteoarticular tuberculosis.[197] As shown in Figure 14b, MSNs was coated onto the large pore surface of β-TCP scaffold by a vacuum impregnation procedure (MSNs-β-TCP). After co-loading of antitubercular drugs (isoniazid: INH and rifampicin: RFP), drug-loaded MSNs-β-TCP was further coated with a layer of bioactive glass (BG) forming a composite scaffold drug delivery system (CS-DDS). The drug loading capacities of CS-DDS for two kinds of drugs (INH: 37.89 mg/g, RFP: 3.77 mg/g) were significantly higher than those in initial β-TCP (INH: 8.53 mg/g, RFP: 0.91 mg/g) due to the contributions by introduced MSNs. Both INH and RFP concentrations reached maxima on the fifth day from CS-DDS, while they reached maxima only in the third day from pure β-TCP either in the blood or in the tissue. Importantly, the drugs released from CS-DDS remained their concentrations above the effective limits for over 42 days. However, the in vivo drug concentrations released from pure β-TCP quickly dropped to near zero in 14 days (Figure 14c). The long-term sustained drug release from CS-DDS was attributed to the sustained release property of encapsulated MSNs covered by a layer of bioactive glass. Further anti-tubercle bacillus tests using extract liquids containing antitubercular drugs released from CS-DDS after implanted for 28 or 42 days and from β-TCP after implanted for 7 or 14 days (denoted as M-28, M-42, T-7 and T14) revealed that almost no Mycobacterium Tuberculosis in M-28, M-42 and T-7 seeded plates survived, while luxuriant growth of the Mycobacterium Tuberculosis was clearly observed on the T-14 seeded agar plate (Figure 14d). This result further demonstrated the long-lasting in vivo maintaining (42 days) of the drug concentrations by exceptionaly sustained releases from CS-DDS, but the pure

Adv. Mater. **2013**,
DOI: 10.1002/adma.201205292

β-TCP failed to sustain the drug releases over 14 days. In addition, the CS-DDS did not cause the long-term lesions to liver and kidney, indicating the good biocompatibility of the composite scaffold.[197]

4. In vivo Diagnostic Imaging Using MSNs-Based Contrast Agents (CAs) for Theranostic Purposes

With the unique structural features of well-defined mesoporosity and intrinsic biocompatibility, MSNs provide an ideal nanomedical platform for the construction of multifunctional MSNs (MMSNs) by integrating various bio-imaging tags in MSNs towards the multifunctionalization for simultaneous biological imaging and diagnostic applications. The endowed diagnostic functions possess the following clinical merits: (1) For pre-therapeutic process, the integration of imaging functionality within MSNs can improve the diagnostic performance of clinically used imaging probes, thus the diseases at their early stages can be detected (*Finding function*); (3) During the therapeutic process, the distribution of NPs and drug-releasing profiles can be real-time monitored (*Fighting function*); (3) After the therapeutic process, the MMSNs can provide more exact information on the progress of pathological changes to predict and validate the effectiveness of therapy, by which doctors can further timely adjust the therapeutic protocols (*Following function*). Therefore, such MMSNs play a "theranostic" role in the concurrent and complementary diagnosis, therapy and monitoring of the therapeutic response. Fortunately, the progress of advanced nanosynthetic chemistry makes the construction of these MMSNs possible. Various imaging agents have been integrated within MSNs to produce novel CAs for magnetic resonance imaging (MRI), optical imaging, positron emission tomography (PET) imaging, ultrasonography, etc., and the varied combinations between/among different imaging modalities towards multimodality bio-imagings have also been attempted for more precise and effective diagnosis.

4.1. In vivo Magnetic Resonance Imaging (MRI)

MRI is one of the most representative imaging modalities clinically due to its intrinsic merits of high spatial resolution and superior three-dimensional soft tissue contrast.[203,204] The introduction of CAs during MR imaging can further enhance the accuracy of diagnosis.[205] Typically, MRI is based on the relaxation of protons triggered by an external magnetic field to transmit an excitation pulse, which was based on either spin-lattice relaxation (relaxation time T_1, longitudinal relaxivity) or spin-spin relaxation (relaxation time T_2 and T_2^*, transverse relaxivity). Different tissues can generate the endogenous contrasts in the time courses of T_1 and T_2 proton relaxations. Although $[Gd(DTPA)]^{2-}$ complex and its analogs have been successfully employed as the exogenous CAs to improve the sensitivity and resolution of clinical MR imaging, their relaxivities and diagnostic performances still need to be improved to detect the diseases at their early stages. MSNs can be functionalized with MRI CAs for efficient T_1- and/or T_2-weighted MRI (**Table 2**).

Superparamagnetic Fe_3O_4 NPs are the most developed CAs for T_2-weighted MRI.[206] Well-defined Fe_3O_4 nanocrystals with small particle size (typically < 100 nm) and highly crystalline structure are generally synthesized by the thermal decomposition process, thus, they are hydrophobic.[207] Coating hydrophobic nanocrystals with mesoporous silica shells can be a good protocol to transform these hydrophobic nanocrystals into hydrophilic media to meet the needs of in vivo use. Additionally, the abundant surface silane chemistry of the coated mesoporous silica shells can be employed for anchoring biomacromolecules (e.g., PEG, PEI-PEG) for prolonged blood circulation half-life time in vivo and/or targeting moieties for targeted diagnosis and therapy. Hyeon et al chose cationic surfactants CTAB as the phase-transforming agent to transform hydrophobic oleic acid-coated Fe_3O_4 NPs from organic media into aqueous solution, followed by subsequent sol-gel process for mesoporous silica coating (**Figure 15**a).[83,84] In this respect, CTAB plays two roles: the stabilizing molecules for the transformation of hydrophobic Fe_3O_4 NPs from organic media into aqueous solution and as the SDAs for the formation of mesoporous silica shell. The r_1 and r_2 relaxivities were 3.40 and 245 mM^{-1} s^{-1}, respectively.[83] After PEGylation, the Fe_3O_4@$mSiO_2$-PEG NPs could accumulate in tumors after intravenous administration into nude mice bearing tumors of 0.5 cm in diameter on the shoulder via EPR effect, as demonstrated by the signal enhancement in the T_2-weighted MR images (Figure 15a). MRI also showed that the injected NPs still remained in the tumor sites after 24 h post-injection, indicating that such NPs could be used for long-term MR imaging.[83] Huang et al found that the chelating of Gd^{3+} ions via DOTA-NHS within the channels of Fe_3O_4@$mSiO_2$ could increase the transverse relaxivity (r_2) from 97 mM^{-1} s^{-1} of Fe_3O_4 to 681 mM^{-1} s^{-1} of Gd^{3+}-chelated Fe_3O_4@$mSiO_2$ NPs.[208] The prepared biocompatible Gd^{3+}-chelated Fe_3O_4@$mSiO_2$ NPs demonstrated the effective in vivo MR imaging effect of lymph nodes.

Although Gd^{3+}-based complex as the representative and preferential T_1-weighted MRI CAs have found the successful clinical applications in disease diagnosis due to their high attainable sensitivity (e.g., Magnevist), FDA has warned that Gd^{3+}-based CAs are associated with nephrogenic systemic fibrosis (NSF) in patients with impaired kidney, hypersensitivity reactions and nephrogenic fibrosing dermopathy (NFD).[209–212] Thereafter, searching alternatives to Gd^{3+} chelates have been urgently recommended and promoted. Manganese is one of the essential elements of high biocompatibility for the metabolism in human bodies and its homeostasis has been efficiently controlled by biological system. Mn (II) ions have been employed as the MRI-T_1 CAs due to their five unpaired electrons with long electronic relaxation time.[213–216] Recently, Hyeon et al employed the coating process to synthesize mesoporous silica-coated hollow manganese oxide NPs (HMnO@$mSiO_2$, Figure 15b), and used them as a novel T_1-weigted MRI CAs for the labeling and MRI tracking of adipose-derived MSCs (Figure 15c and d).[209] However, the MRI performance is still not satisfactory as can be known from the low r_1 value (0.99 $mM^{-1}s^{-1}$, 11.7 T), largely due to the shielding of the active manganese ions on the surface by mesoporous silica coating. Although they claimed that mesopores facilitated the diffusion of water molecules to interact with hollow manganese oxide core, the low imaging

Table 2. Summary of representative examples of MSNs-based CAs for in vivo MR imaging.

MSNs type	Integrated functions	Imaging modalities	Parameters $mM^{-1}s^{-1}$ (Tesla)	Animal models	Purposes	Ref.
MCM41	Gd-Si-DTTA	MRI-T_1	r_1 = 28.8 (3.0 T)	DBA/1J mouse	Aorta imaging	[91]
MCM41	Gd_2O_3	MRI-T_1	/	Nasopharyngeal carcinoma CNE-2 xeno-grafted tumors	Tumor imaging	[247]
MCM41	Gd_2O_3	MRI-T_1	r_1 = 13.48 (3.0 T)	Balb/c nude mice bearing nasopharyngeal carcinoma tumors	Tumor imaging	[218]
MCM41	Gd-Si-DTTA	MRI-T_1	/	Female BALB/c mice bearing 4T1 metastasis tumors	Imaging of tumor metastasis	[223]
MCM41	Gd-DTPA	MRI-T_1	r_1 = 25.7 (1.5 T)	Female athymic nude mice	Targeted imaging	[248]
MCM41	Gd-DTPA	MRI-T_1	r_1 = 23 (1.5 T)	Male nude mice	Stem cell tracking	[92]
APMS	Gd-DTPA	MRI-T_1	r_1 = 2.8 (1.5 T)	C57BL/6 mouse	Bladder imaging	[249]
HMnO@$mSiO_2$	MnO	MRI-T_1	r_1 = 0.99 (11.7 T)	C15/BL6 male mice	In vivo cell transplants	[209]
MCM41	MnOx	MRI-T_1	r_1 = 2.28 (3.0 T)	SD female mouse bearing walk 256 tumors	Tumor imaging	[94]
SBA15	MnOx	MRI-T_1	r_1 = 1.37 (3.0 T)	SD female mouse bearing walk 256 tumors	Tumor imaging	[94]
HMSNs	MnOx	MRI-T_1	r_1 = 8.81 (3.0T)	SD female mouse bearing walk 256 tumors	Tumor imaging	[93]
NaYF4:Tm/Yb/Gd@$mSiO_2$	Gd doping	MRI-T_1	r_1 = 3.07 (3.0 T)	SD female mouse bearing walk 256 tumors	Tumor imaging	[88]
Fe_3O_4@$mSiO_2$	Fe_3O_4	MRI-T_2	r_2 = 245 (1.5 T)	Nude mice bearing MCF-7 tumors	Tumor imaging	[83]
Fe_3O_4@$mSiO_2$	Gd-DOTA & Fe_3O_4	MRI-T_2	r_2 = 681 (3 T)	Male BALB/c mice	Lymph node imaging	[208]
MCM41	Fe_3O_4	MRI-T_2	r_2 = 76.2 (1.5 T)	Nude mice bearing MCF-7 tumors	Tumor imaging	[99]
Fe_3O_4@$mSiO_2$	Fe_3O_4	MRI-T_2	r_2 = 137.8 (3.0 T)	SD female mouse bearing walk 256 tumors	Tumor imaging	[250]
HFe_3O_4@$mSiO_2$	Hollow Fe_3O_4	MRI-T_2	r_2 = 124.3 (3.0 T)	Kunming mice	Liver imaging	[241]

efficacy has indicated that it is not a perfect way to coat manganese oxide NPs for T_1-weighted MRI.

The accessibility of paramagnetic centers by water molecules plays a key role in improving the imaging efficacy of the paradigmatic gadolinium- or manganese-based MRI-T_1 CAs. Mesoporous materials provide an ideal platform to achieve this goal due to the following three reasons. Firstly, it has been demonstrated that the water molecules can diffuse anisotropically within mesopores along mesoporous channel;[217] Secondly, the paramagnetic centers can be highly dispersed into mesoporous channels due to the unique structural characteristics of mesopores, i.e., very large surface area, tunable pore sizes and high pore volume; Finally, the mesopores can behavior as the reservoirs for drugs molecules to combine the merits of chemotherapy and diagnosis into one matrix simultaneously. Based on these considerations, Lin et al grafted silane derivative, Gd-Si-DTTA complex, into mesopores of traditional MSNs to produce a novel but highly efficient T_1-weighted MRI CAs (**Figure 16**a_1).[91] The in vitro r_1 value could reach as high as 28.8 mM^{-1} s^{-1} (3.0 T) and 10.2 mM^{-1} s^{-1} (9.4 T). The in vivo results showed that Gd-MSNs could act as the highly efficient T_1-weighted MRI CAs for intravascular MR imaging (Figure 16a_2 and a_3) and an excellent T_2-weighted CAs for MR imaging of soft tissues when a higher dosage was applied (Figure 16a_4 and 3a_5). Such a high performance is attributed to the extremely high dispersity of Gd-based paramagnetic centers, making them easily interact with water molecules. In addition, Huang et al further modified the mesoporous surface by Gd-DTPA as a delivery system of gadolinium for efficient stem cell tracking.[92] Shao et al recently incorporated Gd_2O_3 clusters within mesopores

Adv. Mater. **2013**,
DOI: 10.1002/adma.201205292

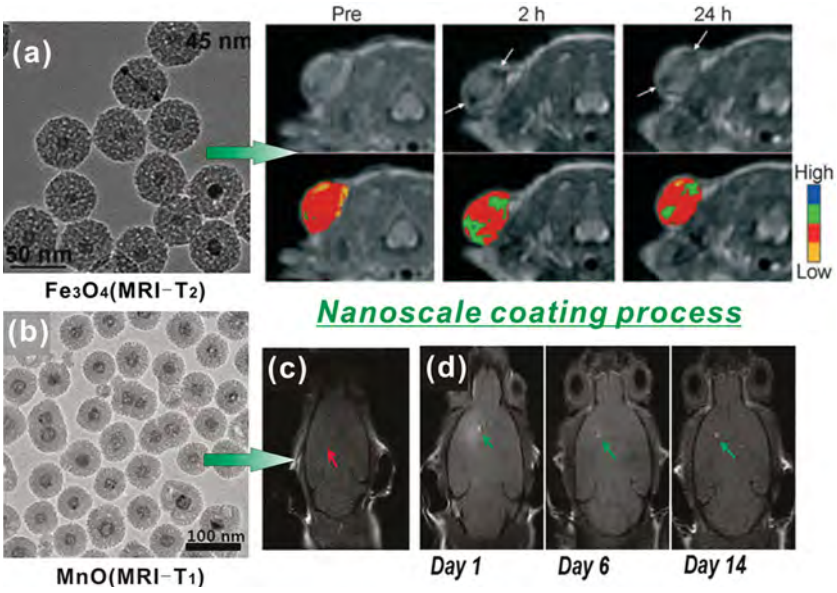

Figure 15. The preparation of core/shell structured mesoporous CAs for MRI by a nanoscale coating process. (a) TEM image of core/shell structured Fe_3O_4@$mSiO_2$ nanoparticles (left image) and in vivo T_2-weighted MRI of tumor-bearing nude mouse before and after intravenous administration of Fe_3O_4@$mSiO_2$ (right images). Reproduced with permission.[83] Copyright 2008, American Chemical Society. (b) TEM image of HMnO@$mSiO_2$. (c, d) *In vivo* MRI of transplanted MSCs before (c) and after (d) transplantation of HMnO@$mSiO_2$-labeled MSCs. Reproduced with permission.[209] Copyright 2011, American Chemical Society.

of MCM41-type MSNs (Figure 16b_1, designated as Gd_2O_3@MCM41), and carried out a systematic preclinical research of Gd_2O_3@MCM41 as MRI-T_1 CAs for tumor imaging.[218] The in vitro r_1 relaxivity of Gd_2O_3@MCM41 (13.48 $mM^{-1}s^{-1}$) was significantly higher than commercial Magnevist (Gd-DTPA, r_1 = 4.75 $mM^{-1}s^{-1}$) under the same test conditions. In vivo T_1-weighted MRI detection of tumor-bearing mouse showed that the MR signals of tumor tissues were significantly enhanced after intravenous administration of Gd_2O_3@MCM41 at the dose of 16 μmol/kg (Figure 16b_2) because of the accumulation of Gd_2O_3@MCM41 by EPR effect.

To optimize the MRI performance of manganese-based MRI CAs, we recently developed an *in-situ* redox process to introduce manganese-based NPs within mesopores by using well-defined mesopores as nanoreactors to disperse manganese paramagnetic centers as highly as possible (Figure 16c_1–c_3).[94] The principal is very similar to Lin's concept of highly dispersing Gd-based complexes within mesopores,[91] but the synthetic protocol is different, facile and economic, and much more beneficial to the MRI-T_1 imaging than the previous reported silica or mesoporous silica coating process. The relaxivity rate r_1 of MnOx-MSNs could reach 2.28 $mM^{-1}s^{-1}$, substantially larger than that of MnO NPs and their coated composites. Furthermore, it is known that manganese oxide NPs exhibits the weak acidity-induced dissolving behavior, therefore Mn^{II} in solid CAs is anticipated to be capable of pH-responsible release from the MnOx NPs dissolution to substantially improve the MRI-T_1 performances because the ionized Mn^{II} in liquid have the largest accessibilities to the surrounding water molecules. Additionally, the tumor tissue is more acidic than normal tissues due to the up-regulated glycolytic metabolism, increased generation of lactic acid and lowered cellular pH values thereafter.[219–221] Thus, the integration of MnOx NPs within MSNs could function as the pH-responsive MRI CAs for tumor detection. We chose HMSNs as the matrix to integrate with MnOx NPs (Figure 16c_4).[93] The relaxation rate r_1 of MnOx-HMSNs in the low pH solution (Figure 16c_5, pH = 5.0, r_1 = 8.81 $mM^{-1}s^{-1}$) increased significantly compared to those in the high one (pH = 7.4, r_1 = 0.79 $mM^{-1}s^{-1}$). Such a pH-responsible MRI performance enhancement is very beneficial to the detection of tumor microenvironment because the acidic nature of tumor tissues could greatly improve the performance of HMCNs for MRI, while the normal tissues with neutral essence do not show such an effect. In vivo evaluation showed that the intravenous administration of MnOx-HMSNs could induce the T_1-weighted positive contrast-enhanced MRI effect for tumor tissues. The tumor vasculature in the periphery showed a significant contrast enhancement at the initial stage, demonstrating the accumulation of HMCNs around the tumor tissue by the EPR effect (Figure 16c_6 and c_7). Importantly, the tumor interior exhibited gradual but strong T_1 contrast enhancements in the time course (Figure 16c_8–c_{10}). This effect is attributed to the leaching out of manganese ions responsible for the enhanced T_1-weighted MRI performances upon arriving at the weak acidic tumor microenvironment. This research demonstrated that HMSNs could be used as manganese ion-delivery carriers for in vivo tumor imaging with pH-sensitive effect.

4.2. In Vivo Optical Imaging

Compared with MRI, optical imaging is a versatile, economic and efficient modality for bio-imaging with high sensitivity, large rooms for probe selection and non-ionization safety. Various fluorescent molecules or nanomaterials, such as conventional organic fluorescein, semiconductor quantum dots (QDs), rare-earth co-doped upconversion nanophosphors, etc., have been explored to label and image cancer cells both in vitro and in vivo. Integrating mesoporous silica with fluorescent materials towards multifunctionalization could endow them with simultaneous optical bio-imaging and drug transport capabilities. Additionally, the silica matrix is optically transparent, which means that it has no significant influence on the excitation and emission of light when passing through the silica framework.

One generally adopted strategy towards fluorescent MSNs is to load or modify organic dyes with suitable wavelength (in the NIR range of "biological window": 700–900 nm[222]) into mesopores. Lo et al chose ICG, a FDA-approved NIR contrast agent with suitable excitation/emission wavelengths ($\lambda_{ex}/\lambda_{em}$ = 800/820 nm) in tissue transparent window and high in vivo signal to noise ratio, to be absorbed into the pores of trimethylammonium groups (TA) modified MSNs (MSNs-TA)

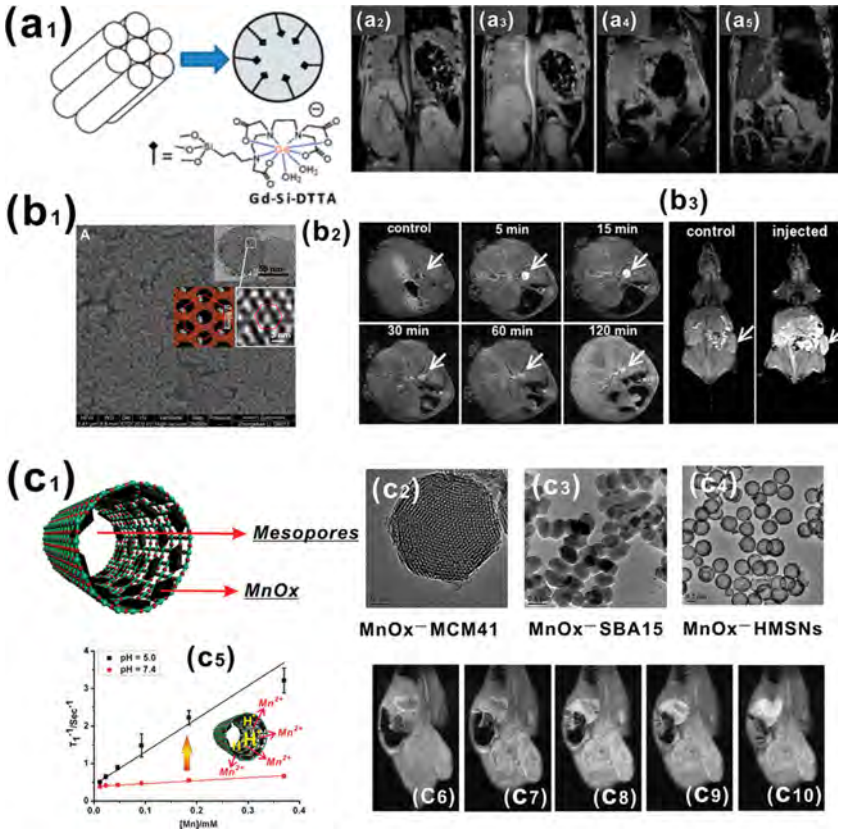

Figure 16. A representative MRI-T_1 CAs obtained using mesopores as the reservoirs for imaging Gd-Si-DTTA molecules. (a_1) Schematic illustration of the Gd-Si-DTTA grafting into mesopores of MSNs; T_1-weighted MRI of mouse showing an aorta signal enhancement before (a_2) and after (a_3) administration of Gd-Si-DTTA grafted MSNs; T_2-weighted MRI of mouse showing liver signal loss before (a_4) and after (a_5) administration of Gd-Si-DTTA grafted MSNs; Reproduced with permission.[91] Copyright 2008, American Chemical Society. (b_1) SEM image of Gd_2O_3@MCM41 (inset is the magnified HRTEM view and simulated supercell structure); (b_2) T_1-weighted MR imagings of the dynamic enhancements of mouse vasculature before and after the intravenous administration of Gd_2O_3@MCM41 nanoparticles for 5, 15, 30, 60 and 120 min; (b_3) T_1-weighted MR imaging of tumor-bearing mouse; Reproduced with permission.[218] Copyright 2012, Elsevier. (c_1) Scheme of the distribution of MnOx NPs within mesopores of MSNs; (c_2, c_3 and c_4) TEM images of MnOx-MCM41, MnOx-SBA15 and MnOx-HMSNs; (c_5) T_1 relaxivity of MnOx-HMSNs after 4 h soaking in buffer solution of different pH values (7.4 and 5.0); (c_6, c_7, c_8, c_9 and c_{10}) T_1-weighted MR imaging of tumor before (c_6) and after intravenous administration of MnOx-HMSNs (c_7: 5 min, c_8: 15 min, c_9: 30 min and c_{10}: 60 min). Reproduced with permission.[94] Copyright 2012, Elsevier.

by electrostatic attraction.[89] The ICG molecules were highly dispersed within mesopores to avoid the self-quenching and degradation. From the fluorescent spectra, it was found that ICG molecules were very stable in neutral and acidic conditions (**Figure 17**a). In vivo fluorescent imaging tests showed that a rather strong and stable fluorescence signal of the MSNs-TA-ICG NPs could be found prominent in the liver ($\lambda_{ex}/\lambda_{em}$ = 800/820 nm, Figure 17d and 17e), while the fluorescence of control MSNs-NH_2-FITC NPs was significantly interfered by the autofluorescence of the hair, skin, urine, viscera, intestine and bladder ($\lambda_{ex}/\lambda_{em}$ = 492/518 nm, Figure 17b and 17c). Chen et al conjugated near-infrared dye ZW800 into MSNs for the optical imaging of a tumor draining sentinel lymph nodes (SLNs).[223] The excitation and emission wavelengths of ZW800-modified MSNs were 770 nm and 795 nm, respectively (Figure 17f). After intravenous administration of such fluorescent MSNs, the probes maintained the fluorescent signals, demonstrating that no quenching effect had occurred on ZW800-modifed MSNs in vivo (Figure 17g). Further optical imaging using 4T1 tumor metastatic model demonstrated that ZW-800-modified MSNs could accumulate in and image the tumor metastatic SLNs (T-SLNs) even after 21 d post-injection (Figure 17j), which was rather similar to bioluminescent signals generated by the injection of the substrate of luciferase (Figure 17h and i) becasue the injected substrate of luciferase could initiate the intrinsic bioluminescent signals upon interacting with metastatic 4T1 cancer cells.

Although the traditional organic dyes have the advantages of excellent biocompatibility, easy preparation and cost-effectiveness, these dyes are prone to bio-erosion, degradation and easy quenching. NPs-based phosphors show the characteristics of tunable wavelengths, high quantum yields, photostability and high resistance to photobleaching, thus very promising in optical bio-imaging. A typical strategy for fluorescent MSNs is to coat mesoporous silica shell onto the surface of fluorescent nanocrystals. Pan et al synthesized PEGylated liposome-coated quantum dots (QDs)/mesoporous silica core/shell NPs for molecular imaging.[224] This strategy simultaneously increases the biocompatibility/stability of QDs and the optical imaging efficiency in labeling cancer cells. The cytotoxicity of traditional Cd-based semiconductor QDs, however, is a serious restriction for their further in vivo translations, and substitutes for them are urgently promoted.[225,226] Rare-earth-based upconversion fluorescent NPs exhibit strong fluorescence under the excitation of 980 nm laser. Especially, because the NIR-Vis upconversion fluorescence possesses high tissue penetration and is unaffected by autofluorescence of tissues, rare-earth nanophosphors capable of NIR-Vis upconversion exhibit much more application prospects than semiconductor QDs for optical bio-imaging, and have been extensively exploited as fluorescent labels in the living cell and whole-body small animal imaging.[227–229] It is also noted that rare-earth nanophosphors have low toxicities due to the absence of heavy metal ions such as Cd. Inspired by previous Hyeon's work on the phase transformation by the surfactants and subsequent sol-gel coating process using the same SDAs,[83,84] we recently successfully coated a thin mesoporous silica layer on the surface of monodispersed $NaYF_4$:Tm/Yb/Gd NPs. The whole particle size was controlled to be less than 50 nm (inset of Figure 17k),[88] which is very beneficial for further in vivo applications. The in vivo fluorescent imaging performances (Figure 17k–m) have been

Adv. Mater. 2013,
DOI: 10.1002/adma.201205292

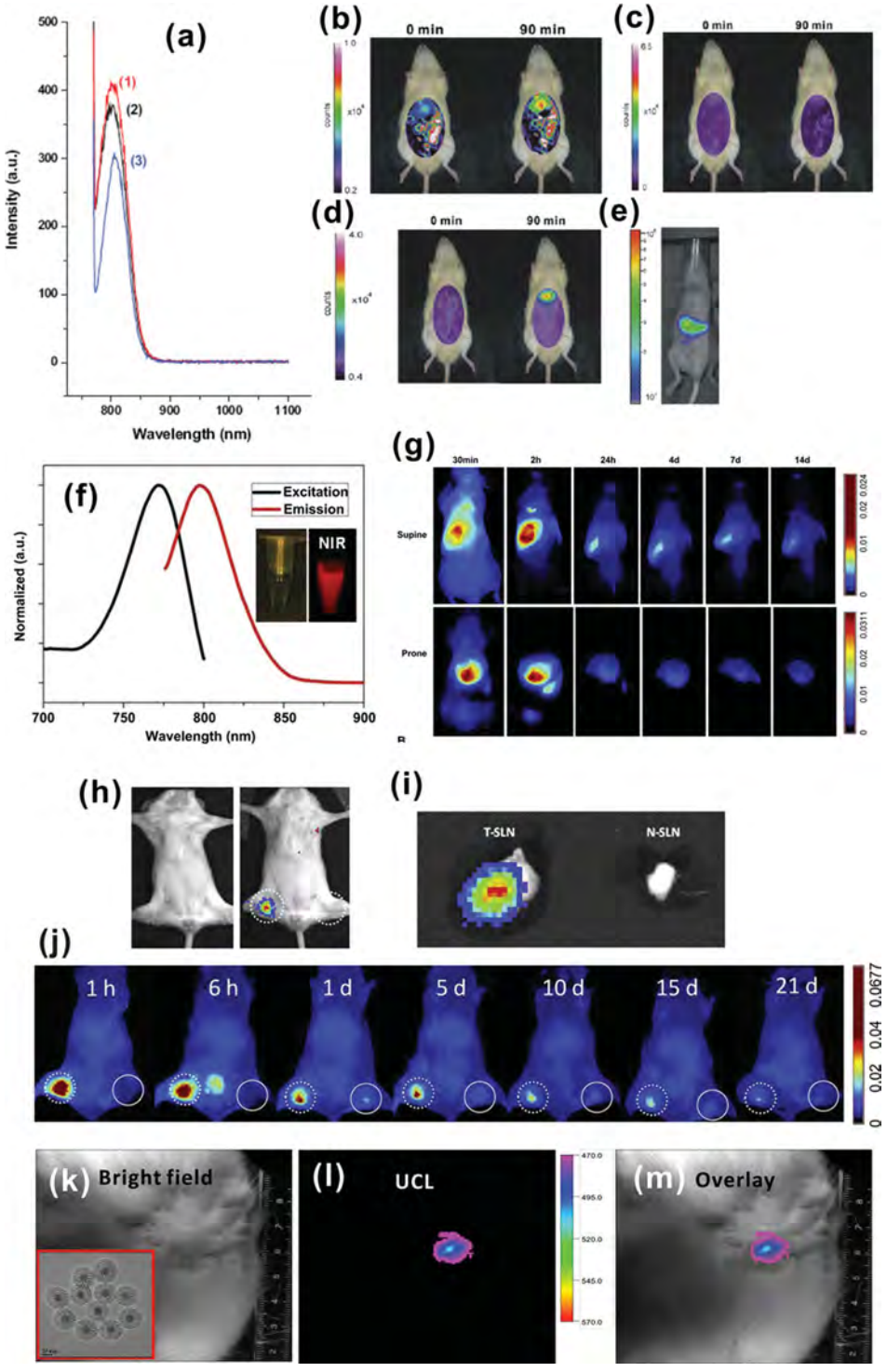

Figure 17. (a) Fluorescent spectra of ICG-loaded MSNs tested in different solutions (1: physiological buffer, 2: 20 mM HCl and 3: 20 mM NaOH); (b and c) In vivo fluorescent imagings before and after (90 min) the intravenous injection of MSNs-NH_2-FITC. The excitation and emission wavelengths were 492 nm and 518 nm, and the shutter time durations for b and c were 60 and 30 s, respectively; (d) In vivo fluorescent imagings in an anesthetized rat before and after injection of MSNs-TA-ICG for 90 min; (e) MSNs-TA-ICG in nude mice in 3 h post-intravenous injection; Reproduced with permission.[89] (f) Excitation and emission spectra of ZW800-modified MSNs; (g) In vivo optical imagings of ZW800-modified MSNs over time; (h) Tracking the tumor metastasis before (left) and after (right) the injection of the substrate of luciferase; (1) *Ex vivo* imagings of T-SLN (left) and N-SLN (right); (j) Fluorescent imagings of tumor metastatic lymph nodes after the injection of ZW800-modified MSNs at different time points (square dot: T-SLN and solid line: N-SLN); Reproduced with permission.[223] Copyright 2012, Elsevier. (k, l and m) upconversion luminescence tumor imagings before after (d, f and g) the administration of $NaYF_4$:Tm/Yb/Gd@$mSiO_2$ NPs (inset of k: TEM image of $NaYF_4$:Tm/Yb/Gd@$mSiO_2$ nanocomposites). Reproduced with permission.[88]

preliminarily demonstrated after the intratumor administration of NPs.

Comparatively, silicon QDs possess the features of excellent biocompatibility and tunable fluorescent properties. Especially, they are much more biodegradable compared to other nanoparticulate phosphors. We have recently developed a bottom-up self-assembly strategy followed by a post thermal treatment to fabricate a new type of oxygen-deficient luminescent MSNs (ODL-MSNs) with controllable morphologies/sizes and integrated mesoporosity-luminescent property.[230] Such luminescent mesoporous materials can not only load and deliver therapeutic agents into cells, but can also luminescently image cells simultaneously by the introduced oxygen deficiency. Importantly, they are potentially much more biocompatible than other reported composite luminescent mesoporous material systems because of their pure silica composition. Such fabrication strategy also provides an alternative way to achieve fluorescent features by engineering the framework of MSNs. Furthermore, very recently we have successfully synthesized a novel kind of silicon QDs-containing mesoporous luminescent NPs by directly in situ carbonizing the surfactant used for directing the formation of mesostructure, during which part of the silica framework was reduced into fluorescent silicon QDs accompanying the formation of carbon in the mesopore channels. Such a framework-functionalized MSNs is capable of loading and delivering hydrophobic anticancer drugs (CPT: 68 mg/g) by the π-π stacking between graphite-like carbon and the insoluble CPT molecules, and simultaneously illuminating the cells in the meantime of drug delivery via intracelluar endocytosis by the Si-QDs embeded in the fraework.[231]

In addition to the successful examples of using ICG and ZW800 incorporated MSNs for preliminary in vivo fluorescent bio-imaging, very few fluorescent mesoporous systems have been stepped into the in vivo stage. Compared to organic fluorescein, inorganic semiconductor QDs show much more application potentials due to their excellent fluorescent properties. However, the toxicity, degradability and excretion of the heavy metal-containing nanophosphors must be taken into consideration. Comparatively, upconversion fluorescent NPs or fluorescent silicon QDs are more priorable from the viewpoint of biocompatibility. However, such biocompatible fluorescent NPs are seldom integrated with mesoporous materials for *in vivo* diagnostic imaging because this research is still in its burgeoning stage and the synthetic techniques for those upconversion nanophosphors or silicon QDs are under development. It is anticipated that upconversion nanophosphors- or silicon QDs-based mesoporous systems are the promising CAs for bio-optical imagings, which need further extensive exploration in the future.

4.3. Other MSN-Based Imaging Modalities for In Vivo Applications

In addition to above MRI and fluorescent agents integrated with MSNs, radionuclide can be introduced into MSNs for PET imaging. It is known that PET is a highly sensitive imaging modality clinically for tumor early-diagnosis. It also possesses the advantages of unlimited depth penetration and

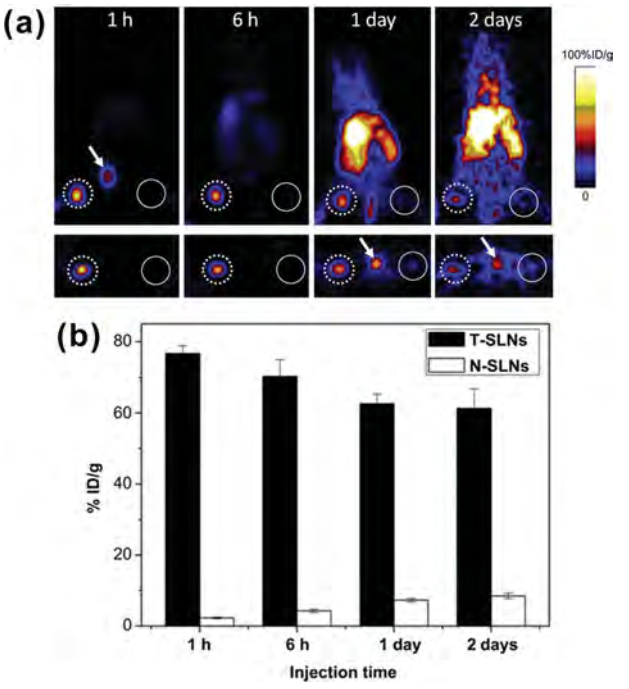

Figure 18. (a) PET imagings of T-SLN (square dot) and N-SLN (solid line) after the intravenous injection of ^{64}Cu-modified MSNs for different time durations (Top: cross section, bottom: transverse section); (b) Quantitative comparison of signal intensities between T-SLN and N-SLN. Reproduced with permission.[223] Copyright 2012, Elsevier.

having a broad range of probes. Chen et al developed radionuclide ^{64}Cu chelated MSNs for in vivo long-term PET imaging of tumor draining sentinel lymph node (SLNs).[223] As shown in **Figure 18**a, the tumor metastatic SLNs (T-SLNs) showed significant radioactivity accumulation compared to normal contra-lateral SLNs (N-SLNs) in 1 h, 6 h, 1 day and 2 days after irradiation. The quantitative results show that signal intensity in T-SLNs was about 35 and 7 folds higher than those in N-SLNs in 1 h and 2 days (Figure 18b), which gives an excellent example of MSNs-based PET probes for the visualization of tumor draining SLNs.

Ultrasound imaging is famous in clinical diagnosis because of its various advantages such as non-invasiveness, non-ionizing, real-time and economy. Compared to clinical MRI, CT or PET, the sensitivity and resolution of ultrasonography is relatively lower. One of the solutions is to develop its CAs with high performances. Although traditional organic microbubbles can enhance the contrast of ultrasonography, the large particle sizes (usually in micrometer size) and instability of these bubbles make them difficult to realize the diagnosis of diseases at their early stages. Recently developed hollow silica NPs showed the excellent echogenic behaviors,[232–235] and they have been preliminarily employed as the CAs for ultrasound imaging of small tumors.[236] Comparatively, HMSNs are much more superior for ultrasonographic applicaiton than non-porous hollow silica NPs because of their well-defined mesoporosity, which can further function as the reservoir for therapeutic and/or phase-transforming agents. We for the first time fabricated monodispersed HMSNs with well-defined mesoporosity for

Adv. Mater. **2013**,
DOI: 10.1002/adma.201205292

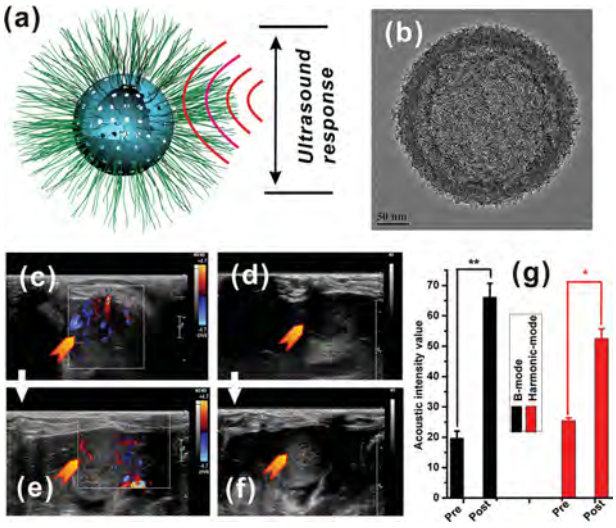

Figure 19. (a) Scheme of PEGylated MnOx-HMSNs and (b) its TEM image; (c-f) In vivo liver tumor ultrasonograms of pre- (c, d) and post- (e, f) puncture administrations of PEGylated MnOx-HMSNs under the guidance of ultrasound imaging (10 mg/mL, 1 mL) using rabbits bearing VX2 tumor as animal model in harmonic (c, e) and conventional B-mode (d, f); (g) The in vivo acoustic intensities (gray value) of the tumor before and after the administration of HMCNs ($n = 3$, $*P < 0.05$, $**P < 0.01$). Reproduced with permission.[93] Copyright 2012, Elsevier.

in vivo ultrasound tumor imaging.[93] The fabricated HMSNs showed well-defined spherical morphology with large hollow interiors (**Figure 19**a and b), and their surface was further PEGylated to improve their stability in saline solution. In vivo assay of the ultrasound contrast-enhanced performances using HMSNs as the CAs was carried out employing New Zealand white rabbits bearing VX2 liver tumor as the disease model. The significant contrast enhancement at the tumor site could be found (Figure 19e and f) after puncture administration of NPs under the ultrasound guidance compared to the control rabbit (Figure 19c and d) under both harmonic- and B-mode, which was further demonstrated by the remarkable increase in quantitative gray values of tumor tissues (Figure 19g). Such an in vivo result suggests that HMSNs can potentially function as the ultrasonographic CAs for the real-time guidance to determine the tumor tissue margins during the surgical process.[93,197,237]

4.4. In vivo Multi-Modality Imaging and Theranostic Applications

Each imaging modality has its intrinsic strengths and limitations.[238] For example, MRI possesses the high spatial resolution, but its sensitivity is relatively low. Optical imaging shows the high sensitivity but the depth penetration of visible light is strongly limited. Comparatively, PET imaging exhibits the very high sensitivity and unlimited depth penetration, but brings about the risks of radiation exposure and high cost. Using MSNs as an integrating platform, smart combinations of different types of imaging modalities with MSNs enable the development of multifunctional nanomedical platforms for multi-modality imagings and/or simultaneous theranostic applications. For example, the integration of fluorescent and magnetic materials can produce bi-modality bio-imaging probes which combines the merits of high sensitivity of fluorescent imaging, noninvasiveness and high spatial resolution of MR imaging for real-time monitoring the evolution of disease as well.[239] Additionally, the integration of MRI and ultrasound imaging shows the clinical potentials because ultrasound can be employed in the surgical process for real-time monitoring and guidance to determine the lesion tissue margins, where MRI can be used for the pre-surgical evaluations.[93] Based on MSNs, Huang et al developed a triple-model nanoprobe by embedding near-infrared dye ZW800 for optical imaging, conjugation of Gd-Si-DTPA for T_1-weighted MRI and labeling with radionuclide ^{64}Cu by chelating chemistry for PET imaging. These multifunctional probes were highly stable, which were further used for longitudinal multimodal imaging to visualize tumor draining sentinel lymph nodes up to three weeks in a 4T1 tumor metastatic model.[223]

MSNs can not only be employed as the compartmental reservoirs for the single or multiple loading of different imaging agents, they can also be further used as the drug carriers for in vivo therapeutic purposes (theranostic function).[99,188,225,240,241] Hyeon et al covalently linked multiple small Fe_3O_4 NPs onto the surface of dye-doped MSNs towards improved simultaneous MRI and anticancer drug (DOX) delivery.[99] In vivo passive targeting and accumulation of these NPs at tumor sites enabled simultaneous T_2-weighted MRI and fluorescent imaging. DOX was successfully delivered to the tumor sites to induce the apoptosis of cancer cells. Stucky et al prepared a fluorescent/magnetic mesoporous NPs for fluorescent and MR bi-modal diagnostic imagings and as the drug (DOX) carriers for magnetically targeted drug delivery.[242] The middle SiO_2 layer between lanthanide-doped upconversion $NaYF_4$ shell and magnetic Fe_3O_4 inner cores were removed by NaOH etching to enhance the drug loading capacity. The promoted particle accumulation via EPR effect and magnetic field greatly suppressed the tumor growth (96%), much higher than free DOX (35%) and the groups without the exposure to the magnetic field (58%). Very recently, we have developed a general polyelectrolyte-mediated self-assembly technique to prepare magnetic/fluorescent bi-functional mesoporous composites as the effective biological bimodal imaging probe and magnetically targeted anticancer drug delivery systems.[239] The positively charged polyelectrolyte (PAH) and negatively charged QDs were successfully and homogeneously assembled onto the surface of ellipsoidal Fe_3O_4@SiO_2@mSiO_2 composite nanostructures by charge modulations. The presence of solid/mesoporous silica layers between the black magnetic NPs and QDs efficiently prevented fluorescence quenching of the QDs.[239,243] The high biocompatibility of the achieved NPs was demonstrated by a cell-cytotoxicity assay, hemolyticity against human red blood cells, and coagulation evaluation of fresh human blood plasma. The bi-modal imaging properties were assessed by confocal microscopic observations of labeling cancer cells and preliminary in vivo evaluation. This synthetic strategy also provides a general but versatile route for incorporating diverse functions into single mesoporous composite NPs. Furthermore, we recently assembled Au nanorods onto the surface of magnetic

mesoporous NPs to obtain a multifunctional platform with MR/thermal dual-modality bio-imagings and simultaneous NIR-induced hyperthermia and chemotherapy.[244] In addition, we designed a novel type of multifunctional hollow nanostructures with hollow interiors, magnetic and mesoporous double-shells by *in situ* decomposition/reduction of a β-FeOOH nanorod core and organosilicate-incorporated silica-shell precursor, which were further covalently conjugated by rhodamine B isothiocyanate (RBITC) and PEG chains for fluorescent cell-labeling and improving their biocompatibility.[241] The achieved hollow magnetic mesoporous NPs have excellent blood compatibility and very low cytotoxicity against HeLa and MCF-7 cells. In vivo MRI results show that the hollow nanocomposites could be used as the T_2-weighted MRI CAs for preferentially imaging liver and spleen. Importantly, these hollow magnetic mesoporous nanocomposites show high loading capacity for water-insoluble anticancer drugs (docetaxel or CPT), and the drug-loaded NPs exhibit greater cytotoxicity than the corresponding free drugs.

Although MSNs with the integrated advantages of each functional component are promising in nano-biomedicine for synchronous efficient diagnosis and therapy, it does not mean that integrating more functions is the better. The multifunctional MSNs with complex structures and compositions need much more systematic and strict in vivo evaluations of their biological behaviors than those with fewer functions. Generally, the potential toxicity of MMSNs is related to two factors: free metal ion leaching from the encapsulated CAs, and the altered biodistribution, profiles of degradation and excretion routes. Based on this consideration, the most important prerequisite for designing multifunctional MSNs is to choose biocompatible functional modules to be integrated with MSNs. The subsequent considerations may be focused on how to integrate every functional module with mesoporous materials based on the organic/inorganic synthetic chemistry.

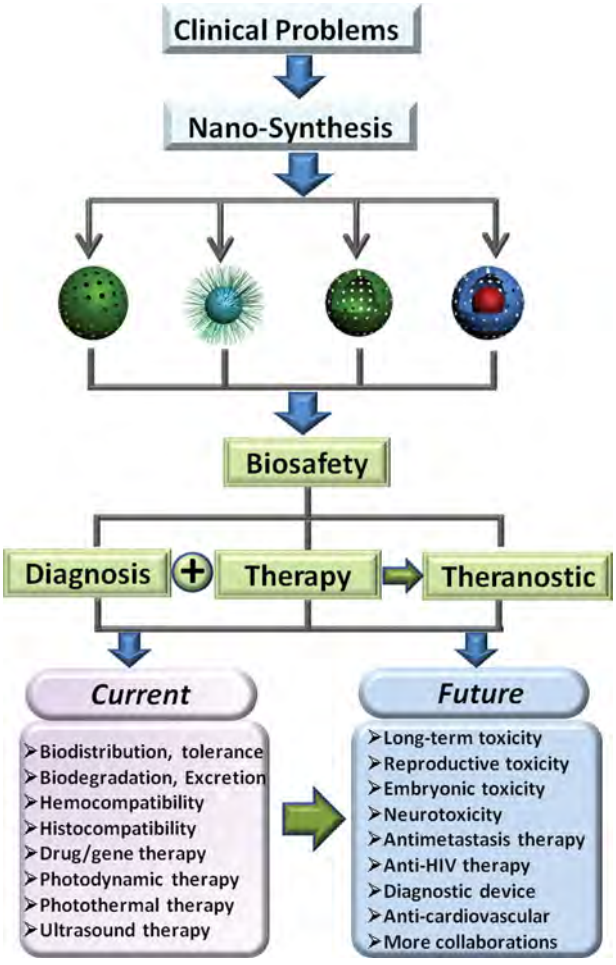

Figure 20. Research protocals, co-relationships among biosafety assay, therapy, diagnostic imaging and theranostics, and current status and future directions of MSNs-based NPs for nano-biomedical applications.

5. Concluding Remarks

The extensive researches have greatly promoted the transformation of nano-technological and nano-biomedical investigations of MSNs from in vitro assays into in vivo evaluations using small-animal models, which mainly focus on the bio-safety evaluations, therapeutic and diagnostic (or theranostic) applications of chemically engineered MSNs, especially on oncology (**Figure 20**). The bio-safety evaluations are the first prerequisite throughout the whole diagnostic imaging and therapeutic processes of diseases. From the materials' point of view, the chemically designed and fabricated MSNs are the bases to cope with the clinical issues. Due to the complex in vivo physiological environment, the structural, compositional and morphological characteristics of MSNs must be carefully tuned and optimized to meet the ever stricter standards for in vivo uses, such as particle size, pore structure, aggregation state, surface status and even the degradation rate, in vivo circulation time and penetration in biological tissues.

For in vivo bio-safety assays, the certified standard testing protocols concerning models, methods and biological platforms are urgently needed while they are still rare and currently under development, by which the data and results obtained from different laboratories will become comparable with each other. Furthermore, the evaluations against the potential risks of MSNs in animal models should be further extended from the assays of acute and subchronic toxicities to chronic toxicities. Although many in vivo results have confirmed the biocompatibility of MSNs, the bio-safety of MSNs-based NPs within the complex biological environment is still far from definition due to the lack of practical clinical trials in human bodies. Additionally, the bio-safety assays should be converted from the general toxicities against major organs and tissues into some specific aspects, such as neurotoxicity and reproductive toxicity. The impact of MSNs on the embryonic development needs to be confirmed in the future. It has been demonstrated that low doses of pristine and oxidized single-wall carbon nanotubes affect the mammalian embryonic development.[245] The influence of MSNs on the embryonic development is still unclear. Although a recent result has demonstrated that the exposure of zebrafish embryos to MSNs did not influence the embryo development and survival,[246] the effect of MSNs on the embryonic development on mammalian still remains unknown.

Adv. Mater. **2013**,
DOI: 10.1002/adma.201205292

For the therapeutic purposes, the degradation behaviors of MSNs still need to be clarified and tuned. Although MSNs can be metabolized into clearable silicate species, the biodegradation rate may be extremely slow in many cases. The therapeutic process is always combined with continuous administration at the special time intervals to achieve the desired drug accumulation. The low degradation rate of the carriers will undoubtedly result in high in vivo accumulation of MSNs after the continuous injection, which might bring about the unexpected toxicity especially in a long term. Preparation of MSNs with hollow interiors to enhance the drug loading capacity is an alternative route to reduce the frequency of administration, thus the accumulation of the carriers can be considerably reduced. To circumvent the accumulation problems of MSNs in organs, the tailoring of the framework compositions to control the degradation behaviors of MSNs should be further considered and attempted. In addition, the strategies of surface engineering should be further developed to overcome the non-specific uptake by mononuclear phagocytic cells and non-targeted cells. Although traditional PEGylation seems to be effective to some extent, the quick and extensive accumulation of MSNs in RES organs such as liver and spleen is still unavoidable, which has now become one of the most prominent problems faced by researches in the field. Thus, the exploration of new targeting ligands to be modified onto the surfaces of MSNs for enhanced drug accumulation at specific cells or sub-cellular organelles but substantially reduced accumulation in RES organs is highly desirable. More essentially, it will be of greater importance to find new and more effective targeting strategies to increase the active tumor cell endocytosis while minimizing the nonspecific uptakes by normal cells/tissues, thus to accomplish the requirements of different patient diseases for personalized medicine.

The biocompatibility of integrated components in the multifunctionalization of MSNs must be kept in the forefront to produce clinically applicable nanoscale formulations. The biomedical applications of MMSNs are not confined to already available therapeutic modalities, such as synergistic therapy, stimuli-responsive drug release, circumvention of drug resistance, traditional theranostics, photothermal/photodynamic therapy, as detailed in this review. Newly emerging applications should be explored using MSNs-based theranostic nano-platform, such as antimetastasis of cancer cells, anti-HIV therapy, blood purification, anti-cardiovascular diseases in terms of disease theray; and other imaging modalities such as computed tomography and photoacoustic imaging in terms of diagnosis. Although it is too early to assert the future successful clinical translation of these MMSNs, the rapid development of new conceptually designed NPs and their unprecedented advantages have shown a promising landscape for the creation of next-generation MSNs-based nanobiomaterials for clinical use.

Although extensive researches have strongly promoted the in vivo nanomedical applications of MSNs forward, large gaps between the synthesis and in vivo applications of MSNs is still present. The rapid progress of nano-synthetic chemistry enables the generation of diverse MSNs-based nanobiomaterials. These NPs have only undergone very preliminary in vitro and in vivo evaluations compared to their individual counterparts. Very few NPs had the opportunities to be evaluated systematically for in vivo use. Such progresses on the synthesis can promote the progress of nano-synthetic chemistry to some extent, but the further in vivo applications are still severely restricted due to the preliminary status of these assays and the strict restrictions for clinic trials. One of the other main reasons is the lack of more tacit and close cooperation between scientists, doctors and technicians from various fields, such as chemical, material, pharmaceutical areas, and even from the companies. Only the simplest MSNs have been being critically and systematically assessed, which have shown the promising clinical translation potentials. Bearing this in mind, more strengths and closer collaborations among experts from different related fields should be devoted to the promotion of MSNs-based "magic bullet" into preclinical and clinical stages, which is highly desired and expected to contribute greatly to the human health and personalized medicine in the near future.

Acknowledgements

This work was supported by the National Nature Science Foundation of China (Grant No. 51132009, 51072212), the National Basic Research Program of China (973 Program, Grant No. 2011CB707905), China National Funds for Distinguished Young Scientists (Grant No.51225202), and Foundation for Youth Scholar of State Key Laboratory of High Performance Ceramics and Superfine Microstructures (Grant No. SKL201203).

Received: December 24, 2012
Revised: February 27, 2013
Published online:

[1] K. Riehemann, S. W. Schneider, T. A. Luger, B. Godin, M. Ferrari, H. Fuchs, *Angew. Chem. Int. Ed.* **2009**, *48*, 872.
[2] M. C. Daniel, D. Astruc, *Chem. Rev.* **2004**, *104*, 293.
[3] J. C. Love, L. A. Estroff, J. K. Kriebel, R. G. Nuzzo, G. M. Whitesides, *Chem. Rev.* **2005**, *105*, 1103.
[4] M. Ferrari, *Nat. Rev. Cancer* **2005**, *5*, 161.
[5] I. W. Hamley, *Angew. Chem. Int. Ed.* **2003**, *42*, 1692.
[6] V. Wagner, A. Dullaart, A. K. Bock, A. Zweck, *Nat. Biotechnol.* **2006**, *24*, 1211.
[7] S. M. Moghimi, A. C. Hunter, J. C. Murray, *FASEB Journal* **2005**, *19*, 311.
[8] R. K. Jain, T. Stylianopoulos, *Nat. Rev. Clin. Oncol.* **2010**, *7*, 653.
[9] M. Vallet-Regi, F. Balas, D. Arcos, *Angew. Chem. Int. Ed.* **2007**, *46*, 7548.
[10] K. E. Uhrich, S. M. Cannizzaro, R. S. Langer, K. M. Shakesheff, *Chem. Rev.* **1999**, *99*, 3181.
[11] H. Koo, M. S. Huh, J. H. Ryu, D. E. Lee, I. C. Sun, K. Choi, K. Kim, I. C. Kwon, *Nano Today* **2011**, *6*, 204.
[12] O. Veiseh, C. Sun, J. Gunn, N. Kohler, P. Gabikian, D. Lee, N. Bhattarai, R. Ellenbogen, R. Sze, A. Hallahan, J. Olson, M. Q. Zhang, *Nano Lett.* **2005**, *5*, 1003.
[13] K. Y. Lee, D. J. Mooney, *Chem. Rev.* **2001**, *101*, 1869.
[14] X. Wang, H. Chen, Y. Chen, M. Ma, K. Zhang, F. Li, Y. Zheng, D. Zeng, Q. Wang, J. Shi, *Adv. Mater.* **2012**, *24*, 785.
[15] Y. Chen, H. R. Chen, Y. Sun, Y. Y. Zheng, D. P. Zeng, F. Q. Li, S. J. Zhang, X. Wang, K. Zhang, M. Ma, Q. J. He, L. L. Zhang, J. L. Shi, *Angew. Chem. Int. Ed.* **2011**, *50*, 12505.
[16] W. Rima, L. Sancey, M.-T. Aloy, E. Armandy, G. B. Alcantara, T. Epicier, A. Malchère, L. Joly-Pottuz, P. Mowat, F. Lux, O. Tillement, B. Burdin, A. Rivoire, C. Boulé, I. Anselme-Bertrand, J. Pourchez, M. Cottier, S. Roux, C. Rodriguez-Lafrasse, P. Perriat, *Biomaterials* **2013**, *34*, 181.

[17] M. Hossain, M. Su, *J. Phy. Chem. C* **2012**, *116*, 23047.
[18] S. Lal, S. E. Clare, N. J. Halas, *Acc. Chem. Res.* **2008**, *41*, 1842.
[19] M. Hu, J. Y. Chen, Z. Y. Li, L. Au, G. V. Hartland, X. D. Li, M. Marquez, Y. N. Xia, *Chem. Soc. Rev.* **2006**, *35*, 1084.
[20] X. H. Huang, I. H. El-Sayed, W. Qian, M. A. El-Sayed, *J. Am. Chem. Soc.* **2006**, *128*, 2115.
[21] D. K. Chatterjee, L. S. Fong, Y. Zhang, *Adv. Drug Deliv. Rev.* **2008**, *60*, 1627.
[22] P. Juzenas, W. Chen, Y. P. Sun, M. A. N. Coelho, R. Generalov, N. Generalova, I. L. Christensen, *Adv. Drug Deliv. Rev.* **2008**, *60*, 1600.
[23] C. F. van Nostrum, *Adv. Drug Deliv. Rev.* **2004**, *56*, 9.
[24] C. R. Thomas, D. P. Ferris, J. H. Lee, E. Choi, M. H. Cho, E. S. Kim, J. F. Stoddart, J. S. Shin, J. Cheon, J. I. Zink, *J. Am. Chem. Soc.* **2010**, *132*, 10623.
[25] M. Vallet-Regi, E. Ruiz-Hernandez, *Adv. Mater.* **2011**, *23*, 5177.
[26] E. Ruiz-Hernandez, A. Lopez-Noriega, D. Arcos, I. Izquierdo-Barba, O. Terasaki, M. Vallet-Regi, *Chem. Mater.* **2007**, *19*, 3455.
[27] E. Ruiz-Hernandez, A. Lopez-Noriega, D. Arcos, M. Vallet-Regi, *Solid State Sci.* **2008**, *10*, 421.
[28] C. T. Wu, W. Fan, Y. F. Zhu, M. Gelinsky, J. Chang, G. Cuniberti, V. Albrecht, T. Friis, Y. Xiao, *Acta Biomater.* **2011**, *7*, 3563.
[29] D. Arcos, V. Fal-Miyar, E. Ruiz-Hernandez, M. Garcia-Hernandez, M. L. Ruiz-Gonzalez, J. Gonzalez-Calbet, M. Vallet-Regi, *J. Mater. Chem.* **2012**, *22*, 64.
[30] D. Peer, J. M. Karp, S. Hong, O. C. FaroKhzad, R. Margalit, R. Langer, *Nat. Nanotechnol.* **2007**, *2*, 751.
[31] M. Elsabahy, K. L. Wooley, *Chem. Soc. Rev.* **2012**, *41*, 2545.
[32] Y. Chen, Y. Gao, H. R. Chen, D. P. Zeng, Y. P. Li, Y. Y. Zheng, F. Q. Li, X. F. Ji, X. Wang, F. Chen, Q. J. He, L. L. Zhang, J. L. Shi, *Adv. Funct. Mater.* **2012**, **22**, 1586–1597.
[33] S. Mornet, S. Vasseur, F. Grasset, E. Duguet, *J. Mater. Chem.* **2004**, *14*, 2161.
[34] S. Laurent, D. Forge, M. Port, A. Roch, C. Robic, L. V. Elst, R. N. Muller, *Chem. Rev.* **2008**, *108*, 2064.
[35] M. Arruebo, R. Fernandez-Pacheco, M. R. Ibarra, J. Santamaria, *Nano Today* **2007**, *2*, 22.
[36] X. Michalet, F. F. Pinaud, L. A. Bentolila, J. M. Tsay, S. Doose, J. J. Li, G. Sundaresan, A. M. Wu, S. S. Gambhir, S. Weiss, *Science* **2005**, *307*, 538.
[37] I. L. Medintz, H. T. Uyeda, E. R. Goldman, H. Mattoussi, *Nat. Mater.* **2005**, 4, 435–446.
[38] X. H. Gao, Y. Y. Cui, R. M. Levenson, L. W. K. Chung, S. M. Nie, *Nat. Biotechnol.* **2004**, *22*, 969.
[39] S. E. Skrabalak, J. Y. Chen, Y. G. Sun, X. M. Lu, L. Au, C. M. Cobley, Y. N. Xia, *Acc. Chem. Res.* **2008**, *41*, 1587.
[40] C. R. Patra, R. Bhattacharya, D. Mukhopadhyay, P. Mukherjee, *Adv. Drug Deliv. Rev.* **2010**, *62*, 346.
[41] R. R. Arvizo, S. Bhattacharyya, R. A. Kudgus, K. Giri, R. Bhattacharya, P. Mukherjee, *Chem. Soc. Rev.* **2012**, *41*, 2943.
[42] S. Beg, M. Rizwan, A. M. Sheikh, M. S. Hasnain, K. Anwer, K. Kohli, *J. Pharm. Pharm.* **2011**, *63*, 141.
[43] J. T. Robinson, S. M. Tabakman, Y. Y. Liang, H. L. Wang, H. S. Casalongue, D. Vinh, H. J. Dai, *J. Am. Chem. Soc.* **2011**, *133*, 6825.
[44] Z. Liu, J. T. Robinson, S. M. Tabakman, K. Yang, H. J. Dai, *Mater. Today* **2011**, *14*, 316.
[45] H. F. Bao, J. P. Yang, Y. Huang, Z. P. Xu, N. Hao, Z. X. Wu, G. Q. Lu, D. Y. Zhao, *Nanoscale* **2011**, *3*, 4069.
[46] M. J. Masarudin, K. Yusoff, R. A. Rahim, M. Z. Hussein, *Nanotechnology* **2009**, *20*, DOI: 10.1088/0957-4484/20/4/045602.
[47] J. M. Rosenholm, V. Mamaeva, C. Sahlgren, M. Linden, *Nanomedicine* **2012**, *7*, 111.
[48] Website: http://www.accessdata.fda.gov/scripts/fcn/gras_notices/GRN000321.pdf.
[49] S. P. Rigby, M. Fairhead, C. F. van der Walle, *Curr. Pharm. Design* **2008**, *14*, 1821.
[50] M. Mahkam, *Curr. Drug Deliv.* **2011**, *8*, 607.
[51] M. Benezra, O. Penate-Medina, P. B. Zanzonico, D. Schaer, H. Ow, A. Burns, E. DeStanchina, V. Longo, E. Herz, S. Iyer, J. Wolchok, S. M. Larson, U. Wiesner, M. S. Bradbury, *J. Clin. Invest.* **2011**, *121*, 2768.
[52] A. Baeza, E. Guisasola, E. Ruiz-Hernandez, M. Vallet-Regi, *Chem. Mater.* **2012**, *24*, 517.
[53] L. Xing, H. Q. Zheng, Y. Y. Cao, S. A. Che, *Adv. Mater.* **2012**, *24*, 6433.
[54] A. Schlossbauer, S. Warncke, P. M. E. Gramlich, J. Kecht, A. Manetto, T. Carell, T. Bein, *Angew. Chem. Int. Ed.* **2010**, *49*, 4734.
[55] E. Climent, R. Martinez-Manez, F. Sancenon, M. D. Marcos, J. Soto, A. Maquieira, P. Amoros, *Angew. Chem. Int. Ed.* **2010**, *49*, 7281.
[56] E. Ruiz-Hernandez, A. Baeza, M. Vallet-Regi, *ACS Nano* **2011**, *5*, 1259.
[57] Y. Chen, P. Xu, H. Chen, Y. Li, W. Bu, Z. Shu, Y. Li, J. Zhang, L. Zhang, L. Pan, X. Cui, Z. Hua, J. Wang, L. Zhang, J. Shi, *Adv. Mater.* **2013**, DOI: 10.1002/adma.201204685.
[58] J. S. Beck, J. C. Vartuli, W. J. Roth, M. E. Leonowicz, C. T. Kresge, K. D. Schmitt, C. T. W. Chu, D. H. Olson, E. W. Sheppard, S. B. McCullen, J. B. Higgins, J. L. Schlenker, *J. Am. Chem. Soc.* **1992**, *114*, 10834.
[59] C. T. Kresge, M. E. Leonowicz, W. J. Roth, J. C. Vartuli, J. S. Beck, *Nature* **1992**, *359*, 710.
[60] D. Y. Zhao, J. L. Feng, Q. S. Huo, N. Melosh, G. H. Fredrickson, B. F. Chmelka, G. D. Stucky, *Science* **1998**, *279*, 548.
[61] Y. Wan, D. Y. Zhao, *Chem. Rev.* **2007**, *107*, 2821.
[62] M. Vallet-Regi, A. Ramila, R. P. del Real, J. Perez-Pariente, *Chem. Mater.* **2001**, *13*, 308.
[63] C. Y. Lai, B. G. Trewyn, D. M. Jeftinija, K. Jeftinija, S. Xu, S. Jeftinija, V. S. Y. Lin, *J. Am. Chem. Soc.* **2003**, *125*, 4451.
[64] C. E. Ashley, E. C. Carnes, G. K. Phillips, D. Padilla, P. N. Durfee, P. A. Brown, T. N. Hanna, J. W. Liu, B. Phillips, M. B. Carter, N. J. Carroll, X. M. Jiang, D. R. Dunphy, C. L. Willman, D. N. Petsev, D. G. Evans, A. N. Parikh, B. Chackerian, W. Wharton, D. S. Peabody, C. J. Brinker, *Nat. Mater.* **2011**, *10*, 389.
[65] S. H. Wu, Y. S. Lin, Y. Hung, Y. H. Chou, Y. H. Hsu, C. Chang, C. Y. Mou, *Chembiochem* **2008**, *9*, 53.
[66] Q. J. He, Z. W. Zhang, F. Gao, Y. P. Li, J. L. Shi, *Small* **2011**, *7*, 271.
[67] H. Meng, M. Xue, T. Xia, Z. X. Ji, D. Y. Tarn, J. I. Zink, A. E. Nel, *ACS Nano* **2011**, *5*, 4131.
[68] Q. J. He, J. M. Zhang, J. L. Shi, Z. Y. Zhu, L. X. Zhang, W. B. Bu, L. M. Guo, Y. Chen, *Biomaterials* **2010**, *31*, 1085.
[69] R. I. Nooney, D. Thirunavukkarasu, Y. M. Chen, R. Josephs, A. E. Ostafin, *Chem. Mater.* **2002**, *14*, 4721.
[70] X. L. Huang, X. Teng, D. Chen, F. Q. Tang, J. Q. He, *Biomaterials* **2010**, *31*, 438.
[71] Y. Chen, H. R. Chen, L. M. Guo, Q. J. He, F. Chen, J. Zhou, J. W. Feng, J. L. Shi, *ACS Nano* **2010**, *4*, 529.
[72] L. M. Pan, Q. J. He, J. N. Liu, Y. Chen, M. Ma, L. L. Zhang, J. L. Shi, *J. Am. Chem. Soc.* **2012**, *134*, 5722.
[73] J. Kobler, K. Moller, T. Bein, *ACS Nano* **2008**, *2*, 791.
[74] V. Cauda, A. Schlossbauer, J. Kecht, A. Zurner, T. Bein, *J. Am. Chem. Soc.* **2009**, *131*, 11361.
[75] M. Mizutani, Y. Yamada, T. Nakamura, K. Yano, *Chem. Mater.* **2008**, *20*, 4777.
[76] M. H. Kim, H. K. Na, Y. K. Kim, S. R. Ryoo, H. S. Cho, K. E. Lee, H. Jeon, R. Ryoo, D. H. Min, *ACS Nano* **2011**, *5*, 3568.
[77] S. B. Hartono, W. Y. Gu, F. Kleitz, J. Liu, L. Z. He, A. P. J. Middelberg, C. Z. Yu, G. Q. Lu, S. Z. Qiao, *ACS Nano* **2012**, *6*, 2104.

[78] H. K. Na, M. H. Kim, K. Park, S. R. Ryoo, K. E. Lee, H. Jeon, R. Ryoo, C. Hyeon, D. H. Min, *Small* **2012**, *8*, 1752.
[79] Y. S. Li, J. L. Shi, Z. L. Hua, H. R. Chen, M. L. Ruan, D. S. Yan, *Nano Lett.* **2003**, *3*, 609.
[80] X. W. Lou, L. A. Archer, Z. C. Yang, *Adv. Mater.* **2008**, *20*, 3987.
[81] D. Chen, L. L. Li, F. Q. Tang, S. O. Qi, *Adv. Mater.* **2009**, *21*, 3804.
[82] Y. Deng, D. Qi, C. Deng, X. Zhang, D. Zhao, *J. Am. Chem. Soc.* **2008**, *130*, 28.
[83] J. Kim, H. S. Kim, N. Lee, T. Kim, H. Kim, T. Yu, I. C. Song, W. K. Moon, T. Hyeon, *Angew. Chem. Int. Ed.* **2008**, *47*, 8438.
[84] W. R. Zhao, J. L. Gu, L. X. Zhang, H. R. Chen, J. L. Shi, *J. Am. Chem. Soc.* **2005**, *127*, 8916.
[85] J. Kim, J. E. Lee, J. Lee, J. H. Yu, B. C. Kim, K. An, Y. Hwang, C. H. Shin, J. G. Park, T. Hyeon, *J. Am. Chem. Soc.* **2006**, *128*, 688.
[86] X. Yang, X. Liu, Z. Liu, F. Pu, J. Ren, X. Qu, *Adv. Mater.* **2012**, *24*, 2890.
[87] Z. Zhang, L. Wang, J. Wang, X. Jiang, X. Li, Z. Hu, Y. Ji, X. Wu, C. Chen, *Adv. Mater.* **2012**, *24*, 1418.
[88] J. N. Liu, W. B. Bu, S. J. Zhang, F. Chen, H. Y. Xing, L. M. Pan, L. P. Zhou, W. J. Peng, J. L. Shi, *Chem. Eur. J.* **2012**, *18*, 2335.
[89] C. H. Lee, S. H. Cheng, Y. J. Wang, Y. C. Chen, N. T. Chen, J. Souris, C. T. Chen, C. Y. Mou, C. S. Yang, L. W. Lo, *Adv. Funct. Mater.* **2009**, *19*, 215.
[90] J. Feng, S. Y. Song, R. P. Deng, W. Q. Fan, H. J. Zhang, *Langmuir* **2010**, *26*, 3596.
[91] K. M. L. Taylor, J. S. Kim, W. J. Rieter, H. An, W. L. Lin, W. B. Lin, *J. Am. Chem. Soc.* **2008**, *130*, 2154.
[92] J. K. Hsiao, C. P. Tsai, T. H. Chung, Y. Hung, M. Yao, H. M. Liu, C. Y. Mou, C. S. Yang, Y. C. Chen, D. M. Huang, *Small* **2008**, *4*, 1445.
[93] Y. Chen, Q. Yin, X. F. Ji, S. J. Zhang, H. R. Chen, Y. Y. Zheng, Y. Sun, H. Y. Qu, Z. Wang, Y. P. Li, X. Wang, K. Zhang, L. L. Zhang, J. L. Shi, *Biomaterials* **2012**, *33*, 7126.
[94] Y. Chen, H. Chen, S. Zhang, F. Chen, S. Sun, Q. He, M. Ma, X. Wang, H. Wu, L. Zhang, L. Zhang, J. Shi, *Biomaterials* **2012**, *33*, 2388.
[95] J. M. Rosenholm, E. Peuhu, L. T. Bate-Eya, J. E. Eriksson, C. Sahlgren, M. Linden, *Small* **2010**, *6*, 1234.
[96] J. M. Rosenholm, E. Peuhu, J. E. Eriksson, C. Sahlgren, M. Linden, *Nano Lett.* **2009**, *9*, 3308.
[97] C. P. Tsai, C. Y. Chen, Y. Hung, F. H. Chang, C. Y. Mou, *J. Mater. Chem.* **2009**, *19*, 5737.
[98] J. M. Rosenholm, A. Meinander, E. Peuhu, R. Niemi, J. E. Eriksson, C. Sahlgren, M. Linden, *ACS Nano* **2009**, *3*, 197.
[99] J. E. Lee, N. Lee, H. Kim, J. Kim, S. H. Choi, J. H. Kim, T. Kim, I. C. Song, S. P. Park, W. K. Moon, T. Hyeon, *J. Am. Chem. Soc.* **2010**, *132*, 552.
[100] Q. J. He, J. L. Shi, *J. Mater. Chem.* **2011**, *21*, 5845.
[101] P. P. Yang, S. L. Gai, J. Lin, *Chem. Soc. Rev.* **2012**, *41*, 3679.
[102] I. I. SlowingJ. L. Vivero-Escoto, C. W. Wu, V. S. Y. Lin, *Adv. Drug Deliv. Rev.* **2008**, *60*, 1278.
[103] J. L. Vivero-Escoto, Slowing, II, B. G. Trewyn, V. S. Y. Lin, *Small* **2010**, *6*, 1952.
[104] Y. S. Lin, K. R. Hurley, C. L. Haynes, *J. Phy. Chem. Lett.* **2012**, *3*, 364.
[105] J. E. Lee, N. Lee, T. Kim, J. Kim, T. Hyeon, *Acc. Chem. Res.* **2011**, *44*, 893.
[106] S. H. Wu, Y. Hung, C. Y. Mou, *Chem. Commun.* **2011**, *47*, 9972.
[107] M. Vallet-Regi, *Chem. Eur. J.* **2006**, *12*, 5934.
[108] B. G. Trewyn, Slowing, II, S. Giri, H. T. Chen, V. S. Y. Lin, *Acc. Chem. Res.* **2007**, *40*, 846.
[109] F. Q. Tang, L. L. Li, D. Chen, *Adv. Mater.* **2012**, *24*, 1504.
[110] Z. X. Li, J. C. Barnes, A. Bosoy, J. F. Stoddart, J. I. Zink, *Chem. Soc. Rev.* **2012**, *41*, 2590.
[111] J. Liu, S. Z. Qiao, J. S. Chen, X. W. Lou, X. R. Xing, G. Q. Lu, *Chem. Commun.* **2011**, *47*, 12578.
[112] Slowing, II, B. G. Trewyn, S. Giri, V. S. Y. Lin, *Adv. Funct. Mater.* **2007**, *17*, 1225.
[113] K. K. Coti, M. E. Belowich, M. Liong, M. W. Ambrogio, Y. A. Lau, H. A. Khatib, J. I. Zink, N. M. Khashab, J. F. Stoddart, *Nanoscale* **2009**, *1*, 16.
[114] H. Jaganathan, B. Godin, *Adv. Drug Deliv. Rev.* **2012**, *64*, 1800.
[115] I. I. Slowing, C. W. Wu, J. L. Vivero-Escoto, V. S. Y. Lin, *Small* **2009**, *5*, 57.
[116] C. Urata, H. Yamada, R. Wakabayashi, Y. Aoyama, S. Hirosawa, S. Arai, S. Takeoka, Y. Yamauchi, K. Kuroda, *J. Am. Chem. Soc.* **2011**, *133*, 8102.
[117] T. Yu, D. Hubbard, A. Ray, H. Ghandehari, *J. Control. Release* **2012**, *163*, 46.
[118] Q. J. He, J. L. Shi, F. Chen, M. Zhu, L. X. Zhang, *Biomaterials* **2010**, *31*, 3335.
[119] Q. J. He, Z. W. Zhang, Y. Gao, J. L. Shi, Y. P. Li, *Small* **2009**, *5*, 2722.
[120] X. L. Huang, L. L. Li, T. L. Liu, N. J. Hao, H. Y. Liu, D. Chen, F. Q. Tang, *ACS Nano* **2011**, *5*, 5390.
[121] X. L. Huang, J. Zhuang, X. Teng, L. L. Li, D. Chen, X. Y. Yan, F. Q. Tang, *Biomaterials* **2010**, *31*, 6142.
[122] J. Lu, Z. X. Li, J. I. Zink, F. Tamanoi, *Nanome-Nanotechnol.* **2012**, *8*, 212.
[123] J. M. Harris, R. B. Chess, *Nat. Rev. Drug Discov.* **2003**, *2*, 214.
[124] J. V. Jokerst, T. Lobovkina, R. N. Zare, S. S. Gambhir, *Nanomedicine* **2011**, *6*, 715.
[125] G. Pasut, F. M. Veronese, *J. Control. Release* **2012**, *161*, 461.
[126] T. Yu, K. Greish, L. D. McGill, A. Ray, H. Ghandehari, *ACS Nano* **2012**, *6*, 2289–2301.
[127] J. Lu, M. Liong, Z. X. Li, J. I. Zink, F. Tamanoi, *Small* **2010**, *6*, 1794.
[128] S. P. Hudson, R. F. Padera, R. Langer, D. S. Kohane, *Biomaterials* **2008**, *29*, 4045.
[129] T. L. Liu, L. L. Li, X. Teng, X. L. Huang, H. Y. Liu, D. Chen, J. Ren, J. Q. He, F. Q. Tang, *Biomaterials* **2011**, *32*, 1657.
[130] V. Cauda, A. Schlossbauer, T. Bein, *Micro. Meso. Mater.* **2010**, *132*, 60.
[131] Q. J. He, J. L. Shi, M. Zhu, Y. Chen, F. Chen, *Micro. Meso. Mater.* **2010**, *131*, 314.
[132] H. Yamada, C. Urata, Y. Aoyama, S. Osada, Y. Yamauchi, K. Kuroda, *Chem. Mater.* **2012**, *24*, 1462.
[133] J. S. Souris, C. H. Lee, S. H. Cheng, C. T. Chen, C. S. Yang, J. A. A. Ho, C. Y. Mou, L. W. Lo, *Biomaterials* **2010**, *31*, 5564.
[134] H. S. Choi, W. Liu, P. Misra, E. Tanaka, J. P. Zimmer, B. I. Ipe, M. G. Bawendi, J. V. Frangioni, *Nat. Biotechnol.* **2007**, *25*, 1165.
[135] Y. S. Lin, C. L. Haynes, *J. Am. Chem. Soc.* **2010**, *132*, 4834.
[136] T. L. Liu, L. L. Li, C. H. Fu, H. Y. Liu, D. Chen, F. Q. Tang, *Biomaterials* **2012**, *33*, 2399.
[137] T. Asefa, Z. Tao, *Chem. Res. Toxicol.* **2012**, *25*, 2265.
[138] L. L. Li, Y. Q. Guan, H. Y. Liu, N. J. Hao, T. L. Liu, X. W. Meng, C. H. Fu, Y. Z. Li, Q. L. Qu, Y. G. Zhang, S. Y. Ji, L. Chen, D. Chen, F. Q. Tang, *ACS Nano* **2011**, *5*, 7462.
[139] Y. F. Zhu, J. L. Shi, W. H. Shen, X. P. Dong, J. W. Feng, M. L. Ruan, Y. S. Li, *Angew. Chem. Int. Ed.* **2005**, *44*, 5083.
[140] W. R. Zhao, H. R. Chen, Y. S. Li, L. Li, M. D. Lang, J. L. Shi, *Adv. Funct. Mater.* **2008**, *18*, 2780.
[141] Y. F. Zhu, J. L. Shi, Y. S. Li, H. R. Chen, W. H. Shen, X. P. Dong, *Micro. Meso. Mater.* **2005**, *85*, 75.
[142] Y. F. Zhu, J. L. Shi, H. R. Chen, W. H. Shen, X. P. Dong, *Micro. Meso. Mater.* **2005**, *84*, 218.
[143] Z. G. Feng, Y. S. Li, D. C. Niu, L. Li, W. R. Zhao, H. R. Chen, J. H. Gao, M. L. Ruan, J. L. Shi, *Chem. Commun.* **2008**, *23*, 2629.
[144] W. R. Zhao, M. D. Lang, Y. S. Li, L. Li, J. L. Shi, *J. Mater. Chem.* **2009**, *19*, 2778.

[145] Y. Chen, C. Chu, Y. C. Zhou, Y. F. Ru, H. R. Chen, F. Chen, Q. J. He, Y. L. Zhang, L. L. Zhang, J. L. Shi, *Small* **2011**, *7*, 2935.
[146] L. L. Li, F. Q. Tang, H. Y. Liu, T. L. Liu, N. J. Hao, D. Chen, X. Teng, J. Q. He, *ACS Nano* **2010**, *4*, 6874.
[147] F. G. Gao, L. L. Li, T. L. Liu, N. J. Hao, H. Y. Liu, L. F. Tan, H. B. Li, X. L. Huang, B. Peng, C. M. Yan, L. Q. Yang, X. L. Wu, D. Chen, F. Q. Tang, *Nanoscale* **2012**, *4*, 3365.
[148] H. X. Wu, G. Liu, S. J. Zhang, J. L. Shi, L. X. Zhang, Y. Chen, F. Chen, H. R. Chen, *J. Mater. Chem.* **2011**, *21*, 3037.
[149] T. T. Wang, F. Chai, Q. Fu, L. Y. Zhang, H. Y. Liu, L. Li, Y. Liao, Z. M. Su, C. A. Wang, B. Y. Duan, D. X. Ren, *J. Mater. Chem.* **2011**, *21*, 5299.
[150] Y. Z. Zhang, J. C. Wang, X. Y. Bai, T. Y. Jiang, Q. Zhang, S. L. Wang, *Mol. Pharm.* **2012**, *9*, 505.
[151] A. M. Chen, M. Zhang, D. G. Wei, D. Stueber, O. Taratula, T. Minko, H. X. He, *Small* **2009**, *5*, 2673.
[152] H. A. Meng, M. Liong, T. A. Xia, Z. X. Li, Z. X. Ji, J. I. Zink, A. E. Nel, *ACS Nano* **2010**, *4*, 4539.
[153] F. Torney, B. G. Trewyn, V. S. Y. Lin, K. Wang, *Nat. Nanotechnol.* **2007**, *2*, 295.
[154] F. Qin, Y. C. Zhou, J. L. Shi, Y. L. Zhang, *J. Biomed. Mater. Res. Part A* **2009**, *90A*, 333.
[155] H. Yan, C. Teh, S. Sreejith, L. L. Zhu, A. Kwok, W. Q. Fang, X. Ma, K. T. Nguyen, V. Korzh, Y. L. Zhao, *Angew. Chem. Int. Ed.* **2012**, *51*, 8373.
[156] N. Singh, A. Karambelkar, L. Gu, K. Lin, J. S. Miller, C. S. Chen, M. J. Sailor, S. N. Bhatia, *J. Am. Chem. Soc.* **2011**, *133*, 19582.
[157] D. Schmaljohann, *Adv. Drug Deliv. Rev.* **2006**, *58*, 1655.
[158] C. D. H. Alarcon, S. Pennadam, C. Alexander, *Chem. Soc. Rev.* **2005**, *34*, 276.
[159] S. Ganta, H. Devalapally, A. Shahiwala, M. Amiji, *J. Control. Release* **2008**, *126*, 187.
[160] N. K. Mal, M. Fujiwara, Y. Tanaka, *Nature* **2003**, *421*, 350.
[161] J. L. Vivero-Escoto, Slowing, II, C. W. Wu, V. S. Y. Lin, *J. Am. Chem. Soc.* **2009**, *131*, 3462.
[162] J. P. Lai, X. Mu, Y. Y. Xu, X. L. Wu, C. L. Wu, C. Li, J. B. Chen, Y. B. Zhao, *Chem. Commun.* **2010**, *46*, 7370.
[163] D. P. Ferris, Y. L. Zhao, N. M. Khashab, H. A. Khatib, J. F. Stoddart, J. I. Zink, *J. Am. Chem. Soc.* **2009**, *131*, 1686.
[164] S. Giri, B. G. Trewyn, M. P. Stellmaker, V. S. Y. Lin, *Angew. Chem. Int. Ed.* **2005**, *44*, 5038.
[165] R. Liu, X. Zhao, T. Wu, P. Y. Feng, *J. Am. Chem. Soc.* **2008**, *130*, 14418.
[166] Q. Yang, S. H. Wang, P. W. Fan, L. F. Wang, Y. Di, K. F. Lin, F. S. Xiao, *Chem. Mater.* **2005**, *17*, 5999.
[167] C. Park, K. Oh, S. C. Lee, C. Kim, *Angew. Chem. Int. Ed.* **2007**, *46*, 1455.
[168] J. T. Sun, C. Y. Hong, C. Y. Pan, *J. Phys. Chem. C* **2010**, *114*, 12481.
[169] C. H. Lee, S. H. Cheng, I. P. Huang, J. S. Souris, C. S. Yang, C. Y. Mou, L. W. Lo, *Angew. Chem. Int. Ed.* **2010**, *49*, 8214.
[170] C. E. Chen, F. Pu, Z. Z. Huang, Z. Liu, J. S. Ren, X. G. Qu, *Nucleic Acids Res.* **2011**, *39*, 1638.
[171] Q. Gao, Y. Xu, D. Wu, Y. H. Sun, X. A. Li, *J. Phys. Chem. C* **2009**, *113*, 12753–12758.
[172] H. J. Kim, H. Matsuda, H. S. Zhou, I. Honma, *Adv. Mater.* **2006**, *18*, 3083.
[173] A. Bernardos, E. Aznar, M. D. Marcos, R. Martinez-Manez, F. Sancenon, J. Soto, J. M. Barat, P. Amoros, *Angew. Chem. Int. Ed.* **2009**, *48*, 5884.
[174] A. Bernardos, L. Mondragon, E. Aznar, M. D. Marcos, R. Martinez-Manez, F. Sancenon, J. Soto, J. M. Barat, E. Perez-Paya, C. Guillem, P. Amoros, *ACS Nano* **2010**, *4*, 6353.
[175] C. Coll, L. Mondragon, R. Martinez-Manez, F. Sancenon, M. D. Marcos, J. Soto, P. Amoros, E. Perez-Paya, *Angew. Chem. Int. Ed.* **2011**, *50*, 2138.
[176] K. Patel, S. Angelos, W. R. Dichtel, A. Coskun, Y. W. Yang, J. I. Zink, J. F. Stoddart, *J. Am. Chem. Soc.* **2008**, *130*, 2382.
[177] C. Park, H. Kim, S. Kim, C. Kim, *J. Am. Chem. Soc.* **2009**, *131*, 16614.
[178] Y. Z. You, K. K. Kalebaila, S. L. Brock, D. Oupicky, *Chem. Mater.* **2008**, *20*, 3354.
[179] C. Y. Liu, J. Guo, W. L. Yang, J. H. Hu, C. C. Wang, S. K. Fu, *J. Mater. Chem.* **2009**, *19*, 4764.
[180] Y. F. Zhu, S. Kaskel, T. Ikoma, N. Hanagata, *Micro. Meso. Mater.* **2009**, *123*, 107.
[181] E. Climent, A. Bernardos, R. Martinez-Manez, A. Maquieira, M. D. Marcos, N. Pastor-Navarro, R. Puchades, F. Sancenon, J. Soto, P. Amoros, *J. Am. Chem. Soc.* **2009**, *131*, 14075.
[182] Y. N. Zhao, B. G. Trewyn, Slowing, II, V. S. Y. Lin, *J. Am. Chem. Soc.* **2009**, *131*, 8398.
[183] J. V. Jokerst, S. S. Gambhir, *Acc. Chem. Res.* **2011**, *44*, 1050.
[184] H. Y. Liu, T. L. Liu, X. L. Wu, L. L. Li, L. F. Tan, D. Chen, F. Q. Tang, *Adv. Mater.* **2012**, *24*, 755.
[185] H. Y. Liu, D. Chen, L. L. Li, T. L. Liu, L. F. Tan, X. L. Wu, F. Q. Tang, *Angew. Chem. Int. Ed.* **2011**, *50*, 891.
[186] T. J. Dougherty, C. J. Gomer, B. W. Henderson, G. Jori, D. Kessel, M. Korbelik, J. Moan, Q. Peng, *J. Natl. Cancer Inst.* **1998**, *90*, 889.
[187] D. Dolmans, D. Fukumura, R. K. Jain, *Nat. Rev. Cancer* **2003**, *3*, 380.
[188] S. H. Cheng, C. H. Lee, M. C. Chen, J. S. Souris, F. G. Tseng, C. S. Yang, C. Y. Mou, C. T. Chen, L. W. Lo, *J. Mater. Chem.* **2010**, *20*, 6149.
[189] M. Gary-Bobo, Y. Mir, C. Rouxel, D. Brevet, I. Basile, M. Maynadier, O. Vaillant, O. Mongin, M. Blanchard-Desce, A. Morere, M. Garcia, J. O. Durand, L. Raehm, *Angew. Chem. Int. Ed.* **2011**, *50*, 11425.
[190] S. H. Cheng, C. C. Hsieh, N. T. Chen, C. H. Chu, C. M. Huang, P. T. Chou, F. G. Tseng, C. S. Yang, C. Y. Mou, L. W. Lo, *Nano Today* **2011**, *6*, 552.
[191] X. Wang, H. R. Chen, Y. Chen, M. Ma, K. Zhang, F. Q. Li, Y. Y. Zheng, D. P. Zeng, Q. Wang, J. L. Shi, *Adv. Mater.* **2012**, *24*, 785.
[192] J. E. Kennedy, *Nat. Rev. Cancer* **2005**, *5*, 321.
[193] J. E. Kennedy, G. R. ter Haar, D. Cranston, *Brit. J. Radiol.* **2003**, *76*, 590.
[194] C. R. Hill, G. R. terHaar, *Brit. J. Radiol.* **1995**, *68*, 1296.
[195] K. U. Kohrmann, M. S. Michel, J. Gaa, E. Marlinghaus, P. Alken, *J. Urol.* **2002**, *167*, 2397.
[196] M. Vallet-Regi, F. Balas, M. Colilla, M. Manzano, *Prog. Solid State Chem.* **2008**, *36*, 163.
[197] M. Zhu, H. X. Wang, J. Y. Liu, H. L. He, X. G. Hua, Q. J. He, L. X. Zhang, X. J. Ye, J. L. Shi, *Biomaterials* **2011**, *32*, 1986.
[198] I. Izquierdo-Barba, M. Colilla, M. Vallet-Regi, *J. Nanomater.* **2008**, DOI: 10.1155/2008/106970.
[199] I. Izquierdo-Barba, L. Ruiz-Gonzalez, J. C. Doadrio, J. M. Gonzalez-Calbet, M. Vallet-Regi, *Solid State Sci.* **2005**, *7*, 983.
[200] X. Li, J. L. Shi, X. P. Dong, L. X. Zhang, H. Y. Zeng, *J. Biomed. Mater. Res. Part A* **2008**, *84A*, 84.
[201] C. Wu, Y. Ramaswamy, Y. F. Zhu, R. Zheng, R. Appleyard, A. Howard, H. Zreiqat, *Biomaterials* **2009**, *30*, 2199.
[202] C. G. Trejo, D. Lozano, M. Manzano, J. C. Doadrio, A. J. Salinas, S. Dapia, E. Gomez-Barrena, M. Vallet-Regi, N. Garcia-Honduvilla, J. Bujan, P. Esbrit, *Biomaterials* **2010**, *31*, 8564.
[203] K. Glunde, D. Artemov, M. F. Penet, M. A. Jacobs, Z. M. Bhujwalla, *Chem. Rev.* **2010**, *110*, 3043.
[204] A. J. L. Villaraza, A. Bumb, M. W. Brechbiel, *Chem. Rev.* **2010**, *110*, 2921.
[205] H. B. Na, T. Hyeon, *J. Mater. Chem.* **2009**, *19*, 6267.
[206] N. Lee, T. Hyeon, *Chem. Soc. Rev.* **2012**, *41*, 2575.
[207] A. H. Lu, E. L. Salabas, F. Schuth, *Angew. Chem. Int. Ed.* **2007**, *46*, 1222.

[208] C. C. Huang, C. Y. Tsai, H. S. Sheu, K. Y. Chuang, C. H. Su, U. S. Jeng, F. Y. Cheng, H. Y. Lei, C. S. Yeh, *ACS Nano* **2011**, *5*, 3905.
[209] T. Kim, E. Momin, J. Choi, K. Yuan, H. Zaidi, J. Kim, M. Park, N. Lee, M. T. McMahon, A. Quinones-Hinojosa, J. W. M. Bulte, T. Hyeon, A. A. Gilad, *J. Am. Chem. Soc.* **2011**, *133*, 2955.
[210] J. G. Penfield, R. F. Reilly, *Nat. Clin. Pract. Nephrol.* **2007**, *3*, 654.
[211] U. I. Tromsdorf, O. T. Bruns, S. C. Salmen, U. Beisiegel, H. Weller, *Nano Lett.* **2009**, *9*, 4434.
[212] J. Perez-Rodriguez, S. Lai, B. D. Ehst, D. M. Fine, D. A. Bluemke, *Radiology* **2009**, *250*, 371.
[213] E. Terreno, D. D. Castelli, A. Viale, S. Aime, *Chem. Rev.* **2010**, *110*, 3019.
[214] D. D. Schwert, J. A. Davies, N. Richardson, *Contrast Agents I* **2002**, *221*, 165.
[215] T. Kim, E. J. Cho, Y. Chae, M. Kim, A. Oh, J. Jin, E. S. Lee, H. Baik, S. Haam, J. S. Suh, Y. M. Huh, K. Lee, *Angew. Chem. Int. Ed.* **2011**, *50*, 10589.
[216] M. Kueny-Stotz, A. Garofalo, D. Felder-Flesch, *Eur. J. Inorg. Chem.* **2012**, *12*, 1987–2005.
[217] F. Stallmach, J. Karger, C. Krause, M. Jeschke, U. Oberhagemann, *J. Am. Chem. Soc.* **2000**, *122*, 9237.
[218] Y. Z. Shao, X. M. Tian, W. Y. Hu, Y. Y. Zhang, H. Liu, H. Q. He, Y. Y. Shen, F. K. Xie, L. Li, *Biomaterials* **2012**, *33*, 6438.
[219] S. H. Crayton, A. Tsourkas, *ACS Nano* **2011**, *5*, 9592.
[220] P. A. Schornack, R. J. Gillies, *Neoplasia* **2003**, *5*, 135.
[221] E. Torres, F. Mainini, R. Napolitano, F. Fedeli, R. Cavalli, S. Aime, E. Terreno, *J. Control. Release* **2011**, *154*, 196.
[222] S. Mura, P. Couvreur, *Adv. Drug Deliv. Rev.* **2012**, *64*, 1394.
[223] X. L. Huang, F. Zhang, S. Lee, M. Swierczewska, D. O. Kiesewetter, L. X. Lang, G. F. Zhang, L. Zhu, H. K. Gao, H. S. Choi, G. Niu, X. Y. Chen, *Biomaterials* **2012**, *33*, 4370.
[224] J. Pan, D. Wan, J. L. Gong, *Chem. Commun.* **2011**, *47*, 3442.
[225] A. M. Derfus, W. C. W. Chan, S. N. Bhatia, *Nano Lett.* **2004**, *4*, 11.
[226] B. A. Rzigalinski, J. S. Strobl, *Toxicol. Appl. Pharm.* **2009**, *238*, 280.
[227] L. Q. Xiong, T. S. Yang, Y. Yang, C. J. Xu, F. Y. Li, *Biomaterials* **2010**, *31*, 7078.
[228] J. Zhou, Z. Liu, F. Y. Li, *Chem. Soc. Rev.* **2012**, *41*, 1323.
[229] M. Vendrell, D. T. Zhai, J. C. Er, Y. T. Chang, *Chem. Rev.* **2012**, *112*, 4391.
[230] Q. J. He, J. L. Shi, X. Z. Cui, C. Y. Wei, L. X. Zhang, W. Wu, W. B. Bu, H. R. Chen, H. X. Wu, *Chem. Commun.* **2011**, *47*, 7947.
[231] Q. He, M. Ma, C. Wei, J. Shi, *Biomaterials* **2012**, *33*, 4392.
[232] H. Hu, H. Zhou, J. Du, Z. Q. Wang, L. An, H. Yang, F. H. Li, H. X. Wu, S. P. Yang, *J. Mater. Chem.* **2011**, *21*, 6576.
[233] H. P. Martinez, Y. Kono, S. L. Blair, S. Sandoval, J. Wang-Rodriguez, R. F. Mattrey, A. C. Kummel, W. C. Trogler, *Medchemcomm* **2010**, *1*, 266.
[234] H. Hu, H. Zhou, J. Liang, L. An, A. T. Dai, X. J. Li, H. Yang, S. P. Yang, H. X. Wu, *J. Colloid Interface Sci.* **2011**, *358*, 392.
[235] P. L. Lin, R. J. Eckersley, E. A. H. Hall, *Adv. Mater.* **2009**, *21*, 3949.
[236] A. Liberman, H. P. Martinez, C. N. Ta, C. V. Barback, R. F. Mattrey, Y. Kono, S. L. Blair, W. C. Trogler, A. C. Kummel, Z. Wu, *Biomaterials* **2012**, *33*, 5124.
[237] M. A. Malvindi, A. Greco, F. Conversano, A. Figuerola, M. Corti, M. Bonora, A. Lascialfari, H. A. Doumari, M. Moscardini, R. Cingolani, G. Gigli, S. Casciaro, T. Pellegrino, A. Ragusa, *Adv. Funct. Mater.* **2011**, *21*, 2548.
[238] J. H. Ryu, H. Koo, I.-C. Sun, S. H. Yuk, K. Choi, K. Kim, I. C. Kwon, *Adv. Drug Deliv. Rev.* **2012**, *64*, 1447.
[239] Y. Chen, H. R. Chen, S. J. Zhang, F. Chen, L. X. Zhang, J. M. Zhang, M. Zhu, H. X. Wu, L. M. Guo, J. W. Feng, J. L. Shi, *Adv. Funct. Mater.* **2011**, *21*, 270.
[240] M. Liong, J. Lu, M. Kovochich, T. Xia, S. G. Ruehm, A. E. Nel, F. Tamanoi, J. I. Zink, *ACS Nano* **2008**, *2*, 889.
[241] H. X. Wu, S. J. Zhang, J. M. Zhang, G. Liu, J. L. Shi, L. X. Zhang, X. Z. Cui, M. L. Ruan, Q. J. He, W. B. Bu, *Adv. Funct. Mater.* **2011**, *21*, 1850.
[242] F. Zhang, G. B. Braun, A. Pallaoro, Y. C. Zhang, Y. F. Shi, D. X. Cui, M. Moskovits, D. Y. Zhao, G. D. Stucky, *Nano Lett.* **2012**, *12*, 61.
[243] V. Salgueirino-Maceira, M. A. Correa-Duarte, M. Spasova, L. M. Liz-Marzan, M. Farle, *Adv. Funct. Mater.* **2006**, *16*, 509.
[244] M. Ma, H. R. Chen, Y. Chen, X. Wang, F. Chen, X. Z. Cui, J. L. Shi, *Biomaterials* **2012**, *33*, 989.
[245] A. Pietroiusti, M. Massimiani, I. Fenoglio, M. Colonna, F. Valentini, G. Palleschi, A. Camaioni, A. Magrini, G. Siracusa, A. Bergamaschi, A. Sgambato, L. Campagnolo, *ACS Nano* **2011**, *5*, 4624.
[246] F. Sharif, F. Porta, A. H. Meijer, A. Kros, M. K. Richardson, *Int. J. Nanomed.* **2012**, *7*, 1875.
[247] S. A. Li, H. A. Liu, L. Li, N. Q. Luo, R. H. Cao, D. H. Chen, Y. Z. Shao, *Appl. Phys. Lett.* **2011**, *98*, DOI: DOI: 10.1155/2008/106970.
[248] J. L. Vivero-Escoto, K. M. L. Taylor-Pashow, R. C. Huxford, J. Della Rocca, C. Okoruwa, H. Y. An, W. L. Lin, W. B. Lin, *Small* **2011**, *7*, 3519.
[249] J. L. Steinbacher, S. A. Lathrop, K. Cheng, J. M. Hillegass, K. Butnor, R. A. Kauppinen, B. T. Mossman, C. C. Landry, *Small* **2010**, *6*, 2678.
[250] Y. Chen, H. R. Chen, D. P. Zeng, Y. B. Tian, F. Chen, J. W. Feng, J. L. Shi, *ACS Nano* **2010**, *4*, 6001.